The role of myeloid cell type-specific inducible nitric oxide synthase in the development of smoke-induced pulmonary hypertension

Inaugural Dissertation submitted to the Faculty of Medicine in partial fulfillment of the requirements for the PhD-Degree of the Faculties of Veterinary Medicine and Medicine of the Justus Liebig University Giessen

by

Gredić Marija

of

Belgrade, Serbia

Giessen, 2022

From the Department of Medicine

Director/Chairman: Prof. Dr. Werner Seeger

of the Faculty of Medicine of the Justus Liebig University Giessen

First Supervisor and Committee Member: Prof. Dr. Norbert Weißmann

Second Supervisor and Committee Member: Prof. Dr. Tim Lahm

Committee member (Chair): Prof. Dr. Klaus-Dieter Schlüter

Committee member: Prof. Dr. Christiane Herden

Date of Doctoral Defense: 02.08.2022

“I would rather have questions that can’t be answered than answers that can’t be questioned.”

Richard P. Feynman

Index

Index of figures

Index of tables

1. Introduction

1.1. Chronic Obstructive Pulmonary Disease

1.1.1. Definition, symptoms, diagnosis and prevalence of COPD

Chronic obstructive pulmonary disease (COPD) is a progressive and incurable disease characterized by persistent respiratory symptoms and airflow limitation (Chung & Adcock, 2008). The disease is caused by chronic exposure to noxious particles and gases, such as cigarette smoke, in complex interaction with predisposing genetic and developmental factors (W. Shi, Bellusci, & Warburton, 2007). Symptoms of COPD include dyspnea, chronic cough and mucus hypersecretion. Acute exacerbations of these symptoms are triggered by bacterial or viral respiratory infections or environmental pollutants. These episodes of sudden worsening include hypoxemia as a result of worsened abnormalities in ventilation-perfusion matching, increased gas trapping and hyperinflation. In addition, COPD patients often have concomitant systemic effects and comorbid conditions including skeletal muscle wasting, osteoporosis, ischemic heart disease, heart failure, diabetes, and metabolic syndrome (Vogelmeier et al., 2020).

COPD diagnosis and assessment of disease stage are based on a spirometry test, with an airflow limitation criterion, namely post-bronchodilatory forced expiratory volume in one second divided by the forced vital capacity ratio (FEV1/FVC) being fixed below 0.70 (Vogelmeier et al., 2020).

Even though symptoms are under-reported by patients and the disease therefore often remains undiagnosed (Vogelmeier et al., 2020), COPD currently accounts for one of the five most important causes of death worldwide (Pichl et al., 2019). The prevalence is higher in individuals older than 40 years and increases rapidly with age. COPD is also more common among ex-smokers compared to non-smokers. Projected further increase in COPD prevalence caused by the aging of the world’s population, smoking epidemics and exposure to other COPD risk factors urges for understanding the complex pathophysiology of this disease and development of novel treatment options (Vogelmeier et al., 2020).

1.1.2. Pathological changes and underlying molecular mechanisms in COPD

Under the umbrella of “airflow limitation that is not fully reversible”, COPD encompasses chronic bronchitis and emphysema (Tuder & Petrache, 2012). While the first term is used to describe a condition arising from the inflammation and remodeling of the conducting airways in the lung, the latter one implies the loss of gas exchange surface, and therefore represents the disease of distal airways and lung parenchyma (Hadzic et al., 2020; Tuder & Petrache, 2012).

1.1.2.1. Chronic bronchitis

The early pathological changes leading to chronic bronchitis are the airway hyper-responsiveness to noxious particles, increased mucus secretion and impaired ciliary clearance. Prolonged exposure of conducting airways to the stimulus results in chronic inflammation and structural remodeling involving epithelium, submucosal glands and airway smooth muscle cells, as well as the adventitial layer of the airways (Hadzic et al., 2020).

Thickening of the epithelial layer is characterized by squamous cell metaplasia and Goblet cell hyperplasia. Squamous cell metaplasia represents a reversible substitution of columnar with squamous epithelium, which leads to airway obstruction and impaired ciliary clearance. The vast expansion of otherwise scarce Goblet cells accounts for the increase in mucus secretion. Hypertrophy of the submucosal glands is present in the large airways (Chung & Adcock, 2008), further aggravating mucus hypersecretion.

In addition to the thickening of the airway epithelium, there is a dramatic increase in the airway smooth muscle layer in COPD patients. Airway smooth muscles contribute to the pathology not only by their contractile properties, but also by the ability to secrete components of the extracellular matrix, as well as different cytokines, chemokines, proteases and growth factors implicated in the pathology of COPD (Chung & Adcock, 2008).

Pathological changes in the third, adventitial layer of airways involve the accumulation of fibroblast and myofibroblasts and aggregation of inflammatory cells. Remodeling also encompasses an increase of total collagen I and III in this layer and in *lamina propria* (Chung & Adcock, 2008; Hadzic et al., 2020). Importantly, recent findings suggest that the early loss of terminal bronchioles is a prominent feature of the disease,

occurring before described fibrotic changes in the remaining small airways. (Hadzic et al., 2020; Tuder & Petrache, 2012).

1.1.2.2. Emphysema

Another important pathological feature of COPD lungs is the development of emphysema. The term is used to describe an enlargement of alveolar space, associated with the destruction of alveolar walls, but without evident fibrotic changes that are paradoxically present in the adjacent small airways (Chung & Adcock, 2008; Hadzic et al., 2020; Hogg & Timens, 2009). Although underlying pathological mechanisms of alveolar destruction mostly differ from those described for chronic bronchitis, excessive inflammatory cell activation is an important player in this pathological condition as well (Tuder & Petrache, 2012).

Inflammatory cells are the source of enzymes such as neutrophilic elastase and matrix metalloproteinases (MMPs), employed in enhanced matrix proteolysis, a process often considered as the central event of emphysema (Hadzic et al., 2020). This paradigm is substantiated by the occurrence of emphysema in α1-antitrypsin deficient patients and numerous data from preclinical models; however, recent findings are offering a far more complex picture of the alveolar destruction (Tuder & Petrache, 2012).

This broad concept implicates oxidative and nitrosative stress as an important contributor to alveolar destruction (Hadzic et al., 2020). In susceptible lungs challenged by cigarette smoke, oxidative and nitrosative stress arise from mitochondrial dysfunction, upregulation of enzymes including components of nicotinamide adenine dinucleotide phosphate (NADPH) oxidase complex, inducible nitric oxide synthase (iNOS), myeloperoxidases (MPOs) and dysregulation of antioxidant defense mechanisms, primarily orchestrated by nuclear factor erythroid 2–related factor 2 (Nrf2) (Hadzic et al., 2020). Oxidative stress can inhibit anti-proteases and activate proteases, amplifying the process of matrix degradation (Tuder & Petrache, 2012). Reactive oxygen and nitrogen radicals also affect the lung maintenance programs by damaging cellular components and thus initiating apoptosis or replicative senescence (MacNee & Tuder, 2009; Tuder & Petrache, 2012). Moreover, reactions with lipids result in pro-inflammatory signaling mediators (Tuder & Petrache, 2012), while posttranslational changes of enzymes and transcriptional factors such as oxidation/carbonylation, nitration and aldehyde adduct formation, can change their

function to promote pro-inflammatory signaling or modulate immune response (Sundar et al., 2014).

Apart from oxidative stress, apoptosis of the structural cells in lung parenchyma emerged as an important contributor to the failure of lung maintenance programs and consequential development of emphysema (MacNee & Tuder, 2009). A multitude of cellular signaling events including DNA damage, endoplasmic reticulum (ER) stress, autophagy, synthesis of pro-apoptotic sphingolipids, and downregulation of growth factor signaling are triggered by direct exposure to noxious stimuli or resulting oxidative stress, culminating in apoptosis of primarily epithelial and endothelial cells (Tuder & Petrache, 2012). Additionally, apoptosis of progenitor cells abolishes the regenerative potential of the lung and interferes with the injury repair processes (Hadzic et al., 2020). Moreover, alveolar cell injury and ineffective clearance of apoptotic cells can in turn further provoke and modulate the inflammatory response (Hadzic et al., 2020).

Alternatively, accumulated damage on cellular components arising from oxidative stress, as well as some inflammatory mediators (interleukin (IL)-6 and IL-8) can lead to cellular senescence, defined as the “non-proliferative state in which cells are metabolically active and apoptosis-resistant” (MacNee & Tuder, 2009). Higher levels of senescence markers, including senescence-associated β-galactosidase, cyclin-kinase inhibitors p16 and p21, as well as decreased telomere length have been documented in both COPD lungs and animal models of the disease (Adnot et al., 2015). Importantly, senescent cells secrete high amounts of growth factors and pro-inflammatory cytokines, including IL-6, IL-8, IL-13, chemokine (C-C motif) ligand (CCL) 2 and CCL5 (Adnot et al., 2015), thus perpetuating inflammation in emphysematous lungs in yet another positive feedback loop. Consequential progressive lung injury could potentially lead to autoimmunity, another emerging mechanism implicated in the progression of emphysema (MacNee & Tuder, 2009; Tuder & Petrache, 2012).

The described concept of several mutually interconnected, self-perpetuating pathological mechanisms explains the progressive nature of the disease even after smoking cessation (Tuder & Petrache, 2012), as well as the failure of several attempted therapies, but also offers new avenues for the treatment of this devastating disease. Moreover, pulmonary vascular remodeling, a pathological condition present in the lungs of smokers and COPD patients, has been recently proposed as an

important contributor to the onset and progression of the disease (Gredic et al., 2020) and will be addressed in more detail in chapter 2.

1.1.2.3. Inflammatory cell profiles in COPD

Chronic inflammation in COPD is characterized by the accumulation of neutrophils, macrophages, mast cells, cluster of differentiation (CD) 4^+ and $CD8^+$ T cells, B cells and dendritic cells in the lung, particularly around the small airways. Increased circulating levels and/or lung expression of numerous mediators, including IL-1β, IL-6, IL-8, IL-17, IL-22, CCL1, CCL2, CCL3, CCL4, CCL5, CCL11, chemokine (C-X-C motif) ligand (CXCL)1, CXCL5, tumor necrosis factor (TNF)-α and transforming growth factor (TGF)-β have been reported in COPD patients (Chung & Adcock, 2008).

Neutrophils and macrophages are the most studied cells of innate immunity in the context of COPD. These phagocytic cells produce a plethora of cytokines, chemokines, lipid mediators, reactive oxygen radicals and proteolytic enzymes involved in the degradation and remodeling of the extracellular matrix (Chung & Adcock, 2008). Importantly, it was shown that cigarette smoke impairs the phagocytic activity of both macrophages and neutrophils (Chung & Adcock, 2008), which would explain defective clearance of pathogens and apoptotic cells and consequent amplification of the inflammatory stimulus (Chung & Adcock, 2008; MacNee & Tuder, 2009; Tuder & Petrache, 2012).

Adaptive immunity could also play a prominent role in COPD pathology, not only by modulation and amplification of innate immune response, but also by direct effects on lung cells and matrix components. On the one hand, the increase in the number of cytotoxic $CD8^+$ T cells could damage the lung parenchyma directly via the release of lytic substances such as perforin and granzyme (Chung & Adcock, 2008). On the other, the occurrence of bronchus-associated lymphoid tissue in advanced COPD, increase in $CD4^+$ T cells and decrease in regulatory T cells, oligoclonal expansion of $CD4^+$ T cells and B cells could contribute to the development of an autoimmune reaction. The existence of the autoimmune response directed against proteins that could have been damaged by smoke and reactive oxygen and nitrogen species (Chung & Adcock, 2008; Sullivan et al., 2005; Tuder & Petrache, 2012; L. Wen et al., 2018) is supported by the detection of circulating anti-elastin antibodies, anti-epithelial antibodies and tobacco

anti-idiotypic antibodies in COPD patients (Chung & Adcock, 2008; L. Wen et al., 2018).

Overall, environmental noxious stimuli activate a robust inflammatory response, whose amplification by genetic factors, infections, oxidative stress, inflammatory mediators, cell apoptosis and senescence likely creates a self-perpetuating stimulus that evolves with time and propagates the disease even upon the smoke cessation.

1.2. COPD-associated pulmonary hypertension

1.2.1. Prevalence and clinical consequences of pulmonary hypertension in COPD

Pulmonary hypertension (PH) represents an increase in pulmonary arterial blood pressure defined by a mean pulmonary artery pressure (mPAP) higher than 20 mmHg at rest, measured by right heart catheterization (and coupled with pulmonary arterial wedge pressure ≤15 mmHg and pulmonary vascular resistance (PVR) ≥3 Wood Units, in case of pre-capillary PH). This serious, incurable and life-threatening condition encompasses several clinical entities, classified into five groups based on pathophysiological mechanisms, clinical presentation, hemodynamic characteristics and therapeutic management ((Simonneau et al., 2019), Table 1).

Table 1: Current clinical classification of PH. Based on Simonneau 2019.

1.	Pulmonary arterial hypertension (PAH)
2.	PH due to the left heart disease
3.	**PH due to lung diseases and/or hypoxia** 3.1. Obstructive lung diseases 3.2. Restrictive lung diseases 3.3. Other lung diseases with mixed obstructive/restrictive pattern 3.4. Hypoxia without lung disease 3.5. Developmental lung disorders
4.	PH due to pulmonary artery obstructions
5.	PH with unclear and/or multifactorial mechanisms

More than a century before the pulmonary arterial pressures could be measured, sclerosis of the pulmonary artery was known as the morphologic signature of PH. Indeed, structural changes in the normal architecture of the walls of pulmonary arteries

and veins, known as pulmonary vascular remodeling, represent the key structural alteration in pulmonary hypertension (Tuder, 2017). In the end stage of the disease, remodeling process usually involves thickening of all three layers of pulmonary vessels - intimal, medial and adventitial. This thickening arises as a result of hypertrophy and hyperplasia of the resident vascular cells and recruitment of inflammatory and/or progenitor cells, and increased deposition of extracellular matrix components.

Interestingly, it seems likely that one of the first descriptions of this phenomenon was based on the findings from the emphysematous lung (Osler, 1893; Romberg, 1893). Nowadays, COPD-associated PH (COPD-PH), a condition included in group 3 according to the current WHO classification (Table 1), is a common finding in COPD patients. Several studies in patients with severe airway obstruction showed that PH (defined by mPAP > 20 mmHg) is present in up to 90% of cases (Barbera, Peinado, & Santos, 2003; Gredic et al., 2020). Although elevation of mPAP is most often mild to moderate, it is nevertheless associated with increased risk of exacerbations and decreased survival in COPD patients (Barbera et al., 2003; Gredic et al., 2020).

As in other forms of PH, the elevation of mPAP in COPD can result in right ventricular (RV) hypertrophy, termed *cor pulmonale*. While RV hypertrophy is an adaptive response that helps to cope with an increased afterload in the RV, it might ultimately result in maladaptation, RV dilatation and heart failure (Gredic et al., 2020).

Intriguingly, recent findings from preclinical models and COPD patients prompted the hypothesis that pulmonary vascular alterations are an early phenomenon of the COPD pathology and a possible driver of parenchymal destruction (Barbera et al., 2003; Gredic et al., 2020). In smoke-exposed mice and guinea pigs, pulmonary vascular remodeling, the main histopathological feature of COPD-PH, precedes parenchymal destruction (Ferrer et al., 2009; Seimetz et al., 2011; Weissmann et al., 2014; Wright & Churg, 1991) and established therapies for PH affect the development of emphysema (Dominguez-Fandos et al., 2015; Seimetz et al., 2015; Weissmann et al., 2014). Similarly, histopathological signs of pulmonary vascular remodeling have been found in most COPD patients and smokers who had not developed COPD (Magee et al., 1988; Santos et al., 2002; Wilkinson et al., 1988; Wright, Petty, & Thurlbeck, 1992).

Despite the association of PH with increased mortality and morbidity in COPD patients and the possible involvement of pulmonary vascular alterations in the development of

airway obstruction, pathological mechanisms driving COPD-PH are still poorly understood and efficient treatment options are not available (Gredic et al., 2020).

1.2.2. Pathogenesis of COPD-associated PH

Pulmonary vascular remodeling is the main cause of COPD-PH, resulting from the combination of direct effects of cigarette smoke on pulmonary vasculature with chronic hypoxemia, endothelial dysfunction and inflammation. Additional contributors to elevated mPAP in obstructed lungs are vascular pruning, polycythemia, pulmonary thrombosis and hyperinflation due to severe emphysema (Barbera et al., 2003; Chaouat, Naeije, & Weitzenblum, 2008; Gredic et al., 2020).

1.2.2.1. Characteristics of pulmonary vascular remodeling in COPD-PH

Signs of pulmonary vascular remodeling in the intimal and/or medial layer of the pulmonary vessel walls have been found in all stages of COPD and in smokers who had not developed the disease (Magee et al., 1988; Santos et al., 2002; Wilkinson et al., 1988; Wright et al., 1992).

Changes in the intimal layer consist of deposition of elastic and collagen fibers and occurrence of longitudinally oriented smooth muscle cells in this layer (Santos et al., 2002; Wilkinson et al., 1988). Notably, described intimal thickening is evident already in smokers without COPD and in patients with mild to moderate COPD whose mPAP is within the normal range at rest (Magee et al., 1988).

Remodeling of the medial layer occurs in patients with established COPD-PH and includes both the hypertrophy of the existing muscular layer and the occurrence of new circular smooth muscle coat and accompanying internal elastic lamina in normally non-muscularized arterioles (Magee et al., 1988; Wilkinson et al., 1988). Remodeling of the pulmonary microvessels is more prominent in patients with severe COPD-PH than in those with moderately elevated mPAP (Bunel et al., 2019).

Importantly, these observations are supported by recent evidence from animal models, where smoke exposure induces changes in intimal (Ferrer et al., 2009) and medial (Ferrer et al., 2009; Seimetz et al., 2011; Weissmann et al., 2014; Wright & Churg, 1991) layer of pulmonary vessel walls and hemodynamic changes prior to emphysema development and independent from hypoxia.

Finally, the adventitial layer of pulmonary muscular arteries in patients with mild COPD is infiltrated with inflammatory cells, and the size of these infiltrates correlates with pulmonary vascular remodeling (Peinado et al., 1999). Since my work provides further evidence for the pivotal role of inflammation in COPD-PH, this matter will be thoroughly discussed in chapter 1.3.

1.2.2.2. Underlying molecular mechanisms of pulmonary vascular remodeling in COPD-PH

As chronic hypoxia is a well-known trigger of pulmonary vascular remodeling in humans living at high altitudes and in animal models (Gassmann et al., 2020; Weissmann et al., 2006), hypoxemia resulting from alveolar destruction has long been considered the main cause of COPD-PH (Chaouat et al., 2008). Acute alveolar hypoxia leads to hypoxic pulmonary vasoconstriction (HPV), a physiological mechanism that redistributes the blood to the better-ventilated parts of the lung and thus optimizes gas exchange (Gassmann et al., 2020; Weissmann et al., 2006). However, under conditions of global hypoxia or impairment of respiratory function (that occurs in COPD), HPV leads to sustained overall vasoconstriction and consequent increase in PVR and PAP (Gassmann et al., 2020; Weissmann et al., 2006). In addition to HPV, sustained hypoxia results in the expression of hypoxia-sensitive genes including platelet-derived growth factor, TGF-β, vascular endothelial growth factor, the imbalance between proliferation and apoptosis of pulmonary vascular cells and consequent pulmonary vascular remodeling (Tuder et al., 2007).

The concept that such mechanisms play the most important role in COPD-associated pulmonary vascular remodeling has recently been challenged, not only by the notion that long-term oxygen therapy does not reverse COPD-PH (Barbera et al., 2003; Weitzenblum et al., 1985) but also by the growing evidence that pulmonary vascular alterations precede alveolar destruction and hypoxemia in COPD patients (Barbera et al., 2003; Gredic et al., 2020; Santos et al., 2002; Seimetz et al., 2011). Moreover, at least in the animal model, evidence was provided that molecular pathways deregulated in pulmonary vessels upon smoke exposure differ largely from those affected by chronic hypoxia (Seimetz et al., 2011). Instead, other mechanisms might be more important for the development of pulmonary vascular alterations at the early stages of COPD (Figure 1).

One of the proposed mechanisms involves direct effects of cigarette smoking (and noxious substances from smoke) on pulmonary artery smooth muscle cells (PASMC) that lead to changes in signaling pathways known to be important for the development of COPD. For example, soluble guanylate cyclase (sGC), iNOS and NADPH oxidase organizer 1 (NOXO1) are expressed in the pulmonary vasculature of mice. Results from preclinical studies suggest that expression of these proteins is dysregulated upon smoke exposure, and that their pharmacologic or genetic manipulation can prevent and/or reverse smoke-induced PH and emphysema (Seimetz et al., 2011; Seimetz et al., 2020; Weissmann et al., 2014).

Another direct target of cigarette smoke might be the endothelium, a well-known regulator of pulmonary vascular tone that acts through the release of potent vasoactive substances, such as nitric oxide (NO), endothelin (ET)-1, angiotensin and prostacyclin. Endothelial NOS (eNOS) (Barbera et al., 2001) and prostacyclin synthase (Nana-Sinkam et al., 2007) are downregulated in the pulmonary endothelium of COPD patients, and circulating levels of ET-1 are increased (Carratu et al., 2008). Importantly, as some of these mediators are able to modulate inflammatory responses and regulate the proliferation of PASMC, endothelial dysfunction and consequent dysregulation of these pathways can even promote medial hypertrophy (Barbera et al., 2003). For example, angiotensin II (AngII), an octapeptide resulting from proteolytic cleavage of the longer precursor by endothelium-expressed angiotensin-converting enzyme, has important immunomodulatory effects and induces proliferation of PASMC via mitogen-activated protein kinase (MAPK) pathway *in vitro* (Morrell et al., 1999; Suzuki et al., 2003). Accordingly, results from preclinical studies suggest that inhibition of the renin-angiotensin system could be a viable therapeutic strategy in the treatment of COPD-PH (Han et al., 2010).

Additionally, recent findings suggest that inflammation, already known as an important pathogenic mechanism in various other forms of pulmonary vascular remodeling, also plays a role in the onset and progression of vascular alterations in COPD (Eddahibi et al., 2006; Joppa et al., 2006; Peinado et al., 1999). However, it remains unclear whether the same molecular mechanisms responsible for the inflammatory cell activation in other forms of PH (especially, hypoxia-induced PH) are in play here, or the observed effects can again be attributed to the direct effects of cigarette smoke. My current work might tackle this important question, as the effects of genetic

manipulation in myeloid cells on the development of PH have been tested in two animal models – in cigarette smoke exposure and in chronic hypoxia model.

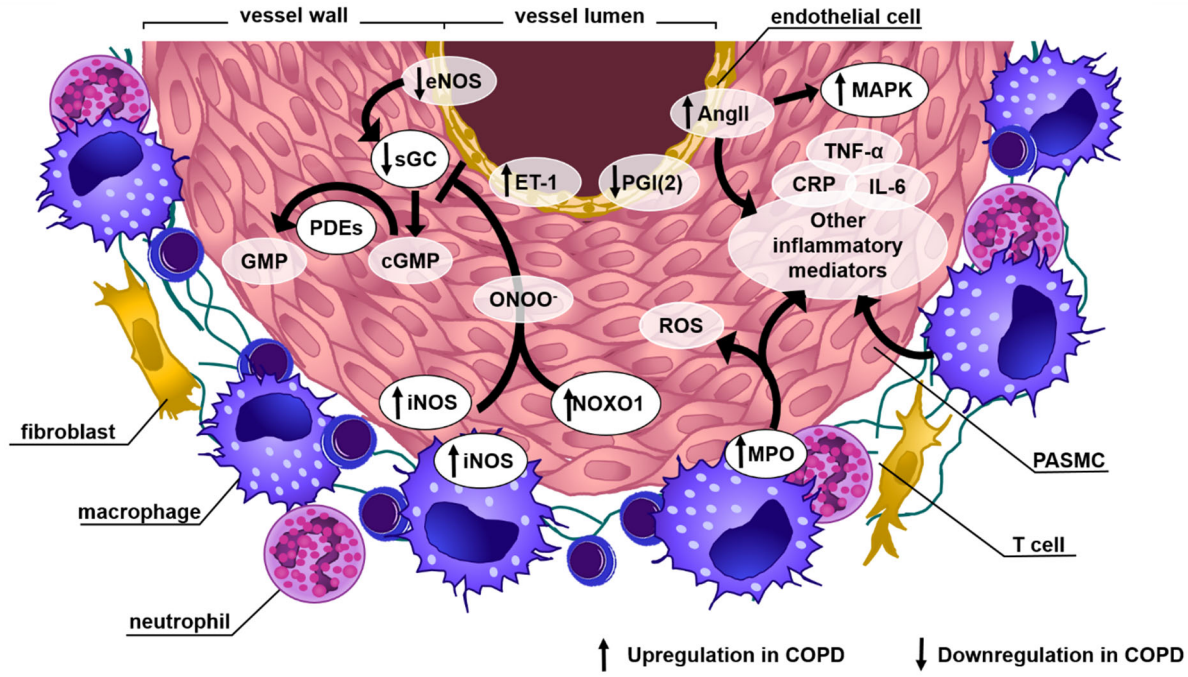

Figure 1: Pathological mechanisms underlying smoke-induced vascular remodeling.

Endothelial dysfunction, smoke-induced changes in pulmonary vascular smooth muscle cells (PASMC) and inflammation are considered to be drivers of pulmonary vascular remodeling in COPD-PH. eNOS: endothelial nitric oxide synthase; iNOS: inducible nitric oxide synthase; NOXO1: nicotinamide adenine dinucleotide phosphate oxidase organizer 1; ET-1: endothelin-1; PGI(2): prostacyclin; AngII: angiotensin II; MAPK: mitogen-activated protein kinase; sGC: soluble guanylate cyclase; cGMP: cyclic guanosine monophosphate; PDEs: phosphodiesterases; $ONOO^-$: peroxynitrite; MPO: myeloperoxidase; ROS: reactive oxygen species; TNF-α: tumor necrosis factor α; IL-6: interleukin-6; CRP: C-reactive protein; COPD: chronic obstructive pulmonary disease. The figure is modified from Gredic et al., 2020.

1.2.2.3. Animal models of COPD-PH

Various animal models that reproduce one or more features of the human COPD pathology can be induced by different triggers, such as cigarette smoke, elastases (pancreatic or neutrophil elastase), lipopolysaccharide (LPS) or inorganic dust, or by diverse genetic modifications in mice (Gredic et al., 2020; Wright, Cosio, & Churg, 2008). However, so far PH was shown only in smoke exposure and elastase models. In addition, transgenic mice overexpressing TNF-α develop both emphysema and PH

(Fujita et al., 2001; Vuillemenot, Rodriguez, & Hoyle, 2004), but they were nevertheless not used to model human COPD until now.

Cigarette smoke exposure models reproduce the majority of the physiological alterations and pathological changes seen in human COPD, which is why these models are of great translational value (Gredic et al., 2020; Wright et al., 2008). In different species, smoke-induced changes include emphysema, epithelial cell metaplasia, airway remodeling and activation of innate immunity, but also pulmonary vascular remodeling and PH as the early phenomena of this disease (Churg & Wright, 2007).

Vascular alterations in the lungs of smoke-exposed rodents mimic important features of pulmonary vascular remodeling seen in COPD-PH. These changes mostly affect the intimal and medial layers of the small pulmonary vessels and lead to the development of PH and RV hypertrophy. Importantly, endothelial dysfunction, small pulmonary vessel muscularization and consequent PAP elevation exist in smoke-exposed mice and guinea pigs well before detectable changes in lung function and development of emphysema (Ferrer et al., 2009; Seimetz et al., 2011). Functional changes and hypertrophy of RV also develop with smoke exposure, but RV failure has not been reported, most likely due to the mild PH occurring in these models (Seimetz et al., 2011; Sussan et al., 2009; Weissmann et al., 2014). It is noteworthy that described pathological alterations occur independently of hypoxia and that vascular gene regulation occurring in smoke-induced PH largely differs from that in remodeled vessels of hypoxic animals (Seimetz et al., 2011).

With regard to the etiology, the model mimics the habit of smoking that is one of the leading causes of COPD in human, but also models the exposure to air pollution, as cigarette smoke contains fine particulate matter and nitrogen oxides (Braun et al., 2021; Ni, Shi, & Qu, 2020). Finally, in rodents exposed to smoke the disease takes long time to develop, similar to the progression seen in human patients.

PH is also observed in the elastase model of emphysema, but pathological mechanisms resulting in elevated PAP in this model probably have a different underlying cause (Icochea, Cooper, & Kuhn, 1982; Luthje et al., 2009; Oliveira et al., 2016).

1.2.2.4. Animal model of hypoxia-induced PH

Exposure of rodents to 50% reduced oxygen concentration (referred to sea level) for more than 2 weeks is a common, well-accepted experimental model for hypoxia-induced PH. Pathological changes seen in this model include elevation of PAP, pulmonary vascular remodeling and right ventricular hypertrophy (Tuder et al., 2007). The remodeling induced by hypoxia in most species (including rodents) is less severe than in PAH and involves *de novo* muscularization of distal arteries, as well as thickening of medial and adventitial layer. An influx of inflammatory cells into hypoxic lungs is less pronounced than in other forms of PH (Gassmann et al., 2020; Tuder et al., 2007).

Described hypoxia-induced changes are mild and gradually fully reversible after returning to a normoxic environment; nevertheless, the model has provided valuable insights into hypoxia-sensing mechanisms, involved in other, more severe forms of human disease (Tuder et al., 2007; Weisel et al., 2014).

1.3. The role of inflammation in pulmonary vascular remodeling

The association between inflammation and pulmonary vascular remodeling is well exemplified by the fact that many conditions that are autoimmune, inflammatory, or infectious (e.g. systemic sclerosis or lupus erythematosus, human immunodeficiency virus [HIV] or herpes infection, schistosomiasis) are recognized as causes of PAH (Kuebler, Bonnet, & Tabuchi, 2018). Similarly, the often employed monocrotaline animal model is based on a direct inflammatory insult and the chronic hypoxia model has an important inflammatory component (Price et al., 2012). However, evidence of the functional role of inflammatory cells and their mediators in pulmonary vascular remodeling goes far beyond these arguments.

Abnormally elevated circulating levels and/or pulmonary expression of numerous cytokines, chemokines and other inflammatory cell mediators in PAH patients have been reported (Pullamsetti et al., 2011). These include IL-1α and β, IL-4, IL-6, IL-8, IL-10, IL-12p70, IL-13, IL-17, IL-21, CX3CL1, CCL2, CCL5 and TNF-α. Furthermore, several types of autoantibodies, C-reactive protein (CRP) and components of the complement system C3 and C4 are increased in the circulation of idiopathic PAH (IPAH) patients. Some of these signaling molecules are biomarkers or the predictors of the clinical outcome in patients, while others are known to directly control matrix

deposition or proliferation, migration and differentiation of pulmonary vascular cells (Price et al., 2012; Pullamsetti et al., 2011; Rabinovitch et al., 2014).

Going beyond, in lungs of PAH patients and animal PH models, the perivascular space and plexiform lesions of remodeled vessels are characterized by infiltrates of inflammatory cells comprising of macrophages, mast cells, T and B lymphocytes and dendritic cells (DC) (Rabinovitch et al., 2014; Savai et al., 2012; Tuder et al., 1994). Reported lymphoid neogenesis, together with changes in activation, phenotype, metabolism and ratios of these cells in PAH pathology contribute to a complex and yet insufficiently understood picture of the inflammatory component of the disease (Rabinovitch et al., 2014).

1.3.1. Macrophages and pulmonary vascular remodeling

$CD68^+$ macrophages are an important constituent of perivascular infiltrates and plexiform lesions in experimental and clinical PAH. Inactivation or depletion of these cells prevents PH in several animal models, including hypoxia-induced PH and portopulmonary hypertension (Rabinovitch et al., 2014). The majority of the cytokines and chemokines deregulated in PAH is secreted by and/or acting on macrophages. Going beyond, recent reports emphasize the importance of a distinct macrophage phenotype in PH.

Traditionally, macrophage activation has been described as a dichotomous event, where “classically activated” or “M1 macrophage phenotype” was elicited by LPS and interferon (IFN)-γ and characterized by the production of IL-6 and a large amount of NO needed for the killing of pathogens. On the other hand, an “alternative activation”, or “M2 macrophage phenotype” resulted from exposure to IL-4 or IL-13. These macrophages expressed arginase and produced IL-10, IL-13, and numerous growth factors to promote wound healing (Mills et al., 2000; Shapouri-Moghaddam et al., 2018). This oversimplified view on macrophage activation has evolved to the point where two described phenotypes are considered as two extremes of a whole spectrum, existing in *in vitro* conditions rather than in living organisms. In other words, the phenotype of macrophages in tissue is probably dynamic and unique for the given situation, constantly modulated and fine-tuned by existing micro-environmental signals and metabolic conditions (Nahrendorf & Swirski, 2016). However, since the M1/M2

paradigm provides a useful framework, the nomenclature persists in the recent literature and will be used here with this word of caution.

In the context of pulmonary vascular remodeling, growing evidence suggests that IL-4 and IL-13 (Th2 cytokines, associated with alternative activation of macrophages) orchestrate pathological changes in scleroderma-associated PH (Angelini et al., 2009; Christmann et al., 2011) and in TGF-β mediated, *Schistosoma mansoni*-induced PAH (Graham et al., 2013; Kumar et al., 2015).

On the other hand, studies in animal models and IPAH patients yielded a concept of fibroblast-activated, pro-inflammatory and pro-remodeling macrophages (El Kasmi et al., 2014; Stenmark, Tuder, & El Kasmi, 2015). These macrophages acquire their intermediate phenotype in constant cross-communication with adventitial fibroblasts through secreted cytokines, chemokines and glycolytic metabolites, among which IL-6 and lactate play key roles. Intriguingly, IL-6 has been recognized recently as an inducer of M2-polarization in macrophages (Braune et al., 2017), also in concert with CCL2 (Roca et al., 2009) and IL-21 (Hashimoto-Kataoka et al., 2015).

Another group reported that early macrophage recruitment and M2 polarization were necessary for the development of hypoxia-induced PH in mice (Vergadi et al., 2011). In line with this finding, CX3CR1 deficiency in mice resulted in protection against hypoxia-induced PH, concomitant with the change from M2 to M1 polarization, whereby the latter macrophage phenotype had reduced ability to induce PASMC proliferation *in vitro* (Amsellem et al., 2017). Following this, a recent study employing two animal models as well as cells and biopsies from IPAH patients confirmed the pronounced ability of M2 macrophages to stimulate proliferation of PASMC. Of note, CCR2 and CCR5 were required for cross-communication between these two cell types and pathological proliferation of PASMC (Abid et al., 2019).

Overall, the importance of macrophage polarization in the pathology of PH is a rather novel concept, but a growing body of evidence suggests that modulation of macrophage phenotype and their communication with vascular cells might be a viable strategy for the treatment of this disease.

1.3.2. Inflammation in COPD-associated PH

Although the pivotal role of inflammatory cells and their mediators in other forms of PH is well substantiated by experimental evidence in rodent models and patients, only few

studies support the role of inflammation in COPD–PH. It has been found that systemic levels of inflammatory mediators such as TNF-α, CRP (Joppa et al., 2006), IL-6 (Eddahibi et al., 2006) and IL-17 (Wang et al., 2019) are increased in COPD patients with PH (Figure 1). In addition, a study from Peinado and colleagues reported the correlation between the number of inflammatory cells in the adventitia and the degree of pulmonary vascular remodeling (Peinado et al., 1999). In animals, a few substances known to affect inflammatory cell function, such as MPO inhibitors (Churg et al., 2012), inhibitors of renin-angiotensin signaling (Han et al., 2010) and statins (J. H. Lee et al., 2005; Wright et al., 2011), were able to prevent or reverse smoke-induced pulmonary vascular remodeling.

1.4. Inducible nitric oxide synthase

iNOS belongs to a three-member family of enzymes called nitric oxide synthases. All three NOS isoforms catalyze the conversion of L-arginine, NADPH and molecular oxygen to L-citrulline, $NADP^+$ and NO, but they differ greatly in the expression pattern and regulation of their activity (M. Lee et al., 2017).

Endothelial NOS (eNOS) and neuronal NOS (nNOS) are constitutively expressed enzymes that produce nanomolar amounts of NO over short periods, primarily for the regulation of vascular tone (eNOS) and neurotransmission (nNOS). The activity of these two enzymes is dependent on increases in cytosolic Ca^{2+}, which allows their rapid and meticulous control. On the other hand, iNOS is usually expressed only upon stimulation of the cell with cytokines or other signals, but it produces micromolar amounts of NO over longer periods in a calcium-independent manner (Alderton, Cooper, & Knowles, 2001; Cinelli et al., 2020). These differences in function and regulation are attributed to specific features in the architecture of each enzyme, but the overall domain organization and cofactor binding is shared among the members of the NOS family (Cinelli et al., 2020).

1.4.1. Structure of the NOS dimer

NOS monomer consists of the N-terminal oxygenase domain and C-terminal reductase domain, separated by calmodulin (CaM) binding site. The N-terminal oxidase domain binds the cofactors heme and tetrahydrobiopterin (BH4) and contains binding pockets for the substrates L-arginine and oxygen. The C-terminal domain contains the binding sites for the cofactors flavin adenine dinucleotide (FAD) and flavin mononucleotide

(FMN). Additionally, all NOS enzymes have catalytically inactive zinc at the dimer interface, required for dimerization (Alderton et al., 2001; Cinelli et al., 2020).

Upon CaM binding (and calcium sensitization), the enzyme goes through a conformational change that brings the FMN subdomain of the first monomer into proximity of the heme bound to the oxygenase domain of the second monomer, thus allowing the electron transfer between these cofactors. (Cinelli et al., 2020). The driving force for the NO production is NADPH, and the catalytic cycle involves an elaborate electron transport chain depicted in Figure 2.

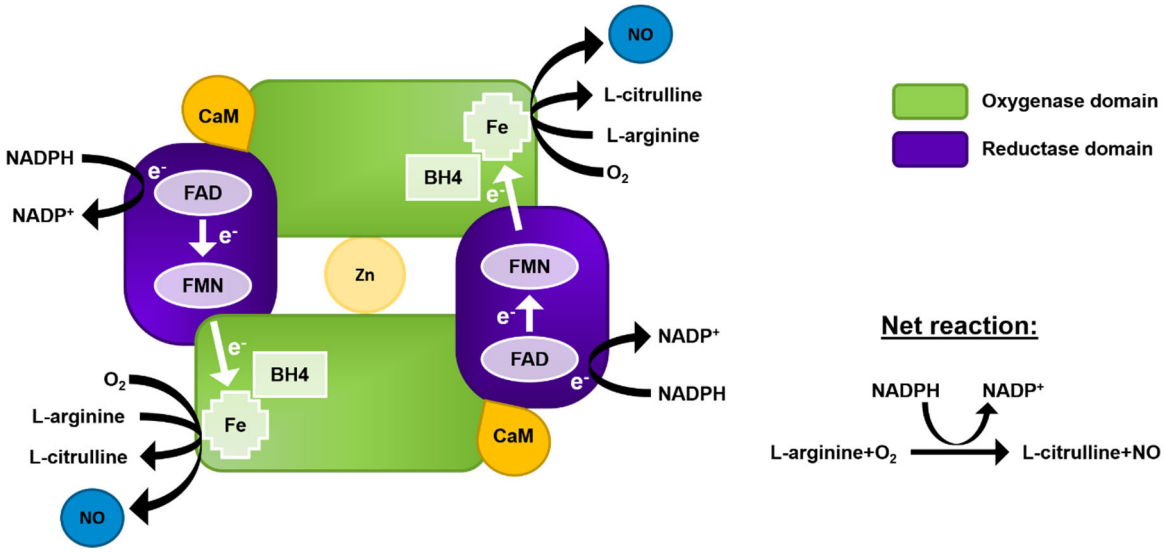

Figure 2: Schematic illustration of the structure of nitric oxide synthases and mechanism of NO synthesis.

CaM: calmodulin; BH4: tetrahydrobiopterin. FAD: flavin adenine dinucleotide; FMN: flavin mononucleotide; NADPH: nicotinamide adenine dinucleotide phosphate.

1.4.2. Regulation of iNOS expression and function

iNOS expression is induced by various stimuli and regulated on the transcriptional, translational and posttranslational levels, in a cell- and species-dependent manner.

The promotor of the *iNOS* gene differs extensively between mouse and human, but in both cases contains binding sites for transcription factors that respond to inflammatory mediators or other stressful stimuli and activate transcription of the *iNOS* in a cooperative manner (M. Lee et al., 2017). For example, promotor of human *iNOS* contains multiple binding sites for nuclear factor kappa-light-chain-enhancer of activated B-cells (NFκB), a transcription factor activated by IL-1β and TNF-α, while

effects of IFN-γ stimulation are mediated by the Janus kinase (JAK)-signal transducer and activator of transcription (STAT)-1 pathway. Additionally, the *iNOS* promotor harbors binding sites for activator protein (AP)-1, a transcription factor downstream of MAP kinases, which are activated by cytokines, growth factors and stress. Another transcription factor critical for human *iNOS* induction is the CCAAT-enhancer-binding protein (C/EBP). Other transcription factors that can potentially induce *iNOS* expression include cyclic adenosine monophosphate-response element-binding protein (CREB), GATA, hypoxia-inducible factor (HIF)-1, Krüppel-like factor (KLF)-6, nuclear factor of activated T-cells (NF-AT), octamer transcription factor (OCT)-1, poly(ADP-ribose) polymerase (PARP)-1 and p53 (M. Lee et al., 2017).

iNOS expression can also be regulated at the translational level. Here, several cytokines stimulate iNOS expression by modifying the availability of RNA-binding proteins which regulate the stability of *iNOS* mRNA. Additionally, iNOS expression is regulated by miRNA-939, and upregulation of this miRNA by cytokines forms one of the negative feedback loops that control the expression of iNOS (M. Lee et al., 2017).

Perhaps the most interesting form of iNOS regulation on the posttranslational level is inhibition of this enzyme by its own product, NO, in a dose-dependent manner. In human mesangial cells, NO regulates iNOS expression biphasically, augmenting mRNA and protein levels at early time points, and inhibiting its expression at later times (Perez-Sala et al., 2001). The major mechanism of iNOS auto-inactivation is S-nitrosylation of the zinc-tetrathiolate cluster, but it can also occur through the direct binding of iNOS to the heme cofactor (M. Lee et al., 2017).

Finally, iNOS can be regulated by the bioavailability of the substrate. The enzyme arginase competes with iNOS for the existing L-arginine pool and thus opposes the production of NO (Cinelli et al., 2020). These two enzymes are often reciprocally expressed in inflammatory responses.

1.4.3. Nitric oxide signaling

The first discovered mechanism through which NO regulates protein activity relies on the direct binding to heme groups or metal cofactors in metalloproteins and serves for the regulation of sGC, cytochrome P450, iNOS, ribonucleotide reductase and others (M. Lee et al., 2017).

In cells such as classically activated macrophages, which produce both NO and superoxide (O_2^-), these molecules often react to produce the oxidizing agent peroxynitrite ($ONOO^-$), which can then react with tyrosine residues of proteins to form 3-nitrotyrosine (M. Lee et al., 2017). Like other reversible posttranslational modifications, nitration of proteins may result in the activation and inactivation of enzymes. NO and peroxynitrite can also perform S-nitrosylation of proteins and by doing so regulate their activity, turnover and folding (M. Lee et al., 2017; Sun, Steenbergen, & Murphy, 2006).

1.4.4. The role of iNOS in inflammatory responses

All genuine immune cells, as well as some other cell types involved in immune response, are able to produce NO. Among others, those are dendritic cells, natural killer (NK) cells, mast cells and phagocytic cells including monocytes, macrophages, microglia, Kupffer cells, eosinophils, and neutrophils, as well as endothelial, epithelial, vascular smooth muscle cells, fibroblasts, keratinocytes, chondrocytes and hepatocytes (Bogdan, 2001).

Large amounts of iNOS-derived NO, generated by macrophages in response to bacterial infections, along with S-nitrosothiols and peroxynitrite, exert important antimicrobial effects primarily via the toxicity to bacterial cells. However, the prominent role of iNOS in the immune system goes beyond its antimicrobial activities and involves effects on the acquisition or modulation of phenotypes and capabilities of the expressing cells, but also on the function and composition of neighboring immune cells (Bogdan, 2001, 2015).

This is especially true for myeloid cell lineage, where iNOS can modulate phagocytosis, expression of major histocompatibility complex (MHC) II, co-stimulatory molecules and cytokines, and can even regulate differentiation, autophagy, proliferation and apoptosis. Additionally, iNOS derived from myeloid cells was shown to regulate T cell proliferation and differentiation into T cell subtypes, as well as their diapedesis into the tissue in a dose-dependent manner (Bogdan, 2015; Sektioglu et al., 2016).

Importantly, iNOS is expressed in T cells and B cells, where it produces small doses of NO to support the survival and differentiation of these cells. Similarly, iNOS-derived NO appears to be required for the functional maturation of NK cells and their responsiveness to IL-12 (Bogdan, 2015; Bogdan, Rollinghoff, & Diefenbach, 2000).

Taken together, these data demonstrate the dramatic functional versatility of iNOS and the existence of complex and still insufficiently investigated mechanisms by which it fine-tunes the cellular phenotypes and orchestrates immune response.

1.5. iNOS in smoke-induced PH and emphysema

Dysregulation of iNOS is implicated in numerous human pathologies, including systemic lupus erythematosus, rheumatoid arthritis, psoriasis and inflammatory bowel disease (M. Lee et al., 2017). Multiple studies suggest that iNOS is also upregulated in the lungs of COPD patients, and that the amount of 3-nitrotyrosine present in the lung inversely correlates with lung function parameters (Brindicci et al., 2009; Ichinose et al., 2000; Maestrelli et al., 2003).

Importantly, a previous study from the laboratory in which the current work was done was the first one to demonstrate a causal link and to identify iNOS as the key player in the pathogenesis of smoke-induced PH and emphysema in mice (Seimetz et al., 2011). iNOS was upregulated in the lungs of smoke-exposed mice, COPD patients and smokers who had not developed COPD, and this upregulation was mirrored by an increased content of nitrotyrosine. Mice lacking iNOS were protected against smoke-induced PH and emphysema. Moreover, treatment with iNOS inhibitor N6-(1-Iminoethyl)-L-lysine (L-NIL) not only prevented pulmonary vascular remodeling, RV hypertrophy and alveolar destruction, but completely reversed fully established disease as well. Experiments with chimeric mice further revealed that smoke-induced PH and emphysema development are driven by iNOS expression in different cell types and therefore can occur independently. In this regard, the group showed that mice lacking iNOS in bone marrow-derived cells were protected against PH, while emphysema development was not affected by iNOS deletion in these cells (Figure 3).

However, it remained unclear which bone marrow-derived cell type drives pulmonary vascular remodeling and what the respective mechanism is. On the one hand, studies using chimeric mice in the past (Fathke et al., 2004; Ishii et al., 2005) have reported an important contribution of non-hematopoietic and/or non-inflammatory cells (mesenchymal stem cells, fibrocytes, endothelial progenitor cells). In line with that, one could speculate that the pathogenic mechanism of COPD-PH relies on the derivation of the portion of pulmonary vascular cells (including smooth muscle cells) from bone-marrow cells. On the other hand, myeloid cell types have previously been implicated

in other forms of PH and chronic inflammation is an important feature of COPD pathology, as described in chapter 1.1.2.3.

Against the background that

1) iNOS is highly expressed and plays important roles in some cells belonging to the myeloid lineage (such as macrophages, chapter 1.4.4.),
2) myeloid cell types are elevated in the pulmonary vasculature upon tobacco smoke exposure (De Cunto et al., 2016; Kosanovic et al., 2014), and
3) they are known contributors to pulmonary vascular remodeling in other forms of PH, (as already described in chapter 1.3.1.)

I hypothesized that pathological signaling leading to smoke-induced PH is triggered by elevated iNOS expression in myeloid cells and that a similar process as in mice may occur in humans.

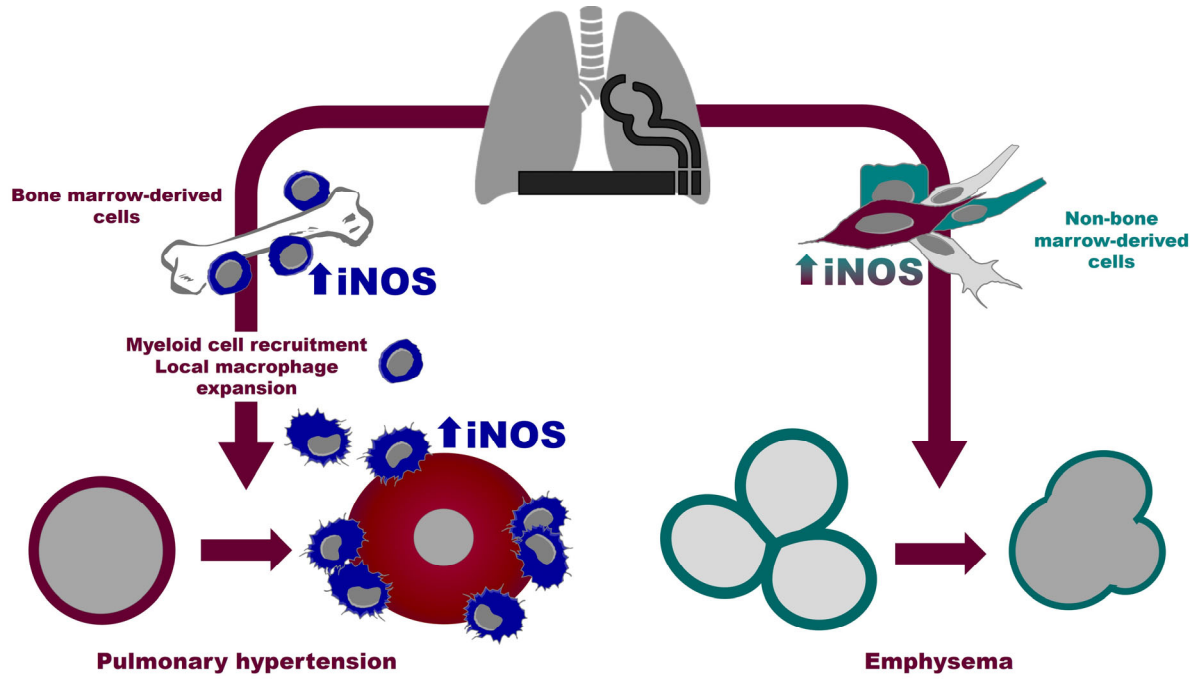

Figure 3: Current understanding of the role of iNOS in COPD-PH and hypothesis of the current thesis.

iNOS expression in bone marrow-derived cells drives smoke-induced vascular remodeling, while upregulation of this enzyme in non-bone marrow-derived lung cells plays an important role in the development of emphysema. The hypothesis of the current thesis proposes that elevation of iNOS expression in myeloid cells, presumably macrophages, plays a key pathogenic role in smoke-induced PH. iNOS: inducible nitric oxide synthase.

1.6. Aims of the study

In line with the above-mentioned hypothesis, the general aims of my study are:

1) to investigate *in vivo* effects of chronic smoke exposure on the pathogenesis of emphysema and PH in myeloid cell-specific iNOS knockout mice,
2) to investigate the effect of myeloid cell-specific iNOS knockout on the development of hypoxia-induced PH in mice
3) to characterize the potential alteration of inflammatory cell profiles in myeloid cell-specific iNOS knockout mice upon exposure to smoke,
4) to analyze the functional role of bone marrow-derived macrophages in the proliferation, migration and apoptosis of PASMC *in vitro*, as the potential underlying mechanism for PH development, and
5) to reveal whether the findings derived from the animal model apply to the situation in COPD patients.

2. Materials and Methods

2.1. Materials

2.1.1. Equipment

Automated microtome (Leica RM 2165)	*Leica Microsystems, Wetzlar, Germany*
Balance for substances (Mettler Toledo PB303 Delta Range®)	*Mettler Toledo, Greifensee, Switzerland*
Blood analyzer (Rapidlab™ 348)	*Bayer Healthcare, Fernwald, Germany*
Cell incubator HERAcell 150	*Thermo Scientific, Dreieich, Germany*
Centrifuge Hematocrit 210	*Hettich, Tuttlingen, Germany*
Centrifuge Mikro 200R	*Hettich, Tuttlingen, Germany*
ChemiDocTM Touch Imaging System	*Biorad, Feldkirchen, Germany*
ChemiDocTM XRS+	*Biorad, Feldkirchen, Germany*
Cigarette smoke generator	*Burghart, Wedel, Germany*
Computer tomograph	
Confocal microscope SP8	*Leica Microsystems, Wetzlar, Germany*
Cooling Plate EG 1150C	*Leica Microsystems, Wetzlar, Germany*
Culture Hood	*Heraeus GmbH, Hanau, Germany*
Flattening bath for paraffin sections (Leica HI 1210)	*Leica Microsystems, Wetzlar, Germany*
FlexiVent mechanical ventilator and data-acquisition system	*SCIREQ, Montreal, Canada*
Fluorescence molecular tomography (FMT) imaging system	*VisEn Medical, Bedford, USA*
Fluorescence-activated cell sorting (FACS) Aria III cell sorter	*BD Biosciences, San Jose, USA*
gentleMACS™ Dissociator	*MiltenyiBiotec, Bergisch Gladbach, Germany*
Heating Block	*VWR, Bruchsal, Germany*
Heating chamber	*Memmert, Schwabach, Germany*

Heating Plate Hi 1220	*Leica Microsystems, Wetzlar, Germany*
Hotplate/Stirrer (371)	*VWR, Bruchsal, Germany*
Hypoxic chamber	*BioSpherix, Parish, USA*
Ice flake machine (Icematic F100 Compact)	*Castelmac SPA, Castelfranco, Italy*
IncuCyte ZOOM	*Essen BioScience, Michigan, USA*
Jess Simple Western™ platform	*ProteinSimple, San Jose, CA, USA*
Laser microdissection system (LMD6000)	*Leica Microsystems, Wetzlar, Germany*
Light microscope (DMLA)	*Leica Microsystems, Wetzlar, Germany*
Low Voltage Power Supplies Power pack P25T	*Biometra, Analytic Jena, Jena, Germany*
LSR II/Fortessa flow cytometer	*BD Biosciences, San Jose, USA*
Microplate reader Infinite M200	*Tecan, Männedorf, Switzerland*
Mini-PROTEAN® electrophoresis cells	*Biorad, Feldkirchen, Germany*
MiniVent type 845 Hugo Sachs	*Elektronik, March-Hugstetten, Germany*
Multimode microplate reader Infinite 200 PRO	*Tecan, Männedorf, Switzerland*
Multimode microplate reader Spark®	*Tecan, Männedorf, Switzerland*
NanoDrop (ND-1000)	*Kisker-Biotech, Steinfurt, Germany*
Paraffin cooling station Leica EG 1150C	*Leica, Wetzlar, Germany*
Paraffin embedding station Leica EG 1140H	*Leica, Wetzlar, Germany*
PCR Plate sealer PX1	*Biorad, Feldkirchen, Germany*
pH meter-766 Calimatic	*Knick, Berlin, Germany*
PowerLab system	*ADInstruments GmbH, Spechbach, Germany*
Precellys® 24 bead beating Tissue Homogenizer	*Thermo Fischer, Massachusetts, USA*
QIAxcel Advanced System	*Qiagen, Hilden, Germany*

Quantum GX µCT scanner	*PerkinElmer, Inc, Waltham, USA*
Real-Time polymerase chain reaction (PCR) Detection System (CFX Connect™)	*Biorad, Feldkirchen, Germany*
Rectal thermometer	*Indus Instruments, Houston, USA*
Roller mixer LLG-uniROLLER 10	*Lab Logistics Group GmbH, Meckenheim, Germany*
Rotary microtome cryostat (CM1520)	*Leica Microsystems, Wetzlar, Germany*
Shaking table Swip	*Edmund Bühler GmbH, Bodelshausen, Germany*
SPR-671 Mikro-Tip® mouse pressure catheter, REF 8406719	*Millar Instruments, Houston, USA*
Table Centrifuge Mikro 200R	*Hettich, Tuttlingen, Germany*
Thermocycler, T3000	*Biometra, Analytic Jena, Jena, Germany*
Thermocycler, Tpersonal	*Biometra, Analytic Jena, Jena, Germany*
Thermoregulation plate TCAT-2LV controller	*Physitemp Instruments, Inc., Clifton, USA*
Trans-Blot® SD Semi-dry Cell	*Biorad, Feldkirchen, Germany*
Trans-Blot® Turbo Semi-dry Cell	*Biorad, Feldkirchen, Germany*
Ultrapure Milli-Q®	*Millipore, Schwalbach, Germany*
Vevo® 2100 high-resolution Imaging System	*FUJIFILM VisualSonics Inc, Toronto, Canada*
Vortexer MS1 Minishaker	*IKA GmbH, Staufen, Germany*
Water bath	*Memmert, Schwabach, Germany*

2.1.2. Substances, chemicals and consumables

0,9% NaCl-Solution (3570160)	*B.Braun, Melsungen, Germany*
20x Tris-buffered saline (TBS, ZUC052-500)	*Zytomed Systems, Berlin, Germany*
3R4F cigarettes	*Kentucky Tobacco Research & Development Center, Lexington, KY, USA*
Acetone (32201)	*Merck KGaA, Darmstadt, Germany*
Agarose (11406)	*SERVA Electrophoresis GmbH, Heidelberg, Germany*
Agarose, low-gelling temperature, suitable for cell culture (A9045)	*Merck KGaA, Darmstadt, Germany*
AlamarBlue cell viability reagent (A50101)	*Thermo Fisher Scientific Inc. Waltham, USA*
Alkaline Phosphatase (AP) Polymer System (POLAP-100)	*Zytomed Systems, Berlin, Germany*
Amersham ECL Plus Western blotting Detections System (29018903)	*GE Healthcare, Munich, Germany*
Ammonium persulfate (APS, A3678)	*Promega, Mannheim, Germany*
Ampuwa® water (3478.1)	*Carl Roth, Karlsruhe, Germany*
Annexin Vivo 750 (NEV11053)	*Perkin Elmer, Waltham, USA)*
Antibody Diluent (ZUC025-100)	*Zytomed Systems, Berlin, Germany*
Apoptosis kinetic assay (ab129817)	*Abcam, Cambridge, UK*
Automatic pipettes (100-1000 µl, 10-100 µl, 1-10 µl)	*Eppendorf AG, Hamburg, Germany*
Background Punisher (BP974)	*Biocare Medical, Pacheco, USA*
Black thread no.16	*Coats GmbH, Kenzingen, Germany*
Bovine Serum Albumin (BSA, A7030)	*Merck KGaA, Darmstadt, Germany*
Bradford assay (5000114)	*Biorad, Feldkirchen, Germany*
Cannulas (16G, 18 G)	*BD Microlane, Franklin Lakes, USA*
CAT Hematoxylin (CATHE-M)	*Biocare Medical, Pacheco, USA*

Cell culture dishes (35er, 60er)	*Sarstedt, Nümbrecht, Germany*
Cell culture plates (6, 12, 24, 96 well)	*Greiner bio-one, Frickenhausen, Germany*
Cell lysis buffer (9803S)	*Cell Signaling Technology, Cambridge, UK*
Cell proliferation ELISA, Bromodeoxyuridine (BrdU, colorimetric, 11 647 229 001)	*Roche, Mannheim, Germany*
Cell scrapers	*Greiner bio-one, Frickenhausen, Germany*
Cell strainers (40 µl, 100 µm)	*Greiner bio-one, Frickenhausen, Germany*
Cellulose swabs Pur-Zellin®	*Paul Hartmann AG, Heidenheim, Germany*
Collagenase (C9891)	*Merck KGaA, Darmstadt, Germany*
Collagenase from Clostridium histolyticum (C5138)	*Merck KGaA, Darmstadt, Germany*
Combtips advanced (5 ml, 10 ml, 25 ml)	*Eppendorf AG, Hamburg, Germany*
Comp-Beads	*BD Biosciences, San Jose, USA*
cOmplete™ Mini EDTA-free Protease-Inhibitor-Cocktail	*Roche, Basel, Switzerland*
Conical centrifuge tubes (15 ml, 50 ml)	*Greiner bio-one, Frickenhausen, Germany*
Coverslips 24x36 mm	*Menzel GmbH&Co.KG, Braunschweig, Germany*
Cryo Tubes	*Sarstedt, Nümbrecht, Germany*
Culture-Inserts 2 Well for self-insertion	*Ibidi, Gräfelfing, Germany*
Cytometer Setup and Tracking beads	*BD Biosciences, San Jose, USA*
DAB Peroxidase Substrate Kit (SK-4100)	*Vector Laboratories, Burlingame, USA*

Dimethylsulfoxide (DMSO, D4540)	*Merck KGaA, Darmstadt, Germany*
Disodiumhydrogenphosphate dihydrate (Na_2HPO4,106580)	*Merck, Darmstadt, Germany*
Distilled Water (3478.1)	*Carl Roth, Karlsruhe, Germany*
Distilled Water (dH_2O, DNAse-/RNAse-free, 10977023)	*Invitrogen™, Thermo Fisher Scientific Inc. Waltham, USA*
DIVA Decloaker (DV2004MX)	*Biocare Medical, Pacheco, USA*
DMEM-F12 (11320-033)	*GIBCO™, Thermo Fisher Scientific Inc. Waltham, USA*
DNAse (04536282001)	*Roche, Mannheim, Germany*
Dulbecco's Modified Eagle Medium (DMEM, 31885023)	*GIBCO™, Thermo Fisher Scientific Inc. Waltham, USA*
Electronic animal identification reusable implanter needles (mini)	*Planet-ID, Essen, Germany*
Embedding cassettes	*Leica Microsystems, Wetzlar, Germany*
Enzyme-free cell dissociation buffer (13151014)	*GIBCO™, Thermo Fisher Scientific Inc. Waltham, USA*
Eosin Y, alcoholic (6766007)	*Thermo Fisher Scientific Inc. Waltham, USA*
Ethanol (pure) for molecular biology (108543)	*Merck, Darmstadt, Germany*
Ethanol 70% (ETO-5000-70-1)	*SAV Liquid Production GmbH, Flintsbach a. Inn, Germany*
Ethanol 96% and 100% (27695 and 27694)	*Otto Fischar GmbH, Saarbrücken, Germany*
Ethylenediaminetetraacetic acid (EDTA, 8043)	*Carl Roth, Karlsruhe, Germany*
FcR blocking reagent (130-092-575)	*MiltenyiBiotec, Bergisch Gladbach, Germany*
Fetal bovine serum (FBS, F0804)	*Merck, Darmstadt, Germany*
Filtered tips (10 µl, 100 µl, 1000 µl)	*Nerbe plus, Winsen, Germany*

Filtopur S (0.2 µm)	*Sarstedt, Nümbrecht, Germany*
Fluoro Care Anti-Fade Mountant (FP 001 G10)	*Biocare Medical, Pacheco, USA*
Formaldehyde (3,5 – 3,7%, stabilized with methanol, 27244)	*Otto Fischar GmbH, Saarbrücken, Germany*
GeneRuler™ 100 bp DNA Ladder (SM0313)	*Thermo Fisher Scientific Inc. Waltham, USA*
GentleMACS C Tubes	*MiltenyiBiotec, Bergisch Gladbach, Germany*
Glass bottles, beakers, cylinders	*Duran, Wertheim, Germany*
Glass bottles, beakers, cylinders	*VWR, Bruchsal, Germany*
Glass bottles, beakers, cylinders	*Fisher Scientific, Schwerte, Germany*
Glass polyethylene naphthalate membrane slides	*Leica, Wetzlar, Germany*
Gloves (Nitra-Tex®)	*Ansell Ltd., Tamworth, UK*
Glycine (A1067)	*AppliChem GmbH, Darmstadt, Germany*
Griess reagent system (G2930)	*Promega, Mannheim, Germany*
Hand towels	*Essity Hygiene and Health, Germany*
Hank's Balanced Salt Solution (HBSS, 14025050)	*GIBCO™, Thermo Fisher Scientific Inc. Waltham, USA*
Heparin (Heparin-Natrium 5000 I.E.)	*Ratiopharm GmbH, Ulm, Germany*
HistoGreen HRP substrate kit (E109)	*LINARIS Biologische Produkte GmbH, Dossenheim, Germany*
Histological glass slides 25x75x1 mm (SuperFrost UltraPlus®)	*R. Langenbrinck, Emmendingen, Germany*
Hydrochloride (HCl, 37%, 4625.1)	*Carl Roth, Karlsruhe, Germany*
Hydrogen-peroxide (30%, 107209)	*Merck, Darmstadt, Germany*
ImmPRESS Anti-Rabbit Ig Polymer Detection-Kit (LS-J1066-15)	*Vector Laboratories, Burlingame, USA*
Iron (II, III)-oxide, powder, <5 micron (31006-9)	*Merck KGaA, Darmstadt, Germany*

iScript complementary DNA (cDNA) Synthesis Kit (1708890)	*Biorad, Feldkirchen, Germany*
Isoflurane (HDG9623)	*Baxter Deutschland GmbH, Unterschleissheim, Germany*
Isopropyl-alcohol (99.8%, 190764)	*Merck KGaA, Darmstadt, Germany*
iTaq Universal SYBR® Green Supermix (1725124)	*Biorad, Feldkirchen, Germany*
Ketamine (Ursotamin)	*Serumwerk, Bernburg, Germany*
Laemly Sample Buffer (4x, 1610747)	*Biorad, Feldkirchen, Germany*
L-Glutamine (P04-80100)	*GIBCO™, Thermo Fisher Scientific Inc. Waltham, USA*
LPS from E.coli (L2630)	*Merck KGaA, Darmstadt, Germany*
lumox® multiwell, 96-well	*Sarstedt, Nümbrecht, Germany*
MACH2 double Stain Polymer 1 (MRCT523)	*Biocare Medical, Pacheco, USA*
Medical adhesive bands (2.5 cm/9.2 m)	*3M Health Care, St.Paul, USA*
Medium 199 (M199, 31150022)	*GIBCO™, Thermo Fisher Scientific Inc. Waltham, USA*
Methanol (99.8%, 32213)	*Merck KGaA, Darmstadt, Germany*
Methyl green (H-3402)	*Vector Laboratories, Burlingame, USA*
Micro tubes (0.5 ml, 1.5 ml, 2.0 ml)	*Sarstedt, Nümbrecht, Germany*
Microtome blades (MX35 Premier)	*Thermo Fisher Scientific Inc. Waltham, USA*
Microtome blades (MX35 Premier)	*Thermo Fisher Scientific Inc. Waltham, USA*
Mounting medium (Pertex®, 41-4012-00)	*Medite GmbH, Burgdorf, Germany*
Mouse IL-4 Quantikine ELISA Kit (M4000B)	*R&D Systems, Abingdon, UK*

Mouse/Rat/Porcine/Canine TGF-beta 1 Quantikine enzyme-linked immunosorbent assay (ELISA) Kit (MB100B)	*R&D Systems, Abingdon, UK*
Mouse-on-mouse horseradish peroxidase (HRP)-Polymer Kit (MM620)	*Biocare Medical, Pacheco, USA*
Multipette E3x	*Eppendorf AG, Hamburg, Germany*
MultiplateTM PCR Plate 96-Well, clear	*Biorad, Feldkirchen, Germany*
N6-(1-Iminoethyl)-L-lysine (L-NIL, 80310)	*Cayman Chemical, Ann Arbor, USA*
Needles (BD Microlance 3®) (18 G /1.2 mm x 40 mm, 20 G /0.9 mm x 40 mm, 26G /0.45 mm x 13 mm)	*Becton Dickinson GmbH, Heidelberg, Germany*
Neubauer counting chamber	*Laboroptik GmbH, Bad Homburg, Germany*
Non-tissue culture treated Petri dishes	*Sarstedt, Nümbrecht, Germany*
Non-tissue culture treated Petri dishes	*Greiner bio-one, Frickenhausen, Germany*
Normocin (ant-nr-1)	*InvivoGen, Toulouse, France*
Nuclear Fast Red (Kernechtrot Aluminiumsulfat, 2E-012)	*Waldeck GmbH & Co.KG, Münster, Germany*
Parafilm®	*Merck KGaA, Darmstadt, Germany*
Paraformaldehyde (PFA, sc-281692)	*Santa Cruz Biotechnology, Inc. Dallas, USA*
Paraplast Plus® for tissue embedding (P3683)	*Merck KGaA, Darmstadt, Germany*
Penicillin/Streptomycin (15070-063)	*GIBCO™, Thermo Fisher Scientific Inc. Waltham, USA*
Phenylmethansulfonylfluorid (PMSF, P7626)	*Merck KGaA, Darmstadt, Germany*

Phenylmethylsulfonyl Fluoride (PVDF)-membrane	*Pall Corporation, Dreieich, Germany*
Phosphate buffered saline (D-PBS, P04-53500)	*PAN Biotech, Aidenbach, Germany*
Polystyrene round-bottom tubes with cell strainer cap (5 ml)	*Greiner bio-one, Frickenhausen, Germany*
Potassium chloride (KCl, 6781.1)	*Merck, Darmstadt, Germany*
Potassiumdihydrogenphosphate (KH_2PO_4, 104873)	*Merck, Darmstadt, Germany*
Povidone-iodine solution (Braunoderm®)	*B.Braun Melsungen AG, Melsungen, Germany*
Precision Plus Protein Dual Color Standards (1610374)	*Biorad, Feldkirchen, Germany*
Primers (listed below)	*Metabion, Planegg, Germany*
Proteinase K Novocastra™ (RE7160-K)	*Leica, Wetzlar, Germany*
Proteome Profiler Mouse XL Cytokine Array (ARY028)	*R&D Systems, Abingdon, UK*
Recombinant murine IFN-γ (315-05)	*PeproTech, Hamburg, Germany*
Recombinant murine IL-4 (214-14)	*PeproTech, Hamburg, Germany*
Recombinant murine macrophage colony-stimulating factor (M-CSF, 315-02)	*PeproTech, Hamburg, Germany*
Red blood cell (RBC) lysis buffer (BD Pharm Lyse™, 555899)	*BD Biosciences, Heidelberg, Germany*
Resorcin-Fuchsin (2E-030)	*Waldeck GmbH & Co.KG, Münster, Germany*
RNeasy®Mini Kit (74106)	*Qiagen, Hilden, Germany*
Rodent Decloaker,10X (RD913)	*Biocare Medical, Pacheco, USA*
SCH772984 (ERK1/2 inhibitor)	*Selleckchem, Houston, USA*

Separation and Detection Modules for automated Western blot analyses	*ProteinSimple, San Jose, CA, USA*
Serological pipette (5 ml, 10 ml, 25 ml, 50 ml)	*BD Falcon, Heidelberg, Germany*
Skimmed milk powder (T145.3)	*Carl-Roth, Karlsruhe, Germany*
Smooth Muscle Cell Basal Medium 2 (C-22262)	*Promo cell, Heidelberg, Germany*
Smooth Muscle Cell Growth Medium 2 (C-22062)	*Promo cell, Heidelberg, Germany*
Smooth Muscle Supplement 2 mix (C-39267)	*Promo cell, Heidelberg, Germany*
Sodium dodecyl sulfate (SDS, AM9820)	*Invitrogen, by Thermo Fisher Scientific Inc. Waltham, USA*
Surgical instruments	*Fine Science Tools GmbH, Heidelberg, Germany*
SYBR® Safe DNA gel stain (S33102)	*Invitrogen, by Thermo Fisher Scientific Inc. Waltham, USA*
Syringes (Injekt®-F) (1 ml, 2 ml, 5 ml, 20 ml)	*B.Braun Melsungen AG, Melsungen, Germany*
Tetramethylethylenediamine (TEMED, 2367.3)	*Carl Roth, Karlsruhe, Germany*
TGX FastCast Kit (12% gels, 1610185)	*Biorad, Feldkirchen, Germany*
Tips for automatic pipettes (200 µl, 1000 µl, 10 µl)	*Sarstedt, Nümbrecht, Germany*
Tissue Tek	*Sakura Finetek, Staufen, Germany*
Transwell Permeable supports (24, 6 well)	*Corning, Wiesbaden, Germany*
TRIS (4855.2)	*Carl Roth, Karlsruhe, Germany*
TRIS-HCl (9090.2)	*Carl Roth, Karlsruhe, Germany*
TritonX-100 (X100)	*Merck KGaA, Darmstadt, Germany*
Trypsin/EDTA (10x, P10-024100)	*PAN-Biotech, Aidenbach, Germany*

Tween® 20 (P1379)	*Merck KGaA, Darmstadt, Germany*
VECTOR NovaRED Peroxidase Substrate Kit (LS-J1084-1)	*Vector Laboratories, Burlingame, USA*
VECTOR VIP Peroxidase Substrate Kit (SK-4600)	*Vector Laboratories, Burlingame, USA*
Warp Red Chromogen Kit (WR 806)	*Biocare Medical, Pacheco, USA*
Water, sterile (00088992)	*B.Braun Melsungen AG, Melsungen, Germany*
Whatman Gel Blotting Paper	*GE Healthcare, Marlborough, USA*
Xylazin 20 mg/ml	*Serumwerk, Bernburg, Germany*
Xylol (9713.2)	*Carl Roth, Karlsruhe, Germany*
β-Mercaptoethanol (4227.3)	*Carl Roth, Karlsruhe, Germany*

2.1.3. Software

GraphPad Prism Version 7	*GraphPad Software, Inc., La Jolla, USA*
LabChart 7	*AD Instruments, Spechbach, Germany*
PowerLab data acquisition system (MPVS-Ultra Single Segment Foundation System)	*AD Instruments, Spechbach, Germany*
Qwin software	*Leica, Wetzlar, Germany*
Vevo Lab Version 5.5.0	*FUJIFILM VisualSonics Inc., Toronto, Canada*
Analyze Pro software	*Analyze Direct, Mayo Clinic, USA*
FlexiVent software	*SCIREQ, Montreal, Canada*
FlowJoVx	*BD Biosciences, Heidelberg, Germany*
Stereology software	*Visiopharm, Hørsholm, Denmark*
IncuCyte® ZOOM Software	*Essen BioScience, Michigan, USA*
Image Lab Version 4.1	*Biorad, Feldkirchen, Germany*

2.1.4. Animals

C57BL/6NCrl	Charles River Laboratories, Sulzfeld, Germany
B6.129P2-Lyz2$^{tm1(cre)Ifo}$/J (Stock ID: 004781)	*Jackson Laboratory, Bar Harbor, USA*
C57BL/6NTac-Nos2$^{tm2904.1Arte}$Tg(CAG-flpe)2Arte	*Bred in house, generated by Taconic Artemis, Cologne, Germany*
Nos2 LysM-Cre (Nos2$^{tm2904.1Arte}$Tg(CAG-flpe)2ArteLyz2$^{tm1(cre)Ifo}$/)	*Bred in house*

2.1.5. Antibodies

Anti-beta Actin antibody (ab8227)	*Abcam, Cambridge, UK*
Anti-CD11b-BV605	*BD Biosciences, Heidelberg, Germany*
Anti-CD206	*BioLegend, Amsterdam, Netherlands*
Anti-CD44-Alexa Fluor700	*BD Biosciences, Heidelberg, Germany*
Anti-CD45-Vio-Blu	*MiltenyiBiotec, Bergisch Gladbach, Germany*
Anti-CD68 antibody [KP1] (ab955)	*Abcam, Cambridge, UK*
Anti-F4/80-PE-Cy7	*BioLegend, Amsterdam, Netherlands*
Anti-iNOS antibody (610329)	*BD Biosciences, Heidelberg, Germany*
Anti-iNOS antibody (ab3523)	*Abcam, Cambridge, UK*
Anti-iNOS antibody (NB300-605),	*Novus Biologicals, Abington, UK*
Anti-Ly6G-APC-Cy7	*BD Biosciences, Heidelberg, Germany*
Anti-Mannose Receptor antibody (anti-CD206, ab64693)	*Abcam, Cambridge, UK*
Anti-MHC-II-APC	*MiltenyiBiotec, Bergisch Gladbach, Germany*
CD68/SR-D1 Antibody (KP1) (NB100-683)	*Novus Biologicals, Abington, UK*

Goat anti-Mouse IgG (H+L) Cross-Adsorbed Secondary Antibody, Alexa Fluor 555	*Thermo Fisher Scientific Inc. Waltham, USA*
Goat anti-Rabbit IgG (H+L) Highly Cross-Adsorbed Secondary Antibody, Alexa Fluor 488	*Thermo Fisher Scientific Inc. Waltham, USA*
Horseradish-peroxidase–labeled anti-mouse (W4011)	*Promega, Mannheim, Germany*
Horseradish-peroxidase–labeled anti-rabbit (W4021)	*Promega, Mannheim, Germany*
p44/p42 (9102S)	*Cell Signaling, Danvers, USA*
Phospho-ERK (p44/p42) (4370S)	*Cell Signaling, Danvers, USA*
Phospho-ERK (p44/p42) (4901S)	
Von-Willebrand-factor (a0082)	*Dako, Hamburg, Germany*
α-smooth muscle actin (A2547)	*Merck KGaA, Darmstadt, Germany*

2.1.6. Primer sequences

Gene	**Forward primer (5'→3'):**	**Reverse primer (5'→3'):**
β-actin (Mus musculus)	GATATCGCTGCGCTGGTC	CATCACACCCTGGTGCCTA
Nos2 (Mus musculus)	CTAAGAGTCACCAAAATGGCTCCC	GTGGCCTTGTGGTGAAGAGTG
Nos2 floxed 1 (genotyping)	GGTGGATCTCTGTGAGTTCAGG	AGGCACACACACAAGTTCAGG
Nos2 floxed 2 (genotyping)	GCATATTCAAACCACCACAGG	AGATACTCCACTGTCTCCCTTCC
Cre recombinase (genotyping)	ATTTGCCTGCATTACCGGTC	ATCAACGTTTTGTTTTCGGA

2.2. Methods

2.2.1. Experimental design and cigarette smoke exposure

Adult male and female *iNos LysM-Cre mice* (*Nos2tm2904.1ArteTg(CAG-flpe)2ArteLyz2tm1(cre)Ifo/*), 3-4 months old, and age and gender-matched *Wildtype* (*Wt*) controls (C57BL/6N, obtained from Charles River Laboratories, Sulzfeld, Germany) were randomly allocated to either tobacco-smoke-exposed or unexposed group. Mice were kept in individually ventilated cages, under controlled temperature conditions (~22ºC), with food and water provided *ad libitum*. 13 animals per group were analyzed by means of hemodynamic and lung function measurements, echocardiography, FMT combined with micro-computed tomography (µCT) and right heart morphometry. Lungs of animals from each experimental group were randomly allocated to be 1) either paraffin-embedded or cryopreserved 2) used for either flow cytometry or RNA and protein isolation (Figure 4). All animal experiments were approved by the local governmental authorities (GI20/10-Nr.G46/2016, Regierungspräsidium Giessen, Germany).

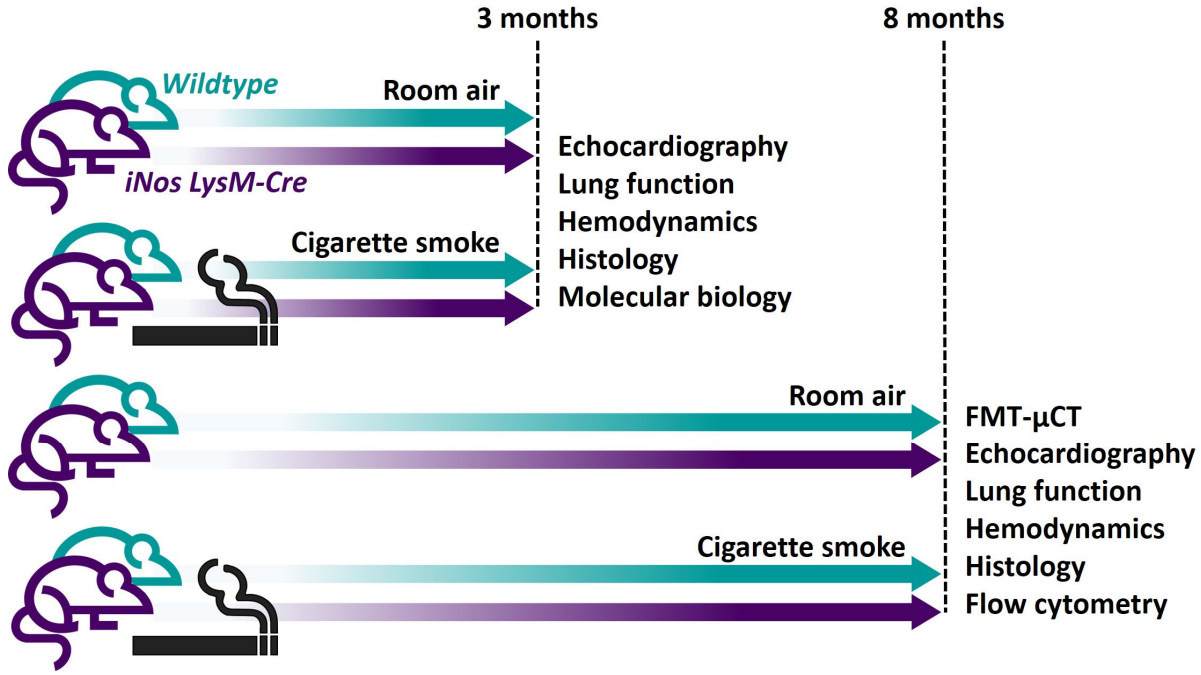

Figure 4. Schematic representation of the study design.
FMT-µCT: Fluorescence molecular tomography combined with micro-computed tomography. Blue: *Wildtype* mice; Purple: *iNos LysM-Cre* mice.

Mice were exposed to mainstream smoke of 3R4F cigarettes (Kentucky Tobacco Research & Development Center, Lexington, USA) for 3 or 8 months (6 hours per day, 5 days per week) produced by a cigarette smoke generator (Burghart, Wedel, Germany, Figure 5) as previously described (Pichl et al., 2019; Weissmann et al., 2014). The concentration of particular matter was measured 3 times per day and kept at 200 mg particulate matter per m^3. Control animals were kept under identical conditions but without exposure to cigarette smoke.

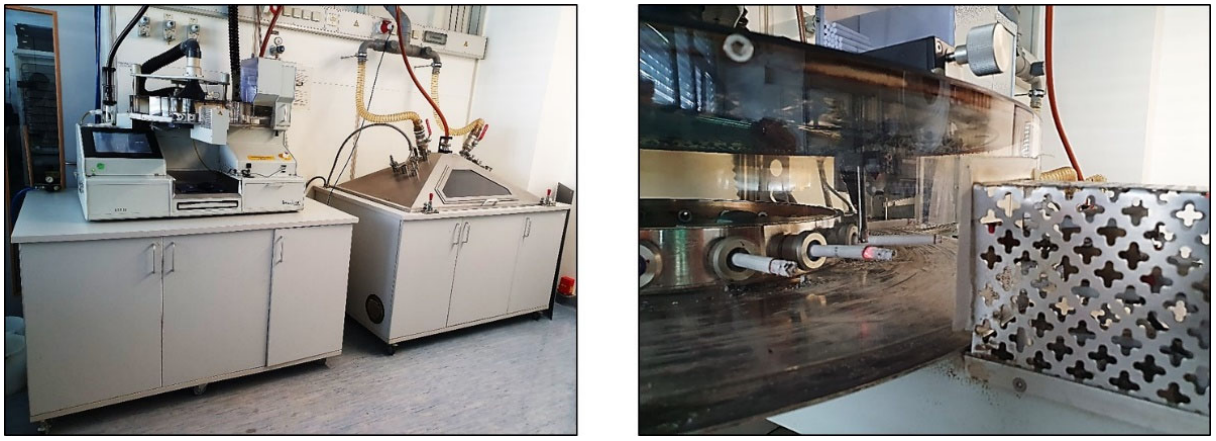

Figure 5. Cigarette smoke generator and smoke exposure chamber.

2.2.2. Exposure to chronic hypoxia

Adult male and female *Nos2 LysM-Cre* mice (*Nos2*$^{tm2904.1Arte}$*Tg(CAG-flpe)2ArteLyz2*$^{tm1(cre)Ifo}$/), 3-4 months old, and age and gender-matched *Wt* controls (C57BL/6N, obtained from Charles River Laboratories, Sulzfeld, Germany) were exposed to either normobaric hypoxia (10% O_2) or normobaric normoxia (21% O_2) in a ventilated chamber under the temperature range from 22-24°C for 28 days. Experiments were approved by the local governmental authorities (GI20/10-Nr.G39/2020, Regierungspräsidium Giessen, Germany).

2.2.3. Echocardiography and FMT-µCT

Transthoracic echocardiography was performed as previously described with subtle modifications (Kojonazarov et al., 2019), by Cheng-Yu Wu (Cardio-Pulmonary Institute, Justus Liebig University, Giessen, Germany). Imaging was done using a Vevo® 2100 high-resolution Imaging System (FUJIFILM VisualSonics, Toronto, Canada) equipped with the high-frequency M550D transducer (22-55 MHz). Mice were

anesthetized with 3% isoflurane and anesthesia was maintained with 1-2% isoflurane supplemented in 100% oxygen. The chest hair was removed before the imaging. The body temperature was monitored using a rectal thermometer and kept at physiological values by a thermoregulation plate. Tricuspid annular plane systolic excursion (TAPSE) was obtained under RV-focused apical 4-chamber view and analyzed using anatomical M-mode.

µCT and FMT-CT were performed using a Quantum GX µCT scanner (PerkinElmer, Inc, Waltham, USA) and FMT (VisEn Medical, Bedford, USA) as previously reported (Kojonazarov et al., 2019), by Dr. Baktybek Kojonazarov (Institute for Lung Health, Justus Liebig University, Giessen, Germany). Mice were anesthetized using 3% isoflurane and placed on a scanner bed with a nose cone supplying constant inhalation of 2% isoflurane supplemented in 100% oxygen. The animal chest was aligned within the center of the field of view. The scanner's complementary metaloxide-semiconductor X-ray flat-panel detector was set for the acquisition of images with an X-ray tube voltage of 90 kV and current of 80 µA. µCT data were collected in list-mode over a single complete gantry rotation with 4 minutes total rotation time (14688 frames collected in total). Raw projection images were processed using a proprietary algorithm for intrinsic retrospective respiratory gating. These were further reconstructed using a filtered back-projection algorithm on a dedicated graphics processing unit and subsequently loaded into Analyze Pro software (Analyze Direct, Mayo Clinic, Minnesota, USA). Lung segmentation and quantitative analysis of the CT density were performed as previously described (Gouveia et al., 2020). Two hours prior FMT-CT imaging, the Annexin Vivo 750 probe (100 µl/25 g mouse, 20 µM solution diluted in PBS) was injected through the tail vein.

2.2.4. *In vivo* lung function and hemodynamic measurement

At the end of the experiments, *in vivo* measurements of the lung function and hemodynamics were performed as described previously (Pichl et al., 2019; Seimetz et al., 2011; Seimetz et al., 2020; Weissmann et al., 2014). Prior to the experiment, anesthesia was induced with 3% isoflurane and maintained during the experiment by 1.5-2% isoflurane supplemented in 100% oxygen. Mice were placed on a thermoregulation plate and body temperature was maintained at 37°C during the measurements. For the assessment of lung function, mice were tracheotomized, connected to the FlexiVent mechanical ventilator and data-acquisition system

(SCIREQ, Montreal, Canada) and ventilated with a tidal volume of 5 ml/kg at a frequency of 150 breaths/min and a positive end-expiratory pressure (PEEP) of 3 cm H_2O. Snapshot and QuickPrime perturbation were imposed, and pressure-volume (PV) loops were generated for assessment of mechanical properties of the respiratory system. Deep inflation was used as a recruitment maneuver. Measurement of the right ventricular systolic pressure (RVSP) was performed after two to three times repeated lung function measurements. The right jugular vein was surgically prepared and catheterized by a micro-tip catheter that was then forwarded into the right ventricle. Measurements were recorded and analyzed using the PowerLab system and LabChart 7.0 software (ADInstruments GmbH, Spechbach, Germany).

2.2.5. Lung tissue processing

After the hemodynamic measurement, the thoracic cavity was opened and bronchoalveolar lavage (BAL) was done using ice-cold PBS buffer. Then, both ventricles of the heart were incised to allow perfusion and the lungs were flushed out of blood through the pulmonary artery with the saline solution under 22 cmH_2O pressure during continuous ventilation (Minivent, Hugo Sachs Electronik, March, Germany). The right lung was harvested for the molecular or flow cytometric analysis, while the left lung was fixed under simultaneous vascular perfusion (22 cmH_2O) and inflation (12 cmH_2O) with formalin. After 20 minutes, lungs were removed from the thoracic cavity, stored in formalin solution at room temperature (RT) overnight and then in PBS at 4°C for at least 24 h. Lung volume was measured using the water displacement method, after which the fixed tissue was put in agarose and cut in 3 mm thick sections. Finally, sections were dehydrated in an automatic dehydration machine and embedded in the paraffin.

2.2.6. Right heart hypertrophy assessment

After lung fixation with formalin, the heart was removed, dissected into the RV and the left ventricle plus septum (LV+S) and weighed. The Fulton index (RV/ (LV+S)) was calculated as a measure of RV hypertrophy.

2.2.7. Flow cytometry and cell sorting

Preparation of lung cell suspensions and flow cytometry was done in collaboration with Dr. Rajkumar Savai (Max Planck Institute for Heart and Lung Research, Bad Nauheim, Germany) and Dr. Andreas Weigert (Institute of Biochemistry I, Faculty of Medicine,

Goethe-University Frankfurt, Frankfurt, Germany). To obtain a single-cell suspension, approximately 0.4 g of fresh, blood-free lung tissue was dissociated using gentleMACS™ Dissociator and then incubated in 1.5 ml of lysis buffer (Table 2) at 37°C for 30 minutes. Lysis was stopped with DMEM medium supplemented with 10% FBS and the sample was passed through 100 µm and 40 µm cell strainers. The suspension was centrifuged for 5 minutes at 2490 x g (Micro 200R, Hettich, Germany) and the pellet was resuspended in 5 ml RBC lysis buffer. After 15 minutes of incubation at RT protected from light, lysis was stopped with 25 ml of PBS. Following centrifugation for 5 minutes at 2490 x g (Micro 200R, Hettich, Germany), the pellet was resuspended in FBS with 10% DMSO and kept on -80°C until use.

Table 2. The composition of the tissue lysis buffer.

Component	**Preparation**	**Volume (per 100 ml)**
Collagenase	Dissolved in HBSS with Mg^{2+} and Ca^{2+} at a concentration of 20 mg/ml (2500 units/ml)	5
DNAse	Dissolved in 20 mM Tris-HCl, 1 mM $MgCl_2$, pH 7.5 at a concentration of 10000 units/ml	1
DMEM medium		47
1xPBS		47

Single-cell suspensions were blocked with FcR blocking reagent in 0.5% PBS-BSA for 20 minutes, stained with fluorochrome-conjugated antibodies and analyzed on an LSR II/Fortessa flow cytometer or sorted using a FACS Aria III cell sorter. Data were analyzed using FlowJoVx. All antibodies and secondary reagents were titrated to determine optimal concentrations. Comp-Beads were used for single-color compensation to create multicolor compensation matrices. For gating, fluorescence minus one controls were used. The instrument calibration was controlled daily using Cytometer Setup and Tracking beads. For characterization of lung macrophages, the following antibodies were used: anti-CD11b-BV605, anti-CD44-AlexaFluor700, anti-Ly6G-APC-Cy7 (BD Biosciences, San Jose, USA), anti-CD45-Vio-Blu, anti-MHC-II-

APC (MiltenyiBiotec, Bergisch Gladbach, Germany), anti-CD206 and anti-F4/80-PE-Cy7 (BioLegend, Amsterdam, Netherlands).

2.2.8. Alveolar and vascular morphometry and design-based stereology

For alveolar morphometry, formalin-fixed and paraffin-embedded lung tissue was cut into 3 µm thick sections, deparaffinized via heat and xylol treatment, rehydrated in a graded ethanol series, and stained with hematoxylin and eosin (H&E). Stained sections were analyzed with the Qwin alveolar morphometry software as previously described (Pichl et al., 2019; Seimetz et al., 2011; Seimetz et al., 2020; Weissmann et al., 2014), to assess alveolar wall thickness, airspace and mean linear intercept. The analysis was done only on the alveolar compartment of the lung, while bronchi and vessels were excluded, as shown in Figure 6.

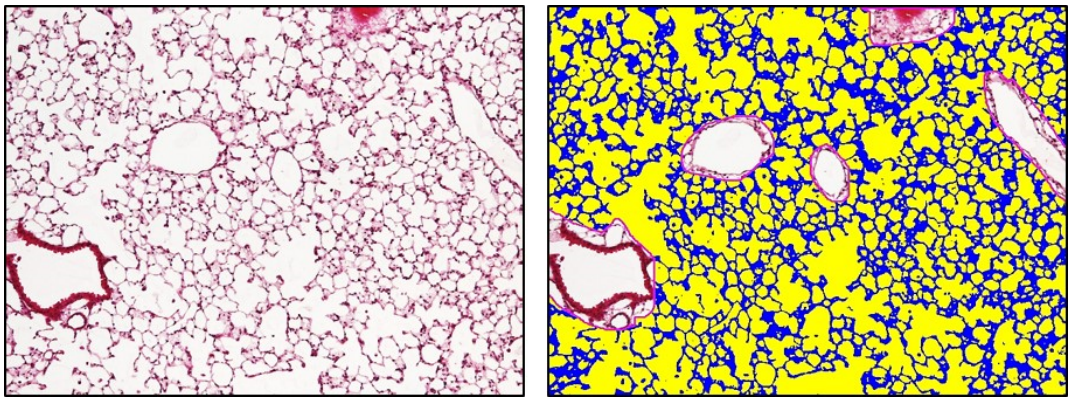

Figure 6. Morphometric analysis of the lung parenchyma using Leica Qwin software. Magnification 100x.

Vascular morphometry was done as previously described (Pichl et al., 2019; Seimetz et al., 2011; Seimetz et al., 2020; Weissmann et al., 2014). 3 µm thick sections were deparaffinized in the heating chamber and then rinsed in xylol and rehydrated in graded ethanol series. The endogenous peroxidase activity was blocked by a freshly prepared solution of hydrogen peroxide (H_2O_2) in methanol (3% v/v) and antigen retrieval was achieved using proteinase K. Non-specific antibody binding was avoided by incubation of sections in 10% BSA, Rodent Block M (prior to anti-α-smooth muscle actin primary antibody) and in normal horse serum (prior to the anti-von Willebrand factor primary antibody) for 30 minutes. Sections were first stained with anti-α-smooth muscle actin primary antibody diluted 1:700 at room temperature for 30 minutes. After washing with PBS, sections were incubated with HRP-labelled anti-mouse secondary antibody. The

purple color of the smooth muscle layer resulted from the reaction of this enzyme with VIP substrate. Next, sections were stained with anti-von Willebrand factor primary antibody at dilution 1:200, for 30 minutes at 37°C. After a few washing steps, slides were incubated with corresponding HRP-labelled secondary antibody. The reaction of DAB substrate with this enzyme determined the brown color of the vessel endothelium. Finally, the sections were counterstained with methyl green. Slides were analyzed using Qwin vascular morphometry software as shown in Figure 7. Muscularization of small pulmonary vessels was assessed based on the categorization of vessels 20-70 µm in outer diameter into non- (less than 5%), partially- (5-70%) and fully (more than 70%) muscularized.

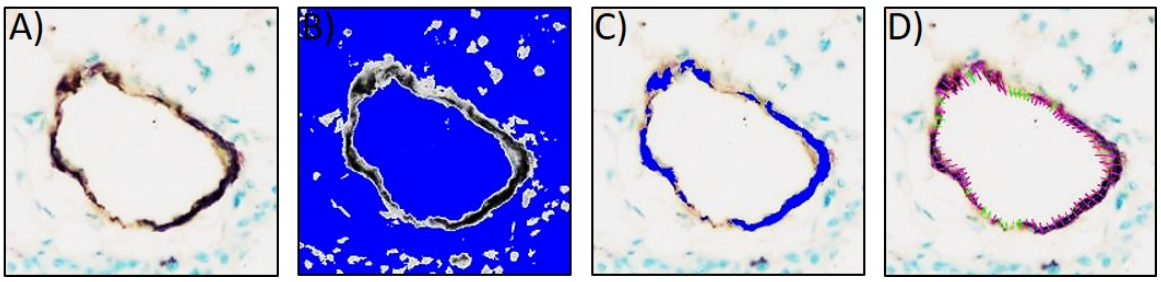

Figure 7. Assessment of muscularization of small pulmonary vessels using Leica Qwin software.

A) Identification of the vessel. B) Detection of the vessel lumen. C) Detection of the purple staining for anti-α-smooth muscle actin. D) Assessment of the muscularization. Magnification 400x.

Design-based stereology was done as previously published (Knust et al., 2009; Seimetz et al., 2020) with the help of Cheng-Yu Wu (Cardio-Pulmonary Institute, Justus Liebig University, Giessen, Germany). For each lung, a pair of 3 µm thick serial sections 3 µm apart from each other represented a physical dissector, allowing the analysis of a three-dimensional network of alveoli. Sections were first deparaffinized in xylol and rehydrated in graded ethanol series, then stained using the resorcinol-fuchsin solution according to Weigert and counterstained with nuclear fast red following standard procedures. The estimation of the alveoli number was done using stereology software (Visiopharm, Hørsholm, Denmark) and uniform random sampling for counting the alveolar openings (represented by elastic fiber bundles) at the level of the free septal edges, where they form a two-dimensional network. The counting process was based on the comparison between the reference section and the look-up section of the physical dissector at a light microscopic level and the identification of structural

changes between them. Mathematically, the number of alveoli was determined by the estimation of the Euler number of the network of alveolar openings.

2.2.9. Immunohistochemical and immunofluorescent staining for CD206, CD68 and iNOS

Human lung samples from donors and COPD patients were used. The study complied with the Declaration of Helsinki, and the tissue donation protocol was approved by the Ethics Committee of the Faculty of Medicine at Justus Liebig University Giessen, Germany (Approval number AZ58/15). Immunohistochemical staining was done as previously reported (Kosanovic et al., 2014; Seimetz et al., 2020) with subtle modifications.

For double staining of human lung tissue for iNOS and CD68, 2 µm thick paraffin-embedded tissue sections were deparaffinized in the heating chamber at 58-60˚C and in xylol, then rehydrated in graded ethanol series to PBS. The endogenous peroxidase activity was blocked by a freshly prepared solution of hydrogen peroxide (H_2O_2) in methanol (3% v/v) and antigen retrieval was achieved by pressure cooking in DIVA decloaker and proteinase K treatment. Non-specific antibody binding was avoided by incubation of sections in 10% BSA for 1 h and in Background Punisher for 15 minutes at RT. Following overnight incubation with both primary antibodies (anti-iNOS 1:250 and anti-CD68 1:200) at 4°C, slides were washed with 1xTBS (pH 7.2) and incubated for 30 minutes at RT with MACH2 double Stain Polymer 1 containing conjugated goat anti-mouse polymer AP and the conjugated goat anti-rabbit polymer HRP. The red color of $CD68^+$ cells resulted from the reaction of AP with Warp Red substrate, while the green color of the $iNOS^+$ cells appeared in reaction with HistoGreen HRP substrate. The slides were counterstained with hematoxylin and coverslipped using a mounting medium.

For staining of CD68 and CD206 in human lung tissue, 2 µm thick serial sections of paraffin-embedded lung tissue were deparaffinized, rehydrated and antigen retrieval was done as mentioned above. Non-specific antibody binding was avoided by incubation of sections in 10% BSA for 1 h and in Background Punisher for 15 minutes at RT. The sections were incubated with primary antibodies (either anti-CD68 or anti-CD206, both diluted 1:200) overnight at 4°C. Following washing with 1xTBS (pH 7.2), slides were incubated with an AP-conjugated secondary antibody polymer. Formation of bright red precipitate in the reaction of AP with Warp Red substrate served for the

visualization of antigen. The slides were counterstained with hematoxylin and coverslipped using a mounting medium.

For immunofluorescent staining of mouse lung sections for CD68 and iNOS, 3 µm thick serial sections of paraffin-embedded lung tissue were deparaffinized, rehydrated and antigen retrieval was done using Rodent Decloaker. Non-specific antibody binding was avoided by incubation of sections in 10% BSA for 1 h and in Background Punisher for 15 minutes at RT. Following overnight incubation with both primary antibodies (anti-iNOS 1:50 and anti-CD68 1:50) at 4°C, slides were washed 3 times with 1x PBS pH 7.4 and incubated with fluorescently labeled secondary antibodies for 2h at RT. After 3 times washing in 1xPBS, sections were counterstained with DAPI and mounted using Fluoro Care Anti-Fade Mountant.

2.2.10. Isolation of mouse PASMC

PASMC were isolated from precapillary vessels of 12-16 week old C57BL/6NCrl mice modified from a previously reported protocol (Marshall et al., 1996). Before the experiment, animals received i.p. injections of anesthesia and anticoagulant at a dosage of 100 mg/kg ketamine, 20 mg/kg xylazine and 1000 IU/kg heparin. After the depth of anesthesia was assessed by loss of a pedal reflex, the animal was sacrificed by exsanguination and the thoracic cavity was opened. Then, both ventricles of the heart were incised to allow perfusion and the lungs were flushed out of blood through the pulmonary artery with PBS. Then, 2-3 ml of a warm 0.5% solution of low-gelling agarose in M199 medium containing 15 mg of iron particles was gently injected into the lung vasculature through the pulmonary artery. Afterwards, the animal was tracheotomized and 2-3 ml of a warm 1% solution of low-gelling agarose was injected into the lung through the trachea. Thereafter, the lung was removed from the thorax and kept in ice-cold PBS to allow polymerization of the agarose. Following the separation of the lung lobes and the transfer to a clean 50 ml tube containing 1 ml of PBS, the lung lobes were cut. After 3 times washing with PBS using a magnetic concentrator, the remaining lung tissue (attached to the iron particles) was resuspended in 10 ml M199 medium containing 800 U of collagenase and incubated for 1 h at 37°C. After the enzymatic digestion was stopped by the medium supplemented with 10% FBS, the tissue was further dissociated by passing through 15 G and 18 G needles. Following the three washing steps, the pulmonary arterial tissue attached to the iron particles was resuspended in PASMC growth medium

(Smooth Muscle Cell Growth Medium 2 + 100 µg/ml Normocin + 10% FBS) and cultured for 5-7 days without passaging. During the first change of the culture medium for the PASMC, vessel pieces were transferred to another culture dish in the fresh PASMC growth medium. Cells on both dishes were cultured until confluence, then seeded for the experiments.

2.2.11. Isolation and differentiation of mouse bone marrow-derived macrophages (BMDM)

Tibiae and femora from 12-16 week old C57BL/6NCrl or Nos2$^{tm2904.1Arte}$Tg(CAG-flpe)2ArteLyz2$^{tm1(cre)Ifo}$/ mice were removed under sterile conditions. Bone ends were cut off and the bone shafts were then flushed with a 24 G needle on a 10 ml syringe with PBS (without Ca^{2+} and Mg^{2+}). The bone marrow was collected in sterile 50 ml tubes and centrifuged for 5 minutes at 400 x g at RT. Cells were resuspended in BMDM differentiation medium (DMEM/F12 with 10 mM L-glutamine, 100 IU/ml penicillin, and 100 µg/ml streptomycin, 10% FBS and 35 ng/ml recombinant mouse M-CSF) and passed through a 40 µm cell strainer. Cells were counted using a Neubauer hemocytometer and the number was adjusted to 7.5 x 10^6 cells/ml. Ten ml of cell suspension was seeded per 10 cm non-tissue culture treated Petri dish and cultured in a humidified atmosphere (5% CO_2 at 37°C) for 7 days, with the addition of 5 ml of differentiation medium on day 3. After 7 days, cells were harvested using enzyme-free cell dissociation buffer, seeded at 10^6 cells/mL in the full BMDM culture medium (DMEM/F12 with 10 mM L-glutamine, 100 IU/ml penicillin, and 100 µg/ml streptomycin, 10% FBS), and stimulated overnight with 100 U/mL IFN-γ to prime them for the differentiation into M1 cells. The following day, IFN-γ was removed and cells were treated with 10 ng/ml LPS to obtain M1 macrophages, or with 100 U/mL IL-4 to elicit M2 cells, with or without 100 µM L-NIL.

2.2.12. CSE preparation

Cigarette smoke extract (CSE) was prepared by pulling the mainstream smoke from one research-grade 3R4F cigarette through the medium. The 3R4F cigarette was vaporized within exactly 1 minute in 10 ml of DMEM/F12 medium to get 100% CSE. Then, CSE was filtered through a 0.2 µm filter, diluted with culture medium to the final concentration needed for the experiment and used within 30 minutes for the treatment of the cells.

2.2.13. Cell viability assay for CSE-treated macrophages

After 6 h of CSE treatment, the new culture medium with 10% alamarBlue Cell Viability Reagent was added. Cell viability was determined 16 h thereafter, by reading fluorescence intensity with microplate reader set to a fluorescence excitation wavelength of 560 nm and an emission of 590 nm.

2.2.14. Co-cultures of macrophages and PASMC

Bone marrow-derived macrophages were seeded at 10^6 cells/mL on Transwell Permeable supports, differentiated into M1 or M2 cells or left in the naïve state. One % CSE was added to the appropriate experimental groups and incubated for 3 h. Meanwhile, PASMC were seeded in 24 well plate dishes at 15.000 cells/well and starved for 24 h in PASMC basal medium supplemented with 0.1% FBS. Prior to co-culturing, the same fresh culture medium was added to both cell types and the co-cultures were kept for 24 h in a humidified atmosphere of 5% CO_2 at 37°C (Figure 8).

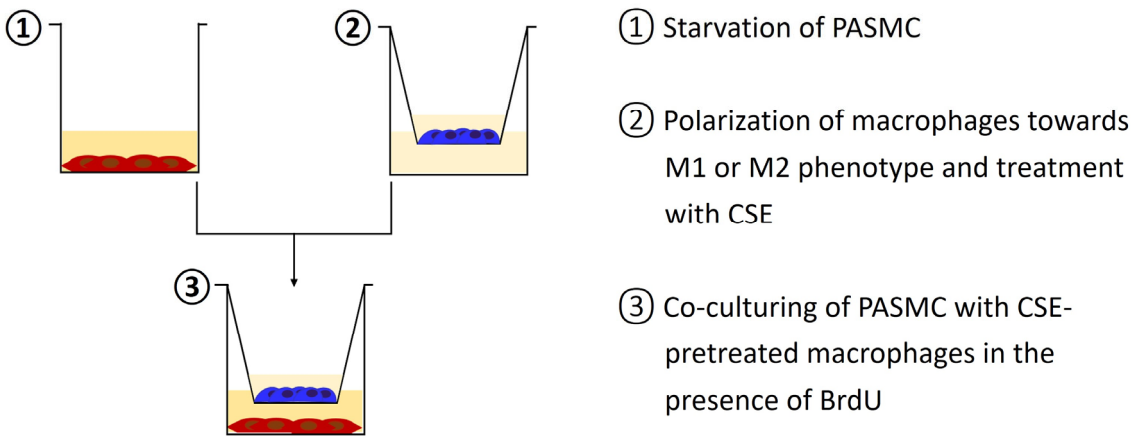

Figure 8. Schematic depiction of the experimental setup for co-culturing bone marrow-derived macrophages with PASMC.
CSE: Cigarette smoke extract. PASMC: Pulmonary artery smooth muscle cells

2.2.15. Proliferation assay

For the assessment of PASMC proliferation in the above-described co-cultures, BrdU labeling solution and/or 100 U/ml of recombinant murine IL-4 was added to the fresh basal PASMC medium before co-culturing. After 6 or 24 h, proliferation of PASMC was measured according to the manufacturer's instructions. Briefly, the PASMC were fixed and the DNA was denatured in one step by incubation with FixDenat for 30 minutes at

RT. Following fixation, cells were incubated for 1.5 h with anti-BrdU antibody conjugated with peroxidase. After removal of the antibody solution, wells were rinsed 3 times with PBS. Upon adding substrate solution, the absorbance of the samples was measured in the microplate reader set to 370 nm (reference wavelength: 492 nm).

For the assessment of PASMC proliferation in response to the macrophage culture-conditioned medium (CM), PASMC were seeded at a density of 12000 cells/well in 24 well plates and starved in for 24 h in PASMC basal medium supplemented with 0,1% FBS. The next day, BrdU labeling solution and 50% of macrophage culture CM or control macrophage growth medium was added to the fresh basal PASMC medium. After 24 h, the proliferation of PASMC was measured according to the above described protocol using microplate reader Infinite M200 PRO.

2.2.16. Experiments with macrophage conditioned medium (CM)

For experiments with macrophage CM, BMDM were seeded at 10^6 cells/mL in 24-well plates and left overnight in a humidified atmosphere of 5% CO_2 at 37°C. Macrophages were differentiated into M1 or M2 cells as described. After the treatment with 1% CSE for 3 h, the medium was changed and macrophages were cultured for the additional 24 h, after which period CM was collected.

PASMC were seeded in 24-well plate dishes at 15.000 cells/well and starved for 24 h in PASMC basal medium supplemented with 0.1% FBS. Then, the medium was replaced by the fresh medium containing BrdU labelling solution and 50% CM collected from macrophage monocultures as described. After 24 h, proliferation was measured according to the previously described protocol and the O.D. values were standardized to the appropriate baseline (PASMC treated with fresh BMDM medium instead of macrophage-CM).

2.2.17. Apoptosis assay

PASMC were seeded at a density of 5000 cells/well in 96 well plates and treated with CSE (to induce apoptosis) and 50% of co-culture CM or control macrophage growth medium (Figure 9). Apoptosis kinetic assay was done according to the manufacturer's instruction and IncuCyte ZOOM was used for visualization. Treatment was done in duplicates and apoptosis was expressed as the average confluence of cells positive for the green fluorescent Annexin V-based probe.

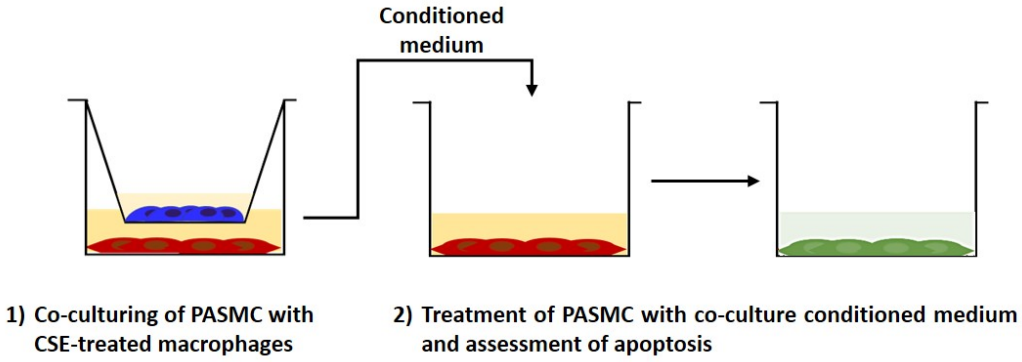

Figure 9. Schematic depiction of the experimental setup for assessment of PASMC apoptosis.

CSE: cigarette-smoke extract. PASMC: pulmonary artery smooth muscle cell

2.2.18. Migration assay

PASMC were seeded in 24 well plates containing 2 Well Culture-Inserts (18000 cells/well) and left overnight (5% CO_2, 37°C). The next day, inserts were removed, cells were washed with PBS twice and treated with 50% of co-culture CM or control macrophage growth medium. Closure of the wound made by insert's removal was followed using the analyzer IncuCyte ZOOM. Three photos per each well/experimental sample were taken every 2 h for 24 h and the average value was calculated and reported.

2.2.19. ERK inhibition experiment

PASMC were seeded in 96-well plate dishes at 5000 cells/well and starved for 24 h in PASMC basal medium supplemented with 0.1% FBS. Cells were pre-treated with DMSO or 100 μM SCH77298 (ERK1/2 inhibitor) for 3 h. Then, cells were given the fresh medium containing 1) BrdU labeling solution, 2) either DMSO (solvent) or 100 μM SCH772984, and 3) 50% of either co-culture CM (collected after 6 h co-culturing) or control CM from PASMC monocultures. After 24 h, proliferation was measured as previously described. Values were standardized to the appropriate baseline (either DMSO + PASMC CM-treated cells or SCH772984 inhibitor + PASMC CM-treated cells). CSE-dependent proliferation was calculated by subtracting proliferation in the group treated with CM from CSE-unexposed co-cultures from the proliferation in the corresponding group treated with CM from CSE-exposed co-cultures (e.g. M2 CSE CM-M2 CM).

2.2.20. Immunocytochemical staining of PASMC

Murine PASMC were seeded on collagen-coated glass coverslips and co-cultured with M2 macrophages as previously described. At the desired time-point, cells were pre-fixed with 2% PFA added in the co-culturing medium for 5 minutes and then fixed with 4% PFA for additional 15 minutes at RT. After washing with PBS, cells were permeabilized with ice-cold 100% methanol for 10 minutes at -20°C and rinsed with PBS. Blocking was done for 1 h at RT using 5% BSA 0.3% TritonX in PBS, and slides were incubated overnight at 4°C with phospho-p44/p42 antibody (Cat#4370, Cell Signaling, 1:200) diluted in 1% BSA 0.3% TritonX in PBS. The next day, slides were washed with PBS and incubated in Cy3-labelled α-smooth muscle actin antibody (Cat#C6198, Merck KGaA, 1:400) and Alexa488-labelled goat anti-rabbit secondary antibody (Cat#A-11034, ThermoFisher Scientific, 1:400) for 2 h at RT. After washing in PBS, cells were counterstained with 2 µg/ml Hoechst in PBS for 10 min. Slides were mounted using Fluoro Care Anti-Fade Mountant (Biocare Medical) and analyzed using the confocal microscope. At least three photos from randomly chosen fields were taken for analysis.

2.2.21. Cytokine array and ELISA assays

CM from co-cultures was harvested after 24 h, centrifuged and kept on -80°C until use. Proteome Profiler Mouse XL Cytokine Array and TGF-β, IL-6 and IL-4 ELISA assays were performed according to the manufacturer's instructions.

For the cytokine array, each membrane (spotted with 111 different antibodies to mouse cytokines in duplicates) was incubated overnight on 4°C with 400 µl of culture CM from the appropriate experimental group (diluted in assay buffer). The following day, membranes were washed and incubated for 1 h at RT with the detection antibody cocktail. Thereafter, membranes were rinsed again and incubated for 30 minutes with the streptavidin-HRP. After washing, membranes were placed into ChemiDoc Touch Imaging System and covered with sufficient amount of Chemi Reagent Mix. Chemiluminescent signal was visualized for all membranes simultaneously every minute for 20 minutes in total.

For the ELISA assays, 50 µl of undiluted cell culture CM was incubated for 2 h at RT in antibody-coated microplates. Following washing 4 times with PBS, an antibody (specific for the assayed cytokine) conjugated with HRP was added to wells and

incubated for 2 h at RT. Wells were rinsed with PBS 4 times and the substrate solution was added to wells and incubated in dark for 30 minutes. Reaction was stopped with stop solution and absorbance was read using plate reader Infinite M200 PRO set to 450 nm (reference wavelength: 540 nm).

2.2.22. Western blot analysis

The sample preparation, SDS polyacrylamide gel electrophoresis, transfer and incubation with primary and secondary antibodies were performed as previously described (Seimetz et al., 2020), with subtle modifications. PASMC were washed in ice-cold PBS and lysed in commercially available lysis buffer containing 1 mM PMSF, while the lung tissue was homogenized in the same lysis buffer using Precellys® 24 bead beating Tissue Homogenizer. Supernatants remaining after 10 minutes centrifugation (14000 × g, 4°C [Micro 200R, Hettich, Germany]) were collected and protein concentration was measured using the spectrophotometric Bradford assay. Following electrophoretic separation (100 Volts, 400 mA, 150 W for 1.5 h) on a 12% polyacrylamide gel, samples were transferred to a PVDF membrane using a semi-dry blotting system. The non-specific binding was blocked by incubation skimmed milk (6% in TBS with Tween [TBST]) for 1 h at RT. After overnight incubation with primary antibodies diluted in blocking solution at 4°C, membranes were washed with TBST and incubated with secondary antibodies conjugated with horseradish peroxidase (anti-rabbit, anti-mouse Promega, Wisconsin, USA) for 1 h at RT. Following washing in TBST, protein bands were visualized using an ECL kit and the ChemiDoc MP Imaging System. Before re-probing with another primary antibody (total extracellular signal-regulated kinase (ERK) or β-actin), membranes were incubated in stripping buffer for 1 h at RT and thoroughly washed.

Primary antibodies were used as follows: phospho-ERK (p44/p42) (Cat#4901S, Cell Signaling) 1:1000; p44/p42 (Cat#9102S, Cell Signaling) 1:1000; iNOS (Cat# 610329, BD Biosciences) 1:1000; β-actin (Cat# ab8227, Abcam), 1:20000.

Table 3. The composition of buffers used in the Western blot procedure.

Buffer	Substance	Amount
Electrophoretic buffer		
	TRIS-Base	3.25 g
	Glycin	14.4 g
	SDS (20%)	10 ml
	H_2O	900 ml
Blotting buffer		
	TRIS-Base	5.8 g
	Glycin	2.8 g
	H_2O	800 ml
	SDS (20%)	1.85 ml
	Methanol	200 ml
Stripping buffer		
	Glycin	0.75 g
	H_2O	100 ml
	37% HCl	2 ml
Washing buffer (TBST)		
	TRIS-base	4.84 g
	NaCl	17.54 g
	H_2O	1000 ml
	Tween 20	1 ml

2.2.23. Laser microdissection and automated Western blot analysis

Laser microdissection was done as described previously with subtle modifications (Seimetz et al., 2020). Briefly, cryopreserved, Tissue tek-embedded lung tissue was cut into 12 µm thick sections and mounted on membrane-coated glass slides. Sections were stained with haematoxylin (diluted 20:30 with distilled H_2O) for 1 min, and dehydrated in the graded ethanol series. 100 vessels per sample were captured by laser microdissection and collected in 30 µl of 0.1X Sample buffer containing a

cOmplete™ Mini EDTA-free Protease-Inhibitor-Cocktail. Samples were sonicated (3 times for 30 seconds) and further prepared and analyzed using the chemiluminescent detection system of the Jess Simple Western™ platform (ProteinSimple, San Jose, CA, USA) according to the manufacturer´s instructions. Antibodies were used as follows: p-p44/p42 phospho-ERK (p44/p42) (Cat#9101S, Cell Signaling Technology, Danvers, MA, USA) 1:4 and p44/p42 (Cat#9102S, Cell Signaling Technology, Danvers, MA, USA), 1:40.

2.2.24. cDNA synthesis and quantitative PCR (qPCR) analysis

Total RNA from mouse PASMC was isolated using RNeasy Mini Kit according to the manufacturer's instructions. 400 ng of RNA was reversely transcribed to cDNA using iScript cDNA Synthesis Kit according to manufacturer's instructions and TPersonal thermocycler set to following conditions: 5 minutes at 25°C, 20 minutes at 46°C, 1 minute at 95°C and stop at 4°C. qPCR analysis was done using iTaq Universal SYBR Green Supermix according to the manufacturer's instructions, with primers designed using Primer BLAST from NCBI and purchased from Metabion. The reaction was carried out in CFX Connect™ Real-Time PCR Detection System set to the following conditions: 1 cycle at 95°C for 10 minutes, then 40 cycles at 95°C for 10 seconds, 59°C for 10 seconds, 72°C for 10 seconds. For the analysis of data, Ct values were first normalized to the internal control (*Hprt* or *β-actin*) to obtain ΔCt values, which were then used to calculate the fold change in RNA expression upon the treatment of cells according to the formula:

$$\text{Fold change} = 2^{-\Delta\Delta Ct}$$

$$\Delta\Delta Ct = \Delta Ct_{treatment} - \Delta Ct_{control}$$

2.2.25. Statistical analysis

Statistical analyses were performed using GraphPad Prism 8. All data are expressed as means ± standard error of the mean (SEM). Normal distribution of residuals was tested and assured visually (using quantile-quantile plot) and formally (using Anderson-Darling, D´Agostino-Pearson, Shapiro-Wilk and Kolmogorov-Smirnov tests). Comparison between multiple groups was performed by analysis of variance (two-way ANOVA and Tukey's post-hoc test for comparison between different groups of non-

matched samples [animal experiments] and Sidak's post-hoc test for matched samples [cell culture experiments]). An independent t-test was used for comparing the equality of means between two groups. p-values of <0.05 were considered statistically significant.

3. Results*

3.1. Deletion of *iNos* in myeloid cells using the *iNos LysM-Cre* driver line

Considering the previous finding that iNOS-expressing, bone marrow-derived cells drive the development of smoke-induced PH (Seimetz et al., 2011), the myeloid cell-specific iNOS knockout mice were generated by crossing *iNos*$^{flox/flox}$ mice with *Lysozyme M* promoter-driven Cre expressing mice (hereafter *LysM-Cre*), to assess the role of myeloid cell-specific iNOS expression in the development of smoke-induced PH *in vivo*. I confirmed the successful generation of the knockout mice *in vitro*, by quantification of iNOS expression in bone marrow-derived, naïve or *in vitro* polarized M1 and M2 macrophages (Figure 10A&B), and *in situ*, by immunofluorescent staining of mouse lung sections (Figure 10C).

*The majority of the data from my thesis presented in this chapter are published as an original research article titled: “Myeloid cell-specific deletion of inducible nitric oxide synthase protects against smoke-induced pulmonary hypertension in mice” (Gredic et al., Eur Respir J, 2021).

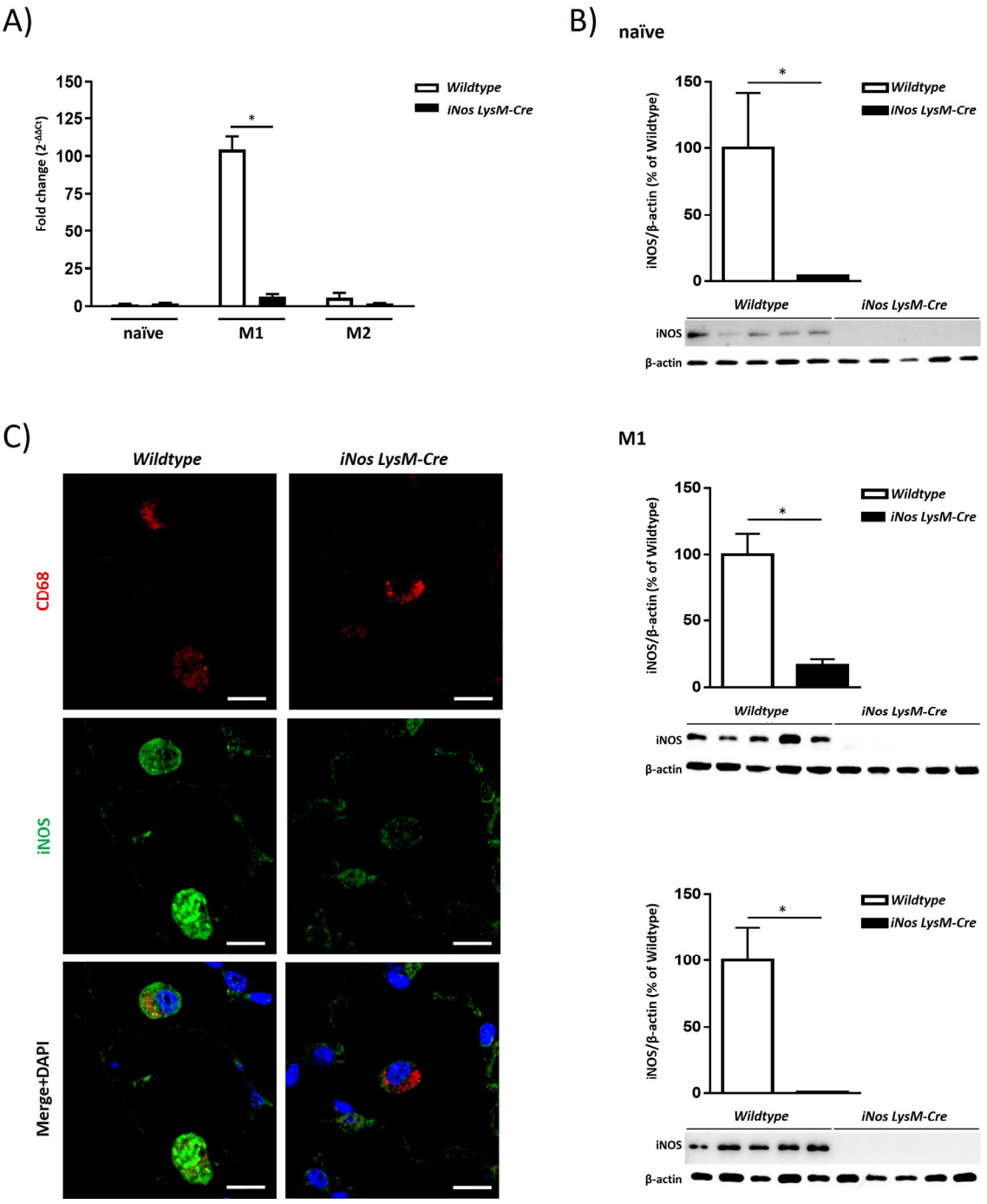

Figure 10. *iNos* gene is successfully deleted in myeloid cells using the *iNos LysM-Cre* driver line.

Bone marrow-derived macrophages were isolated from *Wildtype (Wt)* and *iNos LysM-Cre* mice and polarized *in vitro* using either interferon (IFN)-γ and lipopolysaccharide (LPS) to elicit M1 polarization, or interleukin (IL)-4 to achieve M2 phenotype. A) Expression of *iNos* gene in naïve, M1 and M2 macrophages, quantified by real-time PCR (n=5). Graph shows mean ± SEM. *p < 0.05. Two-way ANOVA (with Sidak´s multiple comparison post-hoc test) was used. B) Western blot quantification of iNOS protein levels in naïve (upper), M1 (middle) and M2 (lower

panel) macrophages (n=5). Graphs show mean ± SEM. *p < 0.05. Unpaired t-test was used. C) Representative images of lung sections from *Wt* and *iNos LysM-Cre* mice stained for CD68 (red) and iNOS (green) and counterstained with DAPI (blue). Scale bar = 10 µm.

3.2. iNOS deletion in myeloid cells prevents PH and right ventricular hypertrophy in smoke-exposed mice

Hemodynamic measurements following chronic smoke exposure revealed increased RVSP in smoke-exposed WT animals compared to unexposed controls, whereas myeloid cell-specific iNOS knockout prevented PH development in mice exposed to smoke for 3 and 8 months (Figure 11).

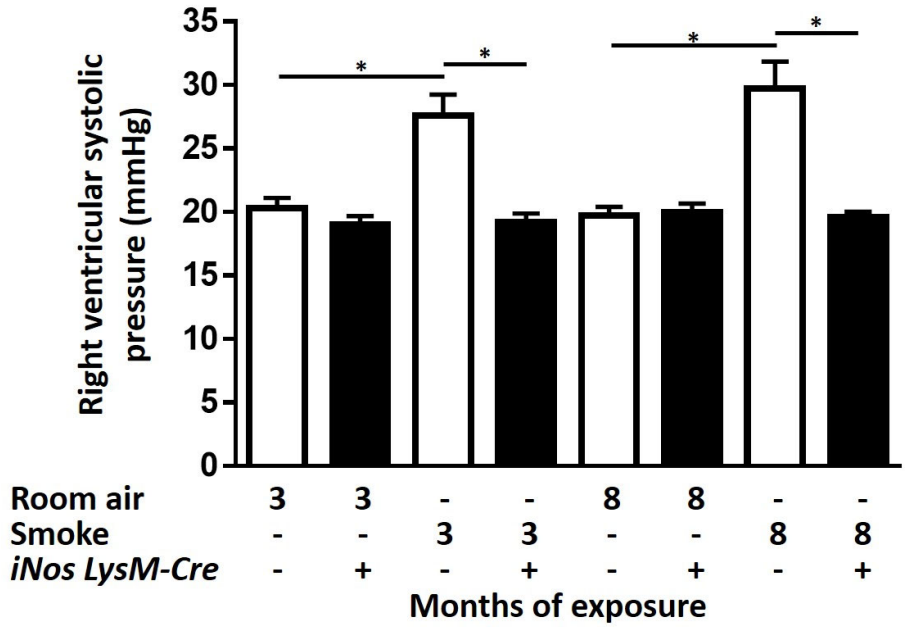

Figure 11. Myeloid cell type-specific iNOS deletion prevents the development of cigarette smoke-induced PH in mice.

Right ventricular systolic pressure (n=9-12) after exposure to either cigarette smoke or room air for 3 and 8 months. Graph shows mean ± SEM. *p < 0.05. Two-way ANOVA (with Tukey´s multiple comparison post-hoc test) was used.

In addition, RV hypertrophy and impaired right heart function occurring after smoke exposure in *Wt* mice were absent in *iNos LysM-Cre* mice, as shown by Fulton index and echocardiography (Figure 12). Of note, echocardiography showed different baseline values of TAPSE in younger animals, probably due to congenital effects.

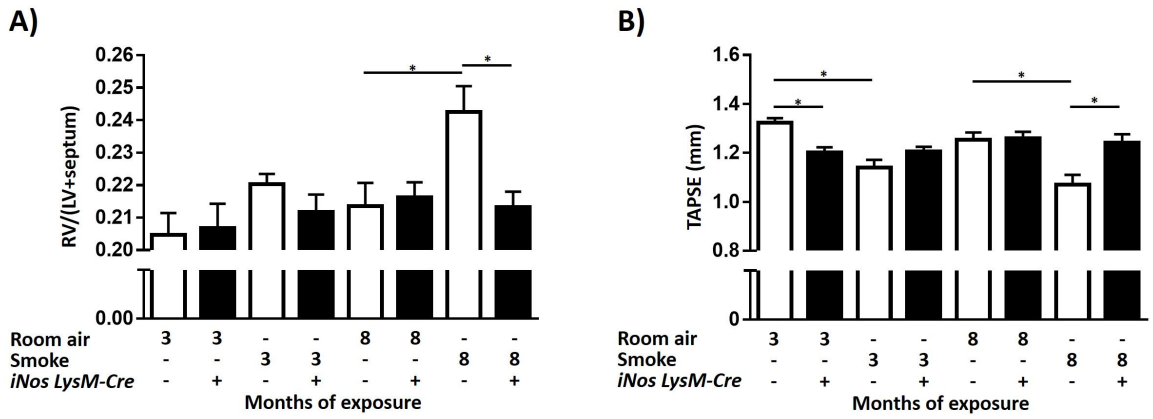

Figure 12. Myeloid cell type-specific iNOS deletion prevents smoke-induced right ventricular (RV) hypertrophy and dysfunction.

A) Changes in the right ventricular structure shown as the ratio of the RV and the left ventricular plus septum (LV+septum) weight (n=9-12). B) Echocardiographic assessment of RV systolic function (n=11-13) depicted through tricuspid annular plane systolic excursion (TAPSE). Graphs show mean ± SEM. *p < 0.05. Two-way ANOVA (with Tukey´s multiple comparison post-hoc test) was used.

Moreover, muscularization of small pulmonary vessels increased in cigarette smoke-exposed *Wt* mice compared to unexposed (room air) controls after 3 and 8 months (Figure 13). In contrast, *iNos LysM-Cre* mice were fully protected against smoke-induced pulmonary vascular remodeling.

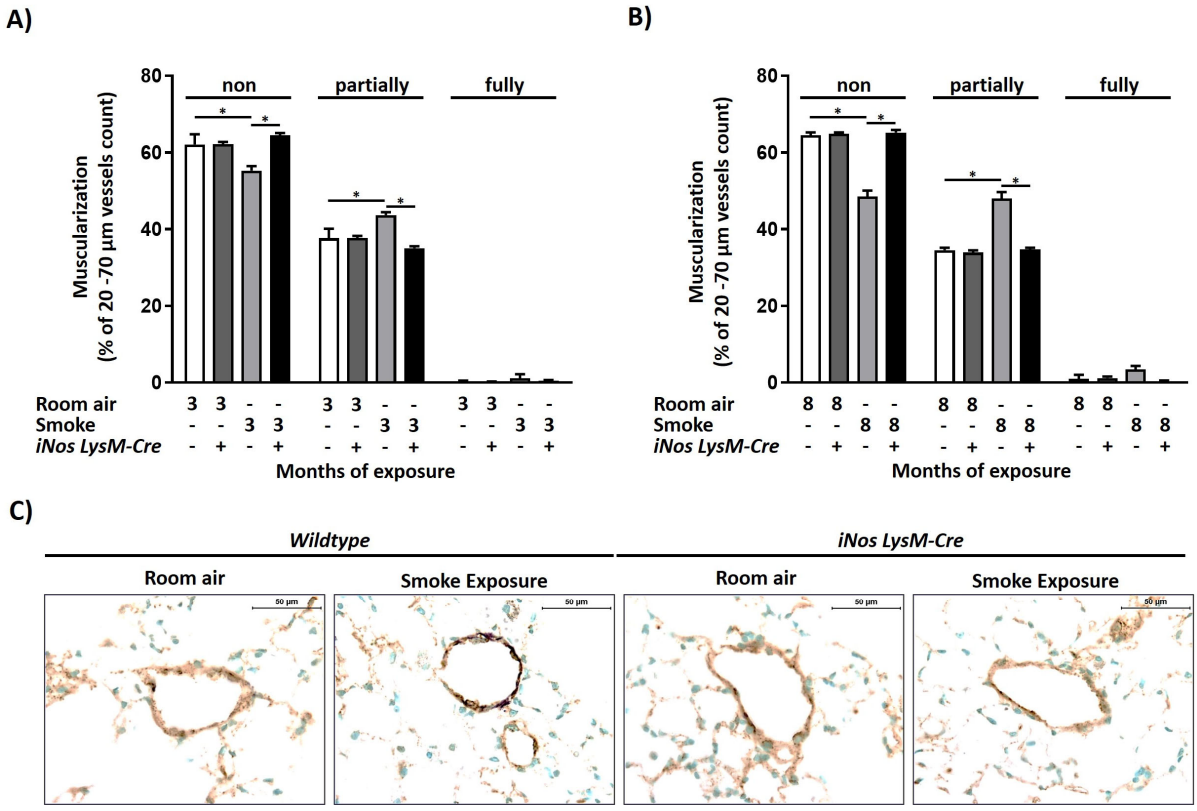

Figure 13. Myeloid cell type-specific iNOS deletion prevents cigarette smoke-induced pulmonary vascular remodeling in mice.

Remodeling of the small pulmonary vessels (20-70 µm outer diameter) presented as the percentage of total vessel count, given for non-, partially- and fully- muscularized vessels after A) 3 (n=4-5) or B) 8 months of smoke exposure (n=5-7), and C) representative images of lung sections from mice exposed to cigarette smoke for 8 months and respective room air controls, co-stained against α-smooth muscle actin (purple) and von Willebrand factor (brown) and counterstained using methyl green (green). Scale bars = 50 µm. Graphs show mean ± SEM. *p < 0.05. Two-way ANOVA (with Tukey´s multiple comparison post-hoc test) was used.

3.3. Myeloid cell-specific iNOS knockout does not prevent emphysema development in mice after chronic smoke exposure

In parallel, I investigated the development of emphysema in *iNos LysM-Cre* mice. Assessment of parenchymal changes *in vivo* with µCT showed that chronic smoke exposure of myeloid cell-specific iNOS knockout mice results in the increase of lung functional residual capacity (FRC) comparable to that observed in WT controls (Figure 14A, left).

Additionally, I used FMT-µCT and Annexin V based imaging probe to quantify apoptosis *in vivo* and found an increase in apoptosis in lungs of both *Wt* and *iNos LysM-Cre* mice after 8 months of smoke exposure, compared to respective unexposed (room air) controls (Figure 14B and C).

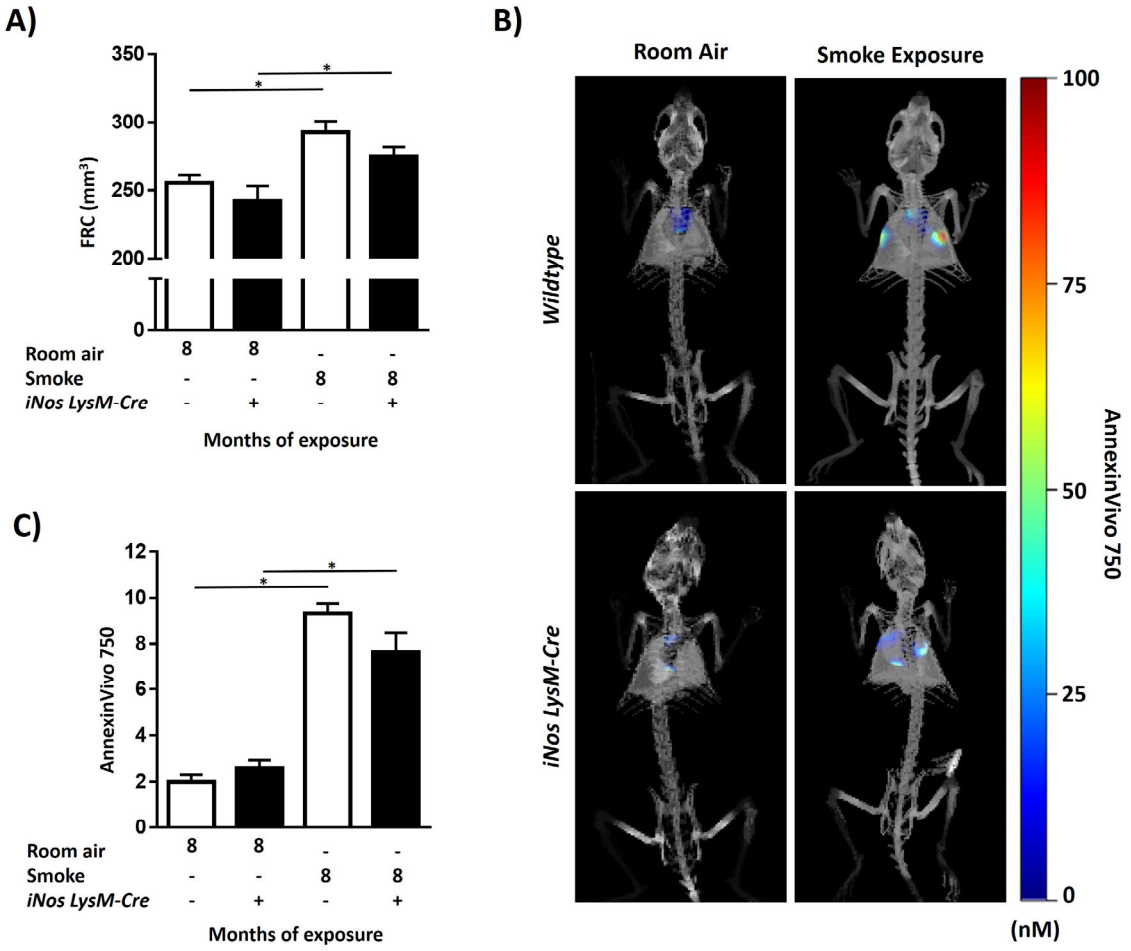

Figure 14. Functional residual capacity (FRC) and apoptosis in the lung of myeloid cell type-specific iNOS knockout mice increase upon chronic smoke exposure.

Mice were exposed either to cigarette smoke or room air for 3 and 8 months. A) Estimation of FRC in lungs of mice exposed to smoke for 8 months and respective unexposed (room air) controls (n=11-13), based on micro-computed tomography (µCT) imaging. B) Representative images of C) *in vivo* quantification of apoptosis in lungs (n=6-7), detected by a fluorescence molecular tomography (FMT) imaging system, using AnnexinVivo 750 probe. Graphs show mean ± SEM. *p < 0.05. Two-way ANOVA (with Tukey´s multiple comparison post-hoc test) was used.

In vivo, functional measurements with the FlexiVent system (Figure 15) showed an increase in lung compliance, a measure inversely related to the elastic recoil of the lung, both during periods of gas flow (dynamic compliance) and at rest (static

compliance), in both WT and knockout animals after chronic smoke exposure. Moreover, the upward shift of respiratory PV loops (Figure 15B) indicated emphysema development in both *Wt* and *iNos LysM-Cre* mice after chronic smoke exposure. Baseline values and temporal dynamic of lung function changes were different in knockout animals, possibly due to congenital effects.

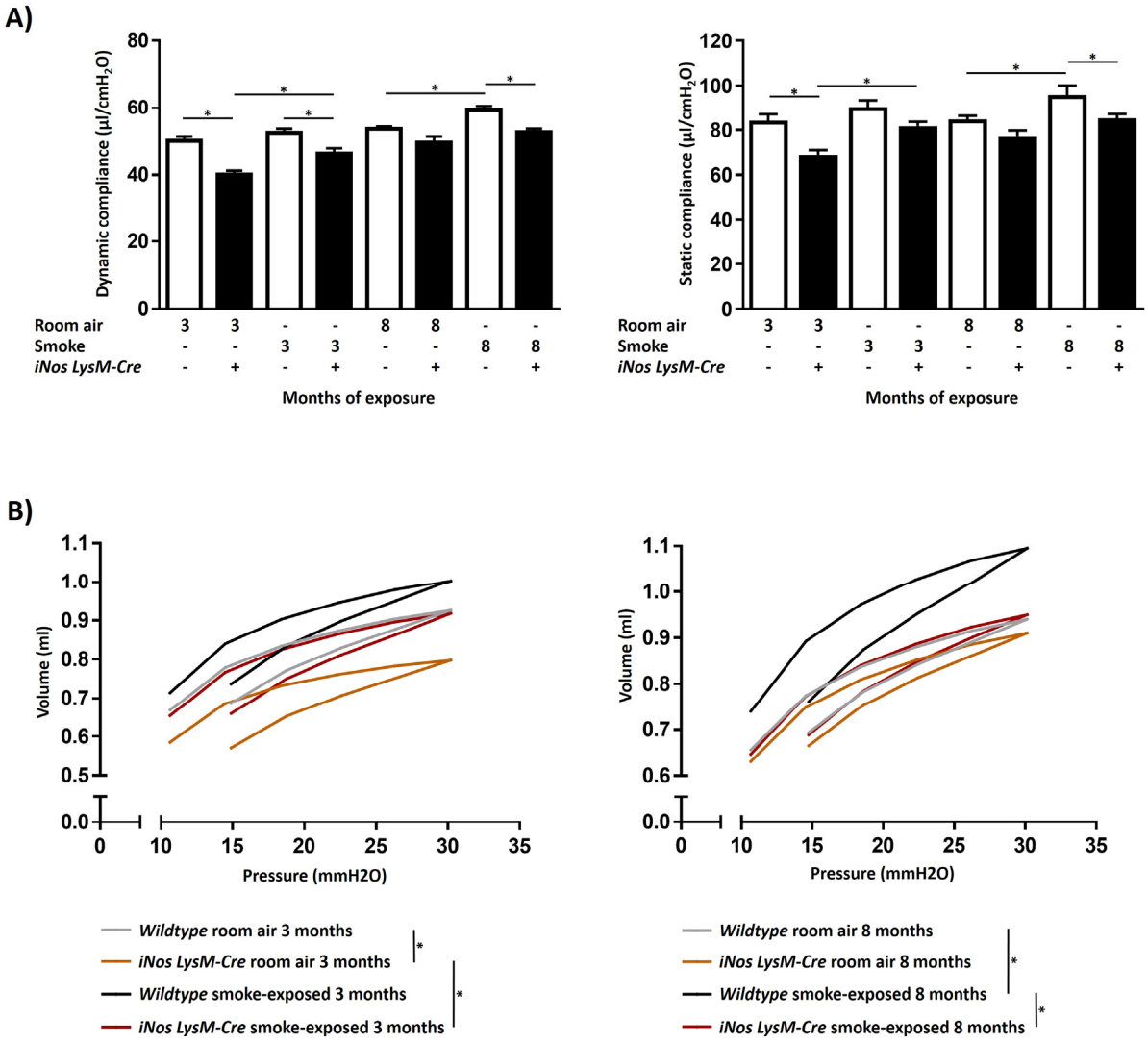

Figure 15. Chronic smoke exposure alters lung function in myeloid cell type-specific iNOS knockout mice.

Lung function (n=8-11) presented as A) dynamic and static compliance and B) respiratory pressure-volume (PV) loops. Graphs show mean ± SEM. *p < 0.05. Two-way ANOVA (with Tukey´s multiple comparison post-hoc test) was used.

Morphometric analysis including design-based stereology confirmed the development of emphysema (Figure 16), characterized by the decrease of the number of alveoli and

septal wall thickness, and increase of airspace, in both mouse strains to the same degree.

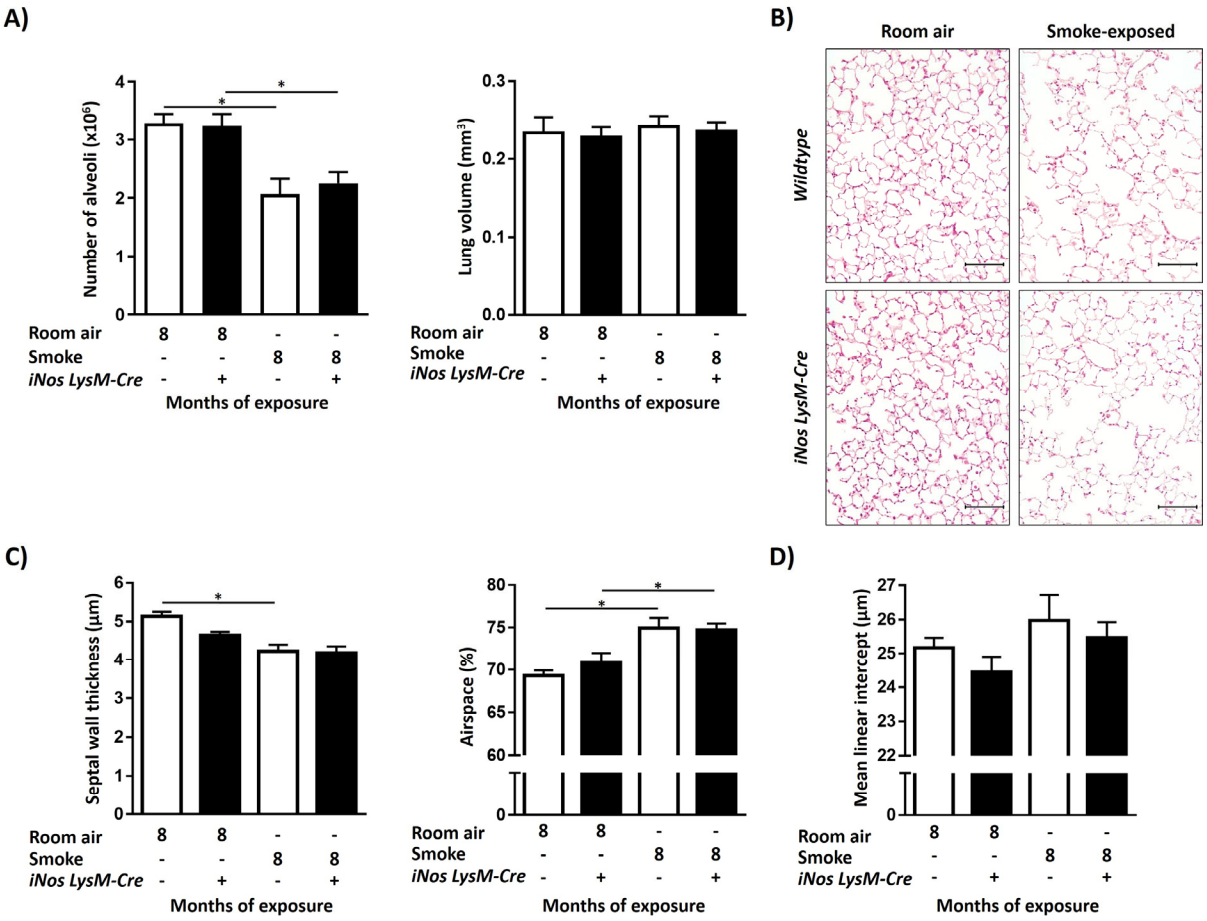

Figure 16. iNOS knockout mice develop emphysema after chronic smoke exposure.

A) Number of alveoli estimated by design-based stereology (left) and corresponding lung volumes (right) assessed by water displacement method (n=7-9). B) Representative images of lung sections from mice after 8 months of smoke exposure stained with hematoxylin-eosin (H&E, scale bar = 100 µm). C) Alveolar morphometry measurements (n=6-7) showing the septal wall thickness (left), percentage of airspace (middle) and mean linear intercept (right) in mice after 8 months of smoke exposure. Graphs show mean ± SEM. *p < 0.05. Two-way ANOVA (with Tukey´s multiple comparison post-hoc test) was used.

3.4. iNOS deletion in myeloid lineage affects the composition of inflammatory cells in the lungs after chronic smoke exposure

As the composition and phenotype of lung inflammatory cells are important factors in other forms of PH, I next examined the effects of myeloid cell-specific iNOS deletion on smoke-induced changes in immune cells in both BAL fluid and lung homogenate using flow cytometry. After 8 months of chronic smoke exposure, a significant increase in the portion of interstitial macrophages in $CD45^+$ cells was found in lung homogenates of smoke-exposed *Wt* animals compared to respective unexposed (room air) controls. However, this smoke-induced effect was absent in *iNos LysM-Cre* mice (Figures 17A&B). Considering the findings that the shift towards an M2-like phenotype of macrophages contributes to pulmonary vascular remodeling in other forms of PH, I next examined the expression of CD206, a marker of M2-like polarization, on interstitial macrophages found in lung homogenate after chronic smoke exposure. Accordingly, in *Wt* animals there was a significant increase in the expression of CD206, suggesting a smoke-induced shift towards an M2-like phenotype of interstitial macrophages. Importantly, expression of CD206 on interstitial macrophages in lungs of *iNos LysM-Cre* mice remained unchanged (Figures 17C&D).

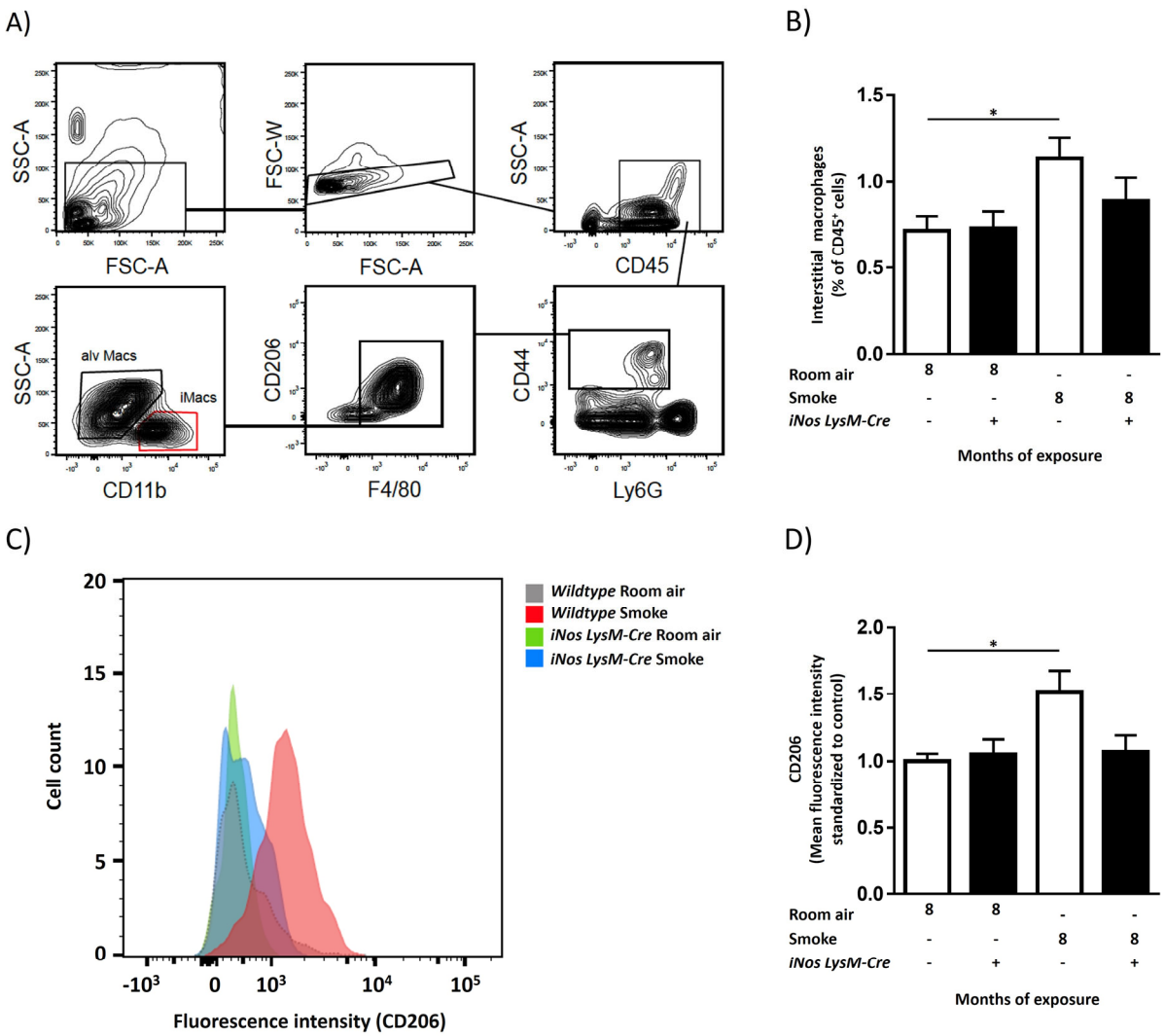

Figure 17. Myeloid cell-specific iNOS deletion prevents smoke-induced accumulation of interstitial macrophages and upregulation of CD206 (the marker of "M2-like" polarization) on these cells.

Mice were exposed either to smoke or room air for 8 months and macrophages in lung homogenates were analyzed by flow cytometry. A) Representative flow cytometry gating scheme, used to separate alveolar and interstitial macrophages (SSC: side scatter; FSC: forward scatter). B) Content of interstitial macrophages in the lungs of smoke-exposed mice and respective unexposed (room air) controls, assessed by flow cytometry and given as the percent of $CD45^+$ cells (n=4-5). C) Representative histogram showing $CD206^+$ cells in lungs of wildtype and myeloid cell-specific iNOS knockout mice. D) CD206 expression on interstitial macrophages (n=4-5), assessed by flow cytometry and given as the mean fluorescence intensity standardized to control. Graphs show mean ± SEM. *p < 0.05. Two-way ANOVA (with Tukey´s multiple comparison post-hoc test) was used for statistical analysis.

Interestingly, I found that the smoke-induced increase in the proportion of $CD4^+$ cells in $CD45^+$ cells found in lung homogenate was significantly higher in *Wt* compared to

iNos LysM-Cre animals (Figure 18A). Similarly, there was a tendency towards a higher smoke-induced increase in both $CD4^+$ and $CD8^+$ T cells in BALF of *Wt* compared *to iNos LysM-Cre mice* (Figure 18B).

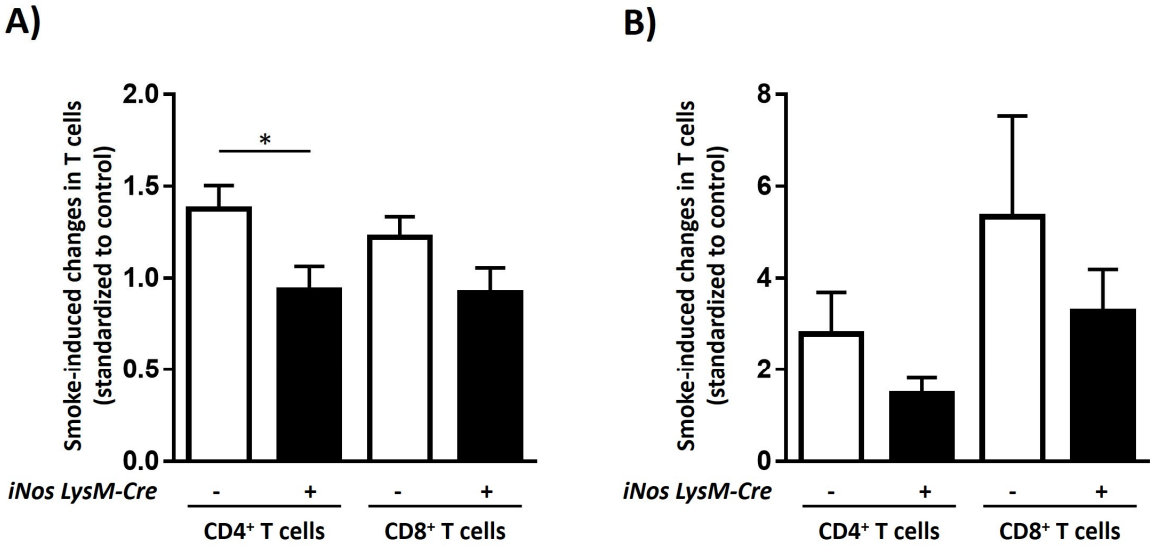

Figure 18. iNOS deletion in myeloid cells ameliorates smoke-induced changes in T cells in the lung homogenates and bronchoalveolar lavage fluid.

Flow cytometry analysis of: A) $CD4^+$ T lymphocytes and $CD8^+$ T lymphocytes found in lung homogenate of mice after 8 months of smoke exposure, B) $CD4^+$ T lymphocytes and $CD8^+$ T lymphocytes found in BALF from mice after 8 months of smoke exposure (n=4-5). All values are given as the percentage of $CD45^+$ cells standardized to non-exposed control. Graphs show mean ± SEM. *$p < 0.05$. An unpaired T-test was used.

3.5. iNOS deletion in myeloid cells does not affect the development of hypoxia-induced PH and right ventricular hypertrophy

As alveolar hypoxia caused by impairment of respiratory function can contribute to vascular remodeling in COPD (Chaouat et al., 2008), and M2 phenotype of macrophages is an important for the development of hypoxic PH (Vergadi et al., 2011), I investigated whether iNOS deletion in myeloid cells can also protect mice against PH after exposure to chronic hypoxia.

However, myeloid cell-specific iNOS knockout mice developed hypoxia-induced PH to the same level as observed in WT mice. This was evident from hemodynamic

measurements, determination of RV hypertrophy and the decrease of RV function (Figure 19).

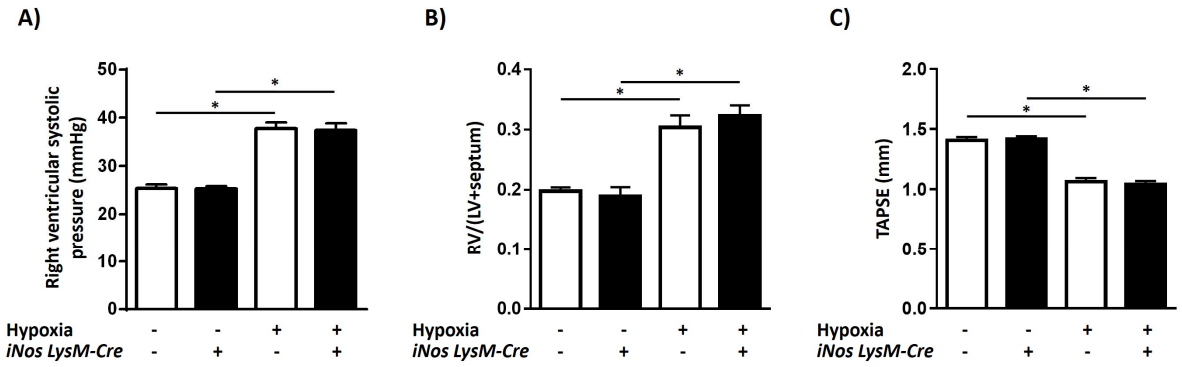

Figure 19. Myeloid cell-specific iNOS knockout does not protect against hypoxia-induced PH in mice.

Mice were exposed to either normobaric normoxia or hypoxia for 28 days. A) Right ventricular systolic pressure (n=6-8). B) Changes in the right ventricular structure shown as the ratio of the RV and the left ventricular plus septum (LV+septum) mass (n=6-8). C) Echocardiographic assessment of RV systolic function (n=6-8) depicted by means of tricuspid annular plane systolic excursion (TAPSE). Graphs show mean ± SEM. *p < 0.05. Two-way ANOVA (with Tukey´s multiple comparison post-hoc test) was used.

Accordingly, muscularization of small pulmonary vessels (20-70 µm in outer diameter) was increased in both *Wt* and *iNos LysM-Cre* mice after chronic hypoxia exposure compared to normoxic controls (Figure 20).

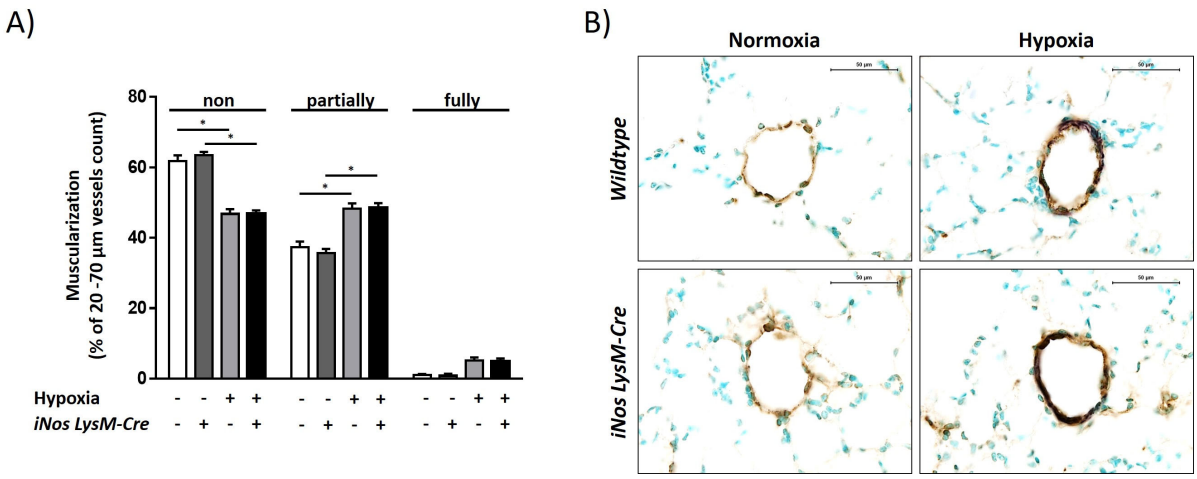

Figure 20. Myeloid cell-specific iNOS knockout does not prevent hypoxia-induced pulmonary vascular remodeling in mice.
Remodeling of the small pulmonary vessels (20-70 µm outer diameter) presented as A) the percentage of total vessel count, given for non-, partially- and fully-muscularized vessels after chronic hypoxia exposure (n=6-8), and B) representative images of lung sections from mice exposed to chronic hypoxia and respective normoxic controls, co-stained against α-smooth muscle actin (purple) and von Willebrand factor (brown) and counterstained using methyl green (green). Scale bars = 50 µm. Graph shows mean ± SEM. *p < 0.05. Two-way ANOVA (with Tukey´s multiple comparison post-hoc test) was used.

3.6. CSE treatment of M2 macrophages increases proliferation of co-cultured PASMC in an iNOS-dependent manner

Considering the prominent iNOS-dependent changes in portion and phenotype of infiltrating macrophages in lungs upon smoke exposure, I next investigated the effects of iNOS deletion on polarization and activity of murine BMDM *in vitro*. iNOS deficient macrophages upregulated the M1-signature genes when stimulated with IFN-γ and LPS, while the expression of the genes associated with M2 phenotype was also successfully elicited with IL-4 treatment (data not shown).

As iNOS deletion in macrophages had no apparent effect on the ability of macrophages to attain M1- or M2-polarization state, I sought to investigate if treatment of these cells with CSE affects the expression and release of mediators that could induce proliferation of PASMC. For all future treatments, I chose a 100 µM concentration of iNOS inhibitor, L-NIL, because it efficiently blocked NO production even in M1 macrophages without effects on cell viability (Figure 21A&B), and a CSE concentration of 1%, because it did not affect viability/metabolic activity of macrophages even during

prolonged exposure (Figure 21B, C&D). Of note, both iNOS inhibition and deletion seemed to mildly potentiate effects that high concentrations of CSE exert on metabolic activity/viability of M2 macrophages (Figure 21D).

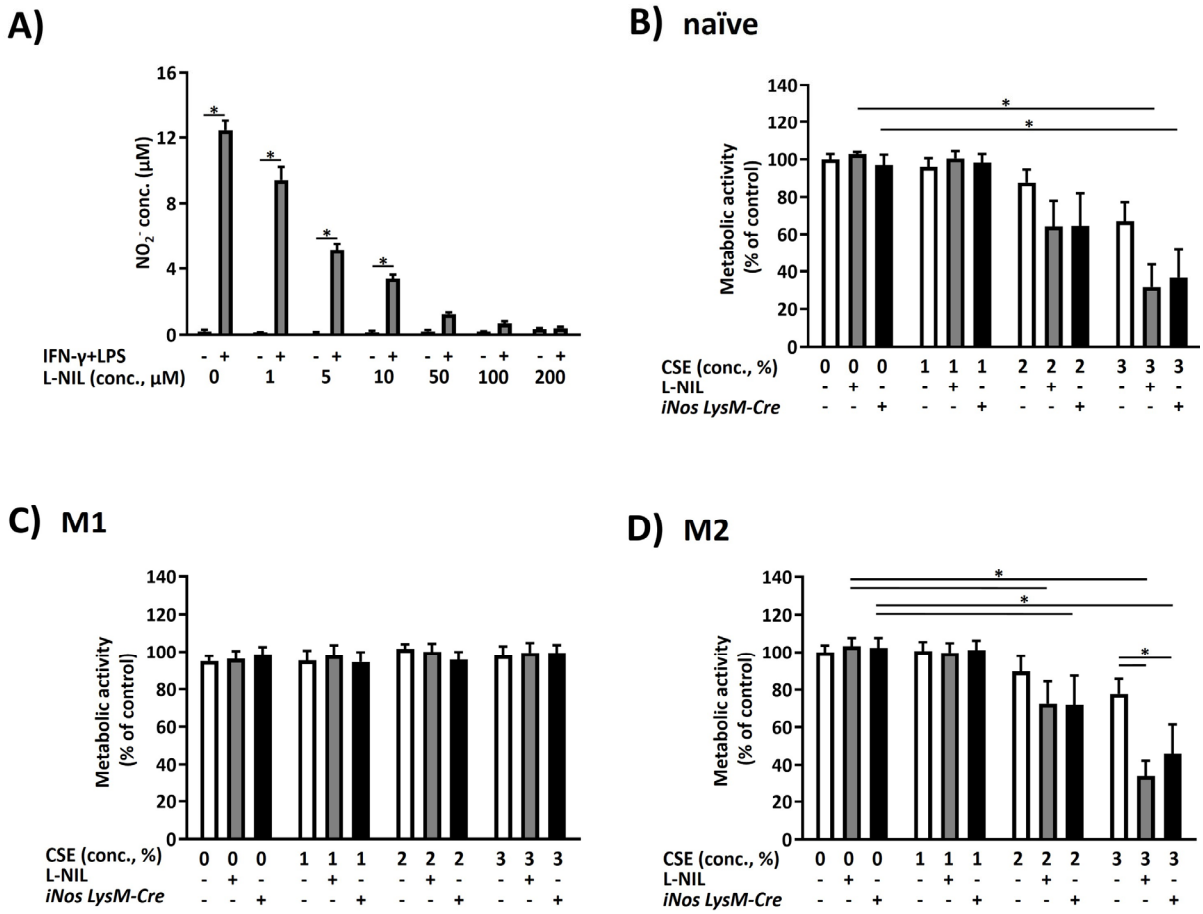

Figure 21. Analysis of iNOS- and cigarette smoke extract (CSE)-induced changes in monocultures of bone marrow-derived macrophages.

A) Inhibition of iNOS by N6-(1-iminoethyl)-L-lysine (L-NIL) in naïve and M1 polarized cells, assessed by the concentration of nitrite (NO_2^-) in the cell culture medium. B, C and D) Metabolic activity of control, iNOS-deficient and L-NIL-treated naïve (B), M1 (C) and M2 (D) macrophages after exposure to CSE, measured by alamarBlue assay and given as the percentage of control (n=6). Graphs show mean ± SEM. *p < 0.05. Two-way ANOVA (with Tukey´s multiple comparison post-hoc test) was used.

For investigating the effects of mediators released by CSE-stimulated BMDM on the proliferation of murine primary PASMC, I employed a Transwell system for co-culturing these two cell types. Pre-treatment of M2 (polarized using IL-4), but not M1 (polarized using IFN-γ and LPS) or naïve macrophages with CSE increased proliferation of PASMC in co-culture after 6 h (Figure 22A) and 24 h (Figure 22B). Importantly, deletion

of iNOS in M2 macrophages abolished the CSE-induced effect on PASMC proliferation. To investigate whether this effect depends on communication between macrophages and PASMC, I quantified the proliferation of PASMC treated with CM from macrophage monocultures. However, the proliferation of PASMC upon treatment with macrophage CM was only slightly increased, and iNOS- or CSE-dependent changes were not observed (Figures 22C and D), suggesting that at least in this setup cross-talk between PASMC and macrophages is an important factor.

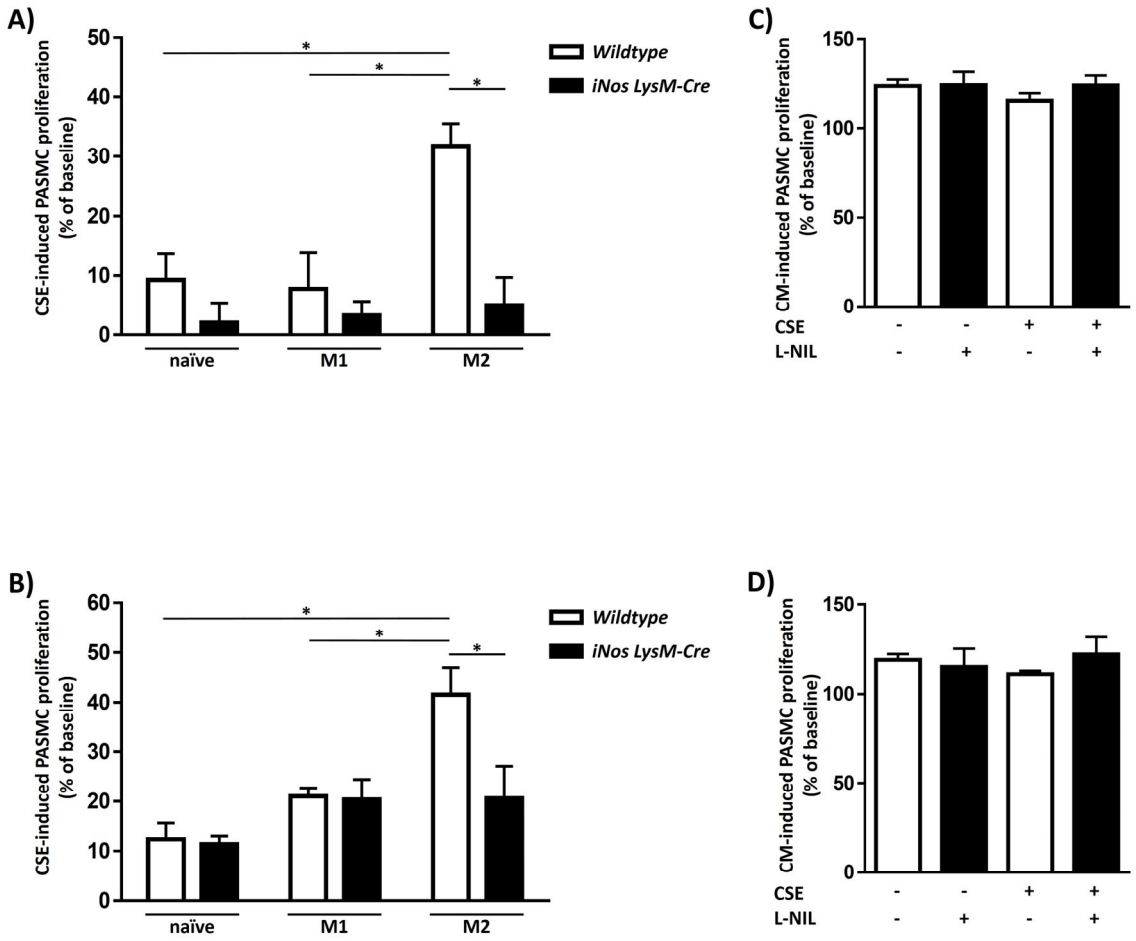

Figure 22. iNOS activity in macrophages affects PASMC proliferation *in vitro*.

A) and B) Pulmonary artery smooth muscle cells (PASMC) were co-cultured with bone marrow-derived naïve, M1- or M2-polarized and macrophages pre-treated for 3 h with 1% cigarette smoke extract (CSE). Proliferation of PASMC in co-cultures with macrophages assessed by BrdU assay after A) 6 h (n=4), and B) 24 h (n=5), standardized to the control PASMC and given as the difference from the co-culturing with non-CSE exposed controls. C) and D) Proliferation of mouse pulmonary artery smooth muscle cells (PASMC) during 24 h of incubation with culture-conditioned medium from C) M1- or D) M2-polarized macrophages pre-treated with CSE, measured by BrdU incorporation assay and given as the percentage of control (n=4). Graphs show mean ± SEM. *p < 0.05. Two-way ANOVA (with Sidak´s multiple comparison post-hoc test) was used.

Next, I investigated the influence of co-culturing macrophages and PASMC on the migration of PASMC by using CM from co-cultures. Like in the case of proliferation of co-cultured (Figure 22) or co-culture CM-treated PASMC (Figure 27), pro-migratory effect of co-culture CM on PASMC was increased by CSE treatment of M2 macrophages and abolished by iNOS inhibition in these cells. In contrast, although CM from M1 co-cultures also potentiated PASMC migration, CSE- or iNOS-dependent changes were not observed (Figure 23A and B).

Additionally, I examined the effects of CM from co-cultures on apoptosis of PASMC in monoculture. CM from both M1 and M2 macrophage-containing co-cultures decreased PASMC apoptosis. The described anti-apoptotic effect was, however, CSE- and iNOS-independent (Figure 23C and D).

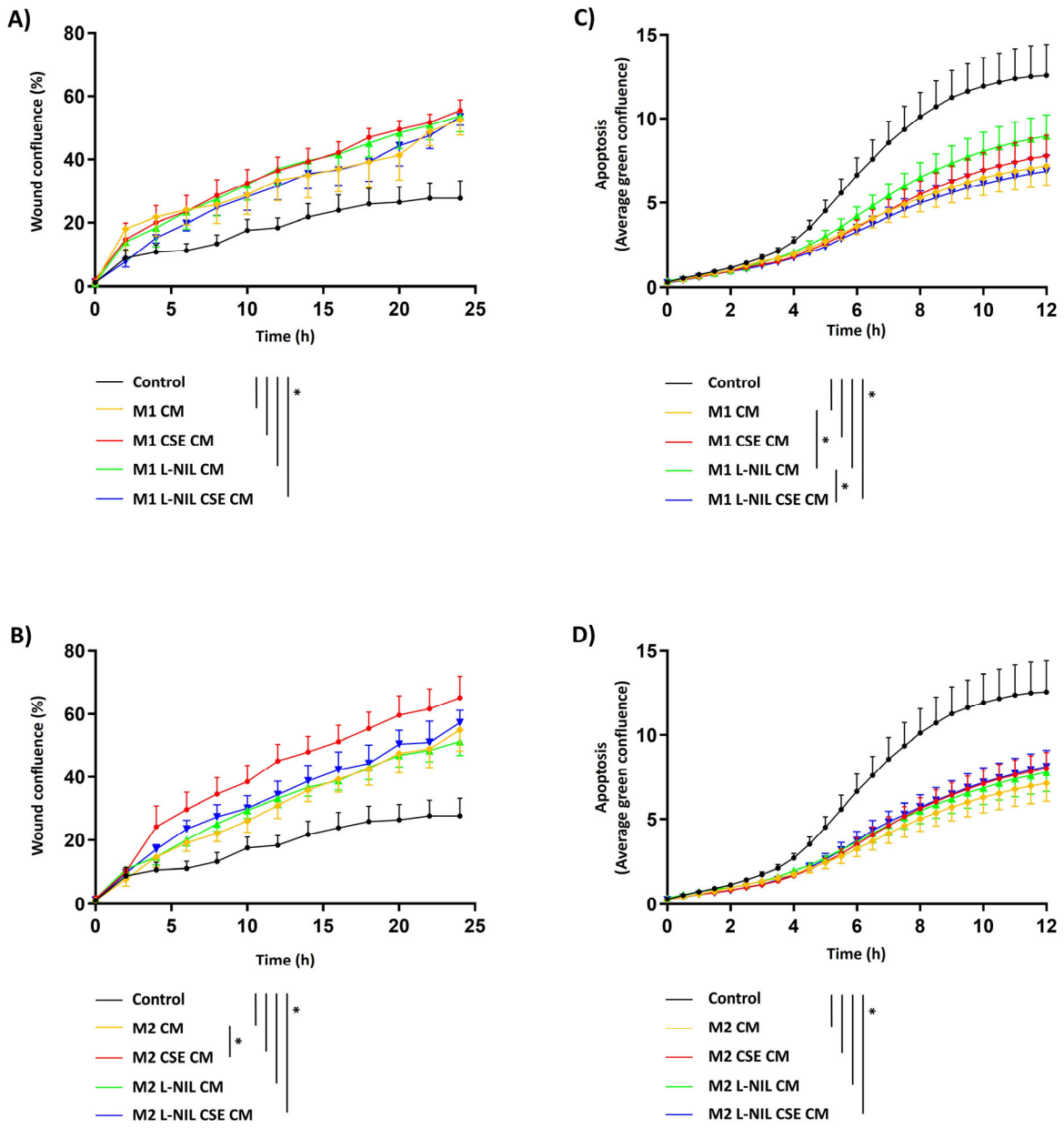

Figure 23. iNOS activity in macrophages affects PASMC migration, but not apoptosis *in vitro*.

A) and B) Migration of the PASMC treated with the conditioned medium from co-cultures of PASMC and CSE and/or L-NIL-treated A) M1 (n=5) and B) M2 macrophages (n=5), given as the wound confluence. C) and D) Apoptosis of the PASMC treated with the conditioned medium from co-cultures of PASMC and CSE and/or L-NIL-treated C) M1 (n=5) and D) M2 macrophages (n=5), given as the confluence of cells labeled with annexin. CM from PASMC monocultures served as a control. Graphs show mean ± SEM. *p < 0.05 at least in the final time point. Two-way ANOVA (with Sidak´s multiple comparison post-hoc test) was used.

3.7. IL-4 signaling might contribute to CSE-induced iNOS-dependent proliferation of PASMC in co-cultures

Next, I wanted to investigate iNOS-dependent changes in autocrine and/or paracrine signals released by CSE-exposed M2 macrophages co-cultured with PASMC that might account for the observed changes in PASMC proliferation. Cytokine profiling in the co-culture medium revealed decreased concentrations of IL-4 in co-cultures of PASMC with M2 macrophages treated with the iNOS inhibitor L-NIL (Figures 24A&B). Functionally, the application of recombinant IL-4 in co-cultures of PASMC with M2 macrophages reversed the reduction of CSE-induced proliferation caused by L-NIL-treatment of M2 macrophages (Figure 24C). As IL-4 was previously reported to increase TGF-β expression (Elovic et al., 1998; F. Q. Wen et al., 2002), I quantified this growth factor in the conditioned medium from the co-cultures. Total TGF-β concentration was changed neither by CSE exposure nor iNOS knockout in macrophages (Figure 24D), leaving however the possibility of its differential activation of in an IL-4-dependent manner, as previously reported (Kumar et al., 2015). Thus, I sought to determine the activation of the mitogenic signaling pathways downstream of TGF-β.

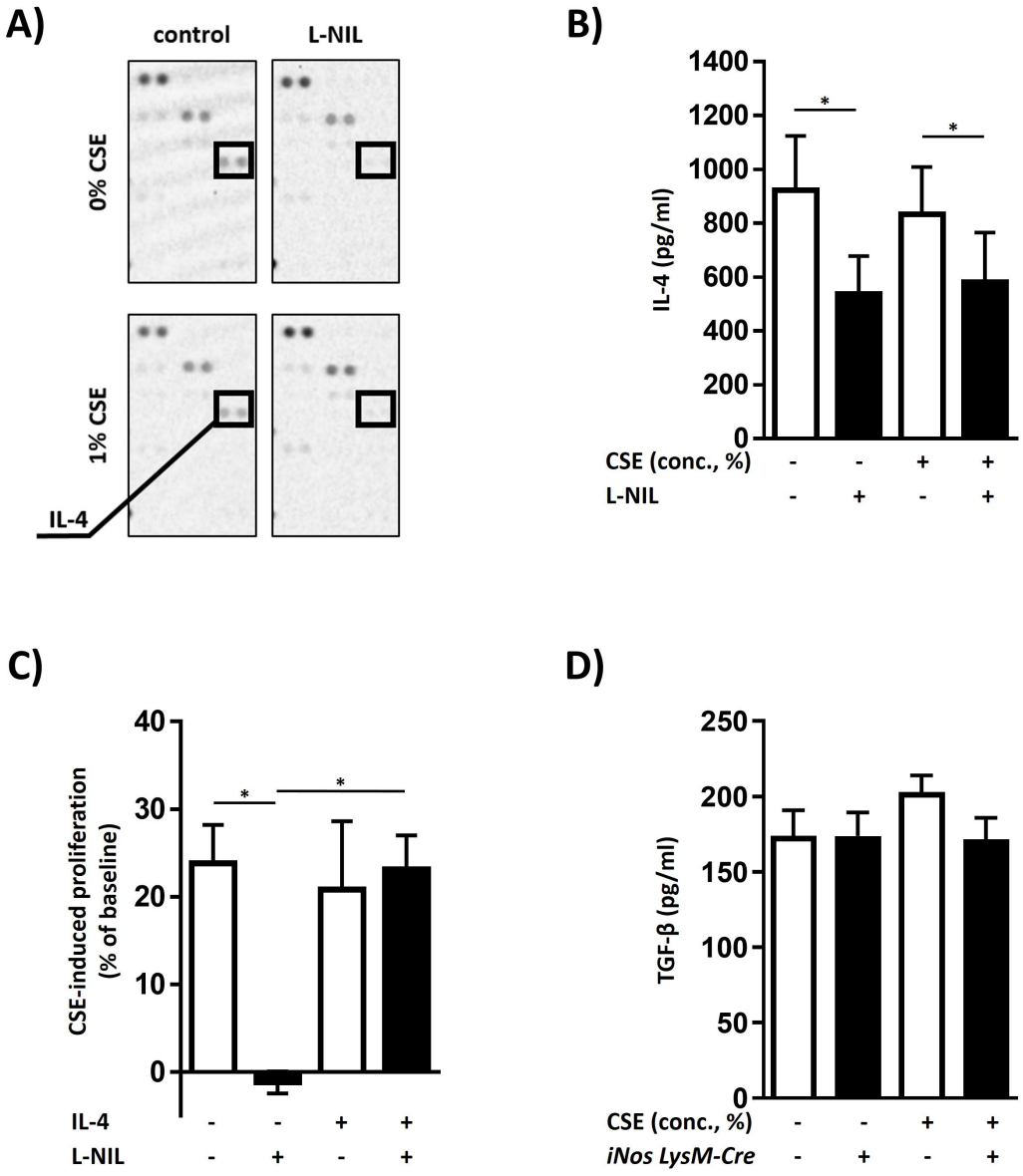

Figure 24. Interleukin (IL)-4 is implicated in CSE-induced pro-proliferative signaling in co-cultures of M2 cells and PASMC.

A) and B) IL-4 in the conditioned medium collected after 24 h of co-culturing of M2 macrophages with PASMC, assessed by A) cytokine array and B) ELISA assay (n=7). C) CSE-induced proliferation of PASMC in co-cultures with control or L-NIL-treated M2 macrophages, in the absence or presence of IL-4 in the co-culture medium (n=6). Proliferation was assessed during 24 h of co-culturing, using BrdU assay and standardized to the control PASMC. Data are given as the difference from the co-culturing with non-CSE exposed controls. D) Transforming growth factor (TGF)-β in conditioned medium from co-cultures of M2 macrophages with PASMC, quantified by ELISA assay. Graphs show mean ± SEM. *$p < 0.05$. Two-way ANOVA (with Sidak´s multiple comparison post-hoc test) was used.

3.8. MAPK signaling pathways mediate CSE-induced iNOS-dependent proliferation of PASMC

Investigation of the proliferative pathways with the focus on those that can be activated by TGF-ß revealed that p-38 and extracellular signal-regulated kinase (ERK) 1/2 are differentially phosphorylated in PASMC co-cultured with L-NIL treated macrophages compared to controls.

On the one hand, I detected an increase in phosphorylation of ERK in PASMC upon co-culturing with CSE-treated M2 macrophages, which was absent in co-cultures with L-NIL-treated phagocytic cells (Figure 25A). These results are consistent with my *in vivo* data, where smoke exposure increases ERK phosphorylation in lung homogenates (Figure 25B) and in pulmonary vessels captured by laser-microdissection (Figure 25C) of WT animals only. Surprisingly, even after 24 h, lower ERK phosphorylation could be observed in PASMC co-cultured with L-NIL-treated M2 cells independent of CSE treatment (Figure 25A).

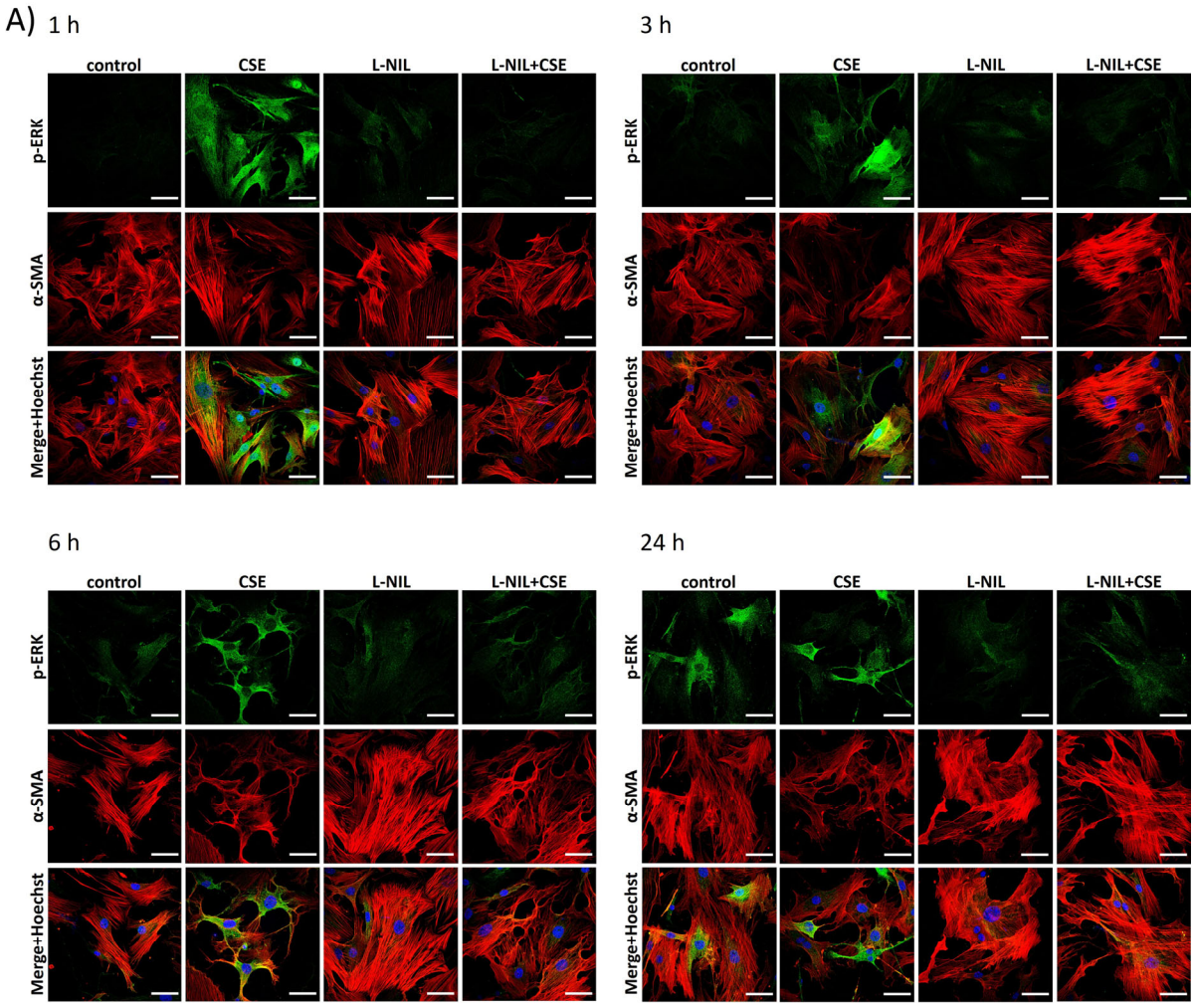

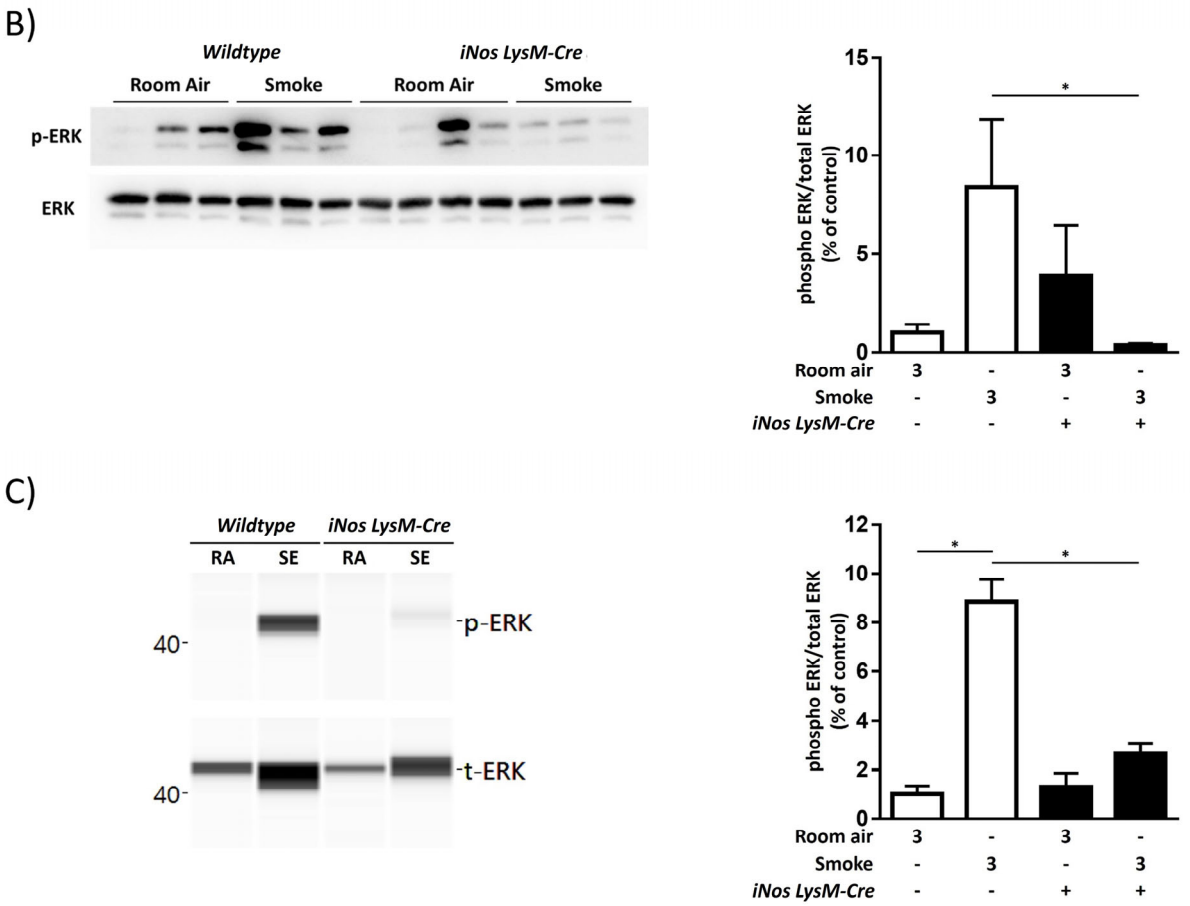

Figure 25. ERK phosphorylation in co-cultured PASMC and mouse lungs depends on iNOS expression in myeloid cells.

A) Representative images showing PASMC co-cultured with CSE- and/or L-NIL treated M2 cells for 1 h, 3 h, 6 h and 24 h, stained for phosphorylated extracellular signal-regulated kinase (ERK, green), α-smooth muscle actin (α-SMA, red) and counterstained with Hoechst (blue). Scale bar = 50 µm. B) Western blot analysis of the ERK phosphorylation in lung homogenates of animals exposed to smoke for 3 months and respective unexposed controls (n=6-7), given as the ratio between phosphorylated and total ERK and standardized to control. C) Western blot analysis of the ERK phosphorylation in pulmonary vessels captured by laser microdissection from lungs of animals exposed to smoke for 3 months and respective unexposed controls (n=3). Data are given as the ratio between phosphorylated and total ERK, standardized to control (unexposed WT). Graphs show mean ± SEM. *p < 0.05. Two-way ANOVA (with Tukey´s multiple comparison post-hoc test) was used.

On the other hand, phosphorylation of p38 kinase at all investigated time-points was lower in PASMC co-cultured with L-NIL-treated M2 macrophages, whereas CSE pre-treatment of M2 cells did not influence p38 activation in co-cultured PASMC (Figure

26A). However, p38 phosphorylation increased in lung homogenates of smoke-exposed WT animals compared to unexposed controls, and this effect was abolished by iNOS knockout in myeloid cells (Figure 26B).

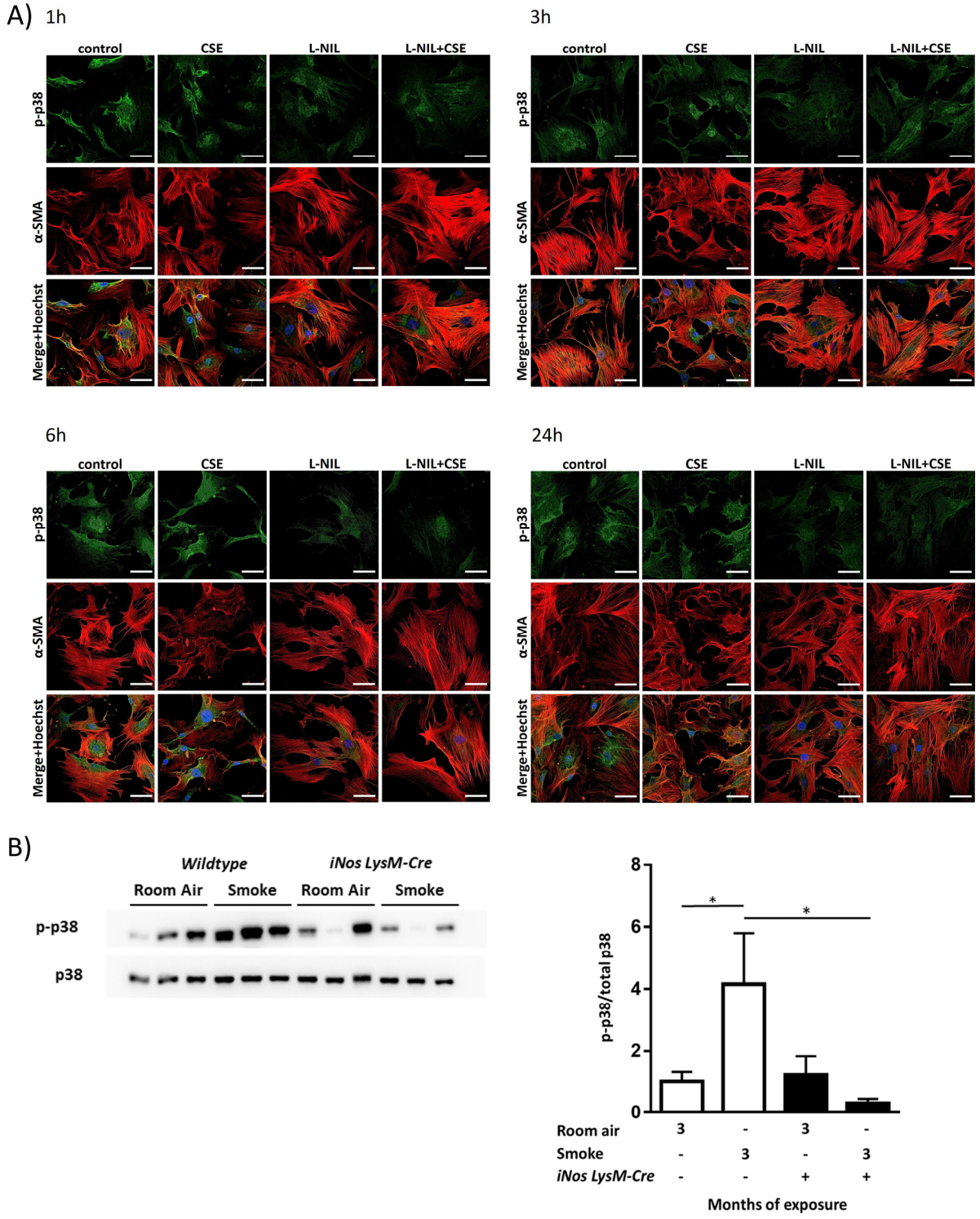

Figure 26. Phosphorylation of p38 in co-cultured PASMC and mouse lung homogenates depend on iNOS expression in myeloid cells

A) Representative images showing PASMC co-cultured with CSE- and/or L-NIL treated M2 cells for 1 h, 3 h, 6 h and 24 h, stained for phosphorylated p38 kinase

(green), α-smooth muscle actin (α-SMA, red) and counterstained with Hoechst (blue). Scale bar = 50 µm. B) Western blot analysis of the p38 phosphorylation in lung homogenates of animals exposed to smoke for 3 months and respective unexposed controls (n=6-7), given as the ratio between phosphorylated and total p38 and standardized to control. Graph shows mean ± SEM. *p < 0.05. Two-way ANOVA (with Tukey´s multiple comparison post-hoc test) was used.

The fact that the ERK phosphorylation in early time-points of co-culturing strongly resembled PASMC proliferation in this setup suggested a functional role of this pathway in CSE- and iNOS-dependent pro-proliferative signaling from M2 macrophages. Therefore, I investigated whether ERK inhibition affected PASMC proliferation when treated with co-culture CM. Indeed, the ERK1/2 inhibitor SCH772984 prevented the increase in PASMC proliferation induced by CM from co-cultures of PASMC with CSE-pretreated M2 cells. This effect was similar to the effect of iNOS inhibition (Figure 27).

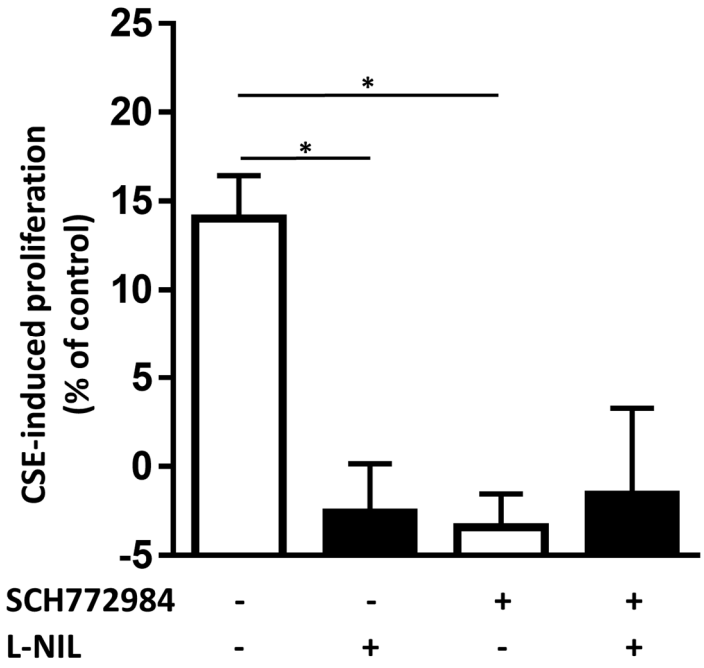

Figure 27. ERK inhibition in PASMC counteracts proliferative signaling from adjacent CSE-treated M2 macrophages.
Proliferation of PASMC treated with ERK inhibitor SCH772984 and conditioned medium (CM) from co-cultures of PASMC and CSE- and/or L-NIL treated M2 macrophages, assessed by BrdU assay. The proliferation is standardized to the control (treatment with PASMC CM) and given as the difference between the effects of CM from CSE-exposed and unexposed co-cultures. Graph shows mean ± SEM. *p < 0.05. Two-way ANOVA (with Sidak´s multiple comparison post-hoc test) was used.

3.9. iNOS$^+$ and CD206$^+$ macrophages accumulate in close proximity of remodeled vessels in the lungs of COPD patients

To investigate the relevance of the described findings for human COPD, I performed double staining of human lung sections for the macrophage marker CD68 and iNOS and found an increased number of iNOS-expressing macrophages in the proximity of the remodeled vessels in COPD patients when compared to donors (Figure 28).

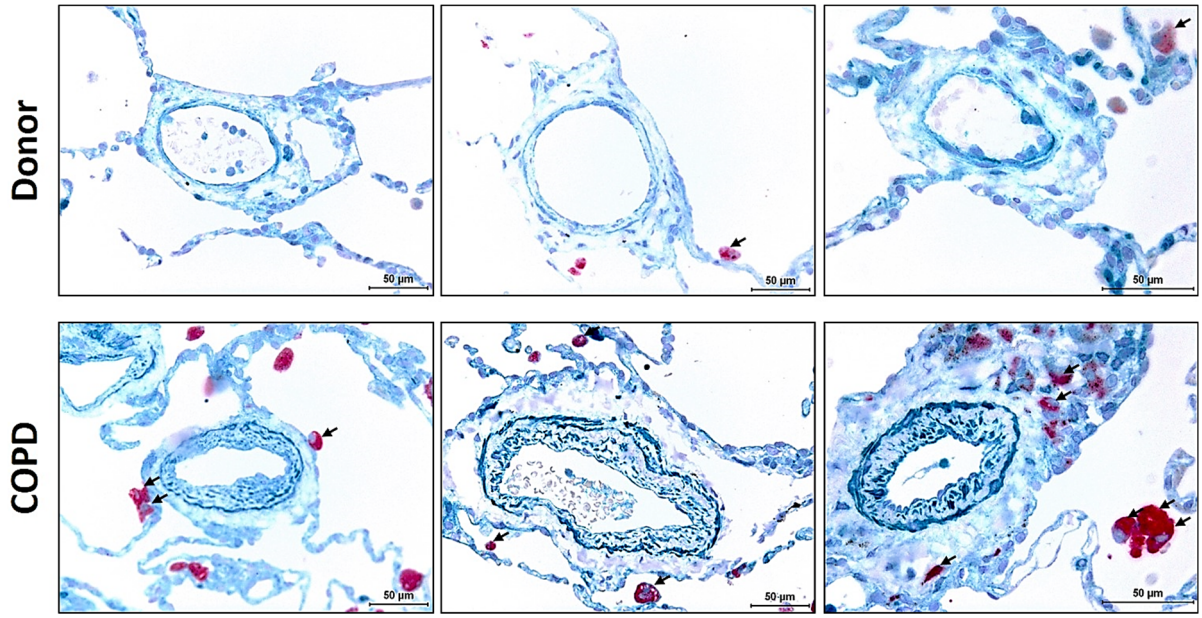

Figure 28. iNOS$^+$ macrophages accumulate in the close proximity of remodeled vessels in the lungs of COPD patients.
Representative images of lung sections from donors and COPD patients are presented. Co-staining of iNOS (green) and CD68 (red). Hematoxylin was used for counterstaining. Arrow: CD68$^+$iNOS$^+$ cells. Scale bar = 50 µm.

Additionally, I stained human COPD lungs for CD68 and CD206, a protein highly expressed by alternatively activated M2-like macrophages, and found numerous double-positive cells around the remodeled vessels in COPD lungs (Figure 29), supporting my hypothesis derived from the mouse data of an important role of M2 macrophages for pulmonary vascular remodeling.

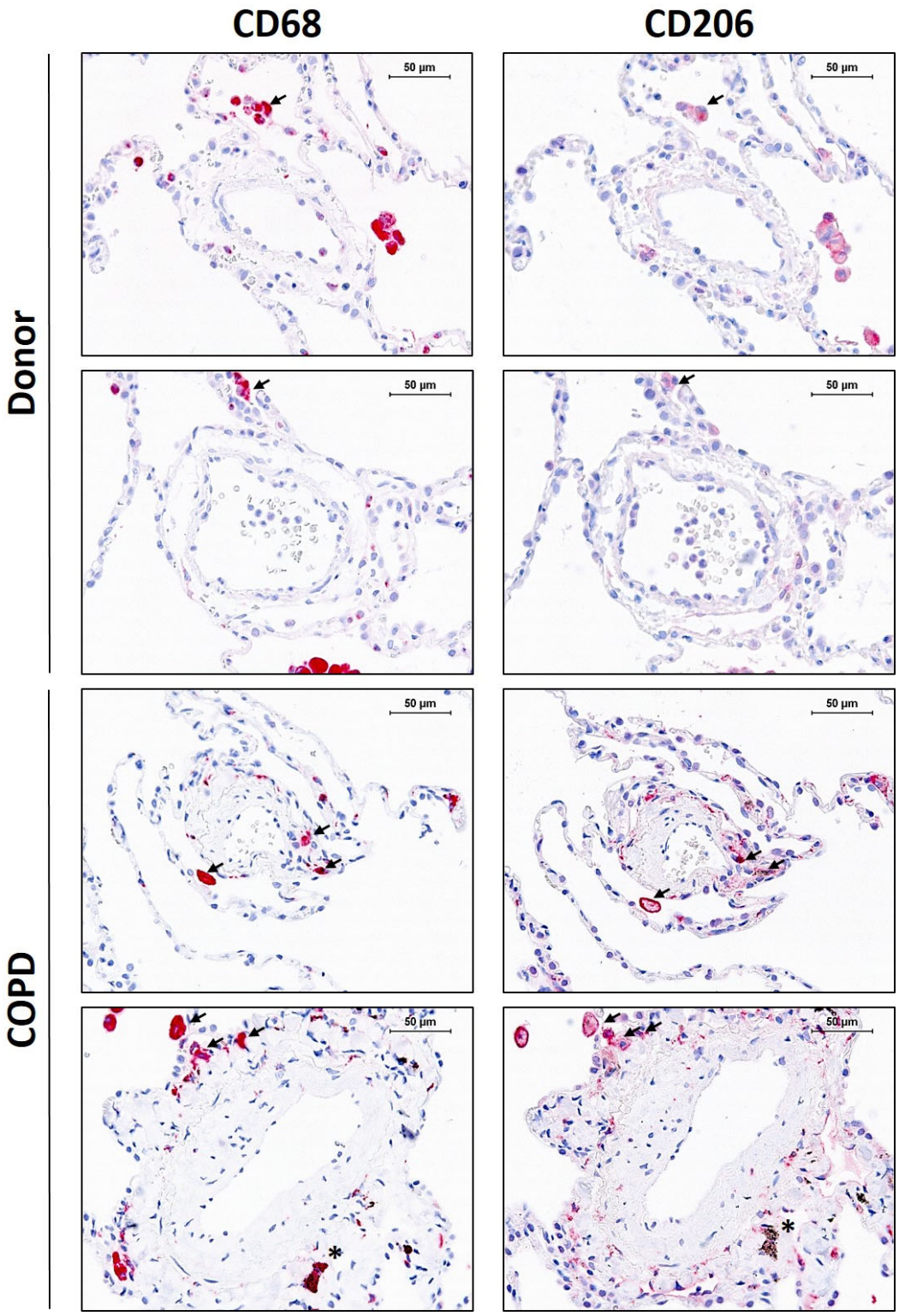

Figure 29. CD206^{+} macrophages accumulate in the close proximity of remodeled vessels in the lungs of COPD patients.

Representative images of serial lung sections from donors and COPD patients stained for CD68 (red, left) and CD206 (red, right), and counterstained with hematoxylin. Arrow: CD68^{+}CD206^{+} cells. Asterisk: CD68^{+}CD206^{-} cells. Scale bar = 50 µm.

3.10. ERK and p38 signaling pathways are activated in remodeled pulmonary vessels in COPD lungs

Since phosphorylation of ERK and p38 was elevated in PASMC co-cultured with WT M2 macrophages and in the lungs of smoke-exposed WT mice, I wanted to investigate whether these pathways are active in remodeled vasculature in lungs of COPD patients. Immunohistochemical staining for phosphorylated forms of ERK and p38 kinase showed the positive signal located in medial layer of the remodeled vessels in COPD lungs (Figure 30).

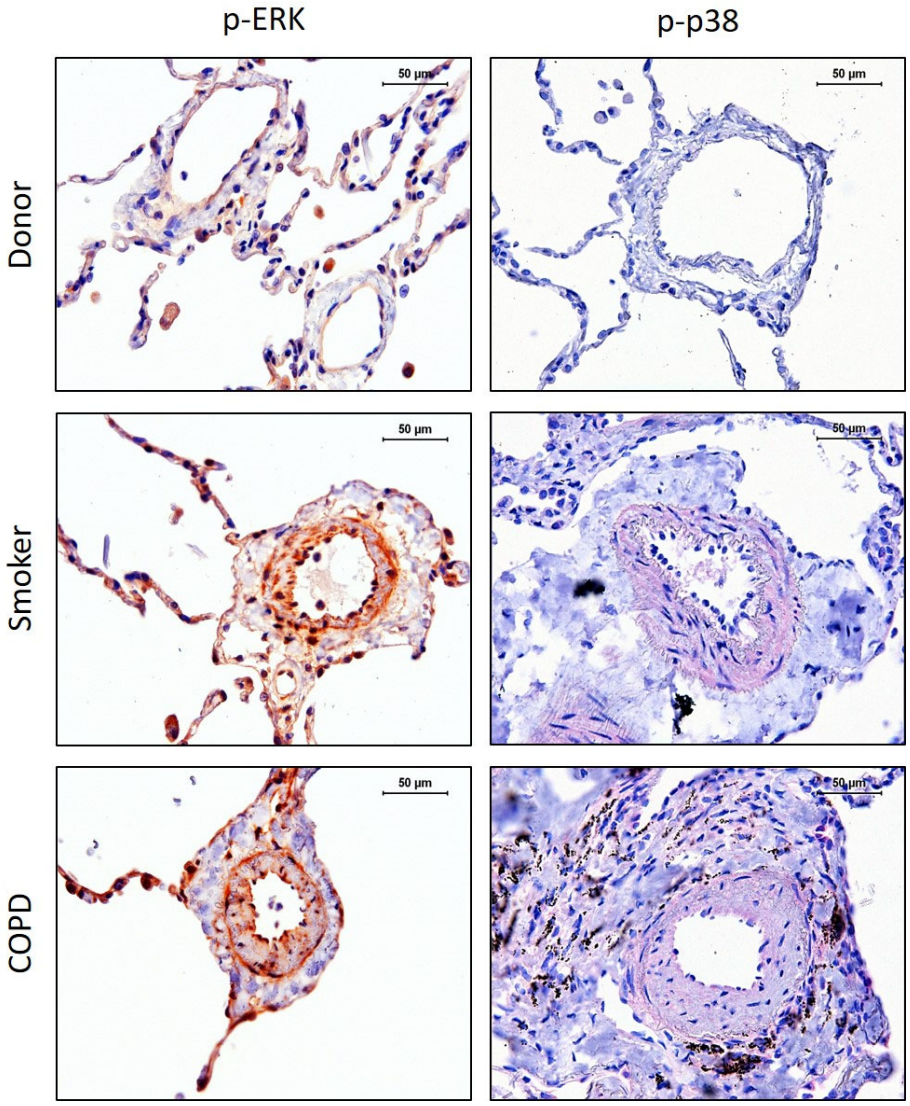

Figure 30. Phosphorylated forms of ERK and p38 kinases are present in remodeled vessels in the lungs of COPD patients.

Representative images of serial lung sections from donors and COPD patients stained for phosphorylated extracellular signal-regulated kinase (ERK) (brownish, left) and phosphorylated p38 kinase (red, right). Scale bar = 50 µm.

4. DISCUSSION

While severe, out-of-proportion PH is rarely present in COPD patients, mild to moderate elevation of mPAP is a common finding for this disease. Importantly, resting mPAP above 20 mmHg, which according to some estimations is present in up to 90% of cases (Scharf et al., 2002; Thabut et al., 2005), imposes higher mortality and morbidity on COPD patients (Douschan et al., 2018; Kessler et al., 1999; Kovacs et al., 2014; Medrek et al., 2017). Surprisingly, a recent study showed that Group 3 PH patients (with underlying lung disease) have worse prognosis than any other PH group patients including PAH (Hurdman et al., 2012). Similarly, enlarged pulmonary arteries were found to be a better baseline predictor of exacerbations than any lung function parameter (Wells et al., 2012). Despite the clinical relevance of PH in COPD, existing PAH therapies are not recommended for most COPD patients and can even lead to severe complications of this disease.

Pulmonary vascular remodeling, as the underlying cause of increased pulmonary vascular resistance and elevated mPAP, has long been considered a consequence of impaired respiratory function. Indeed, in late-stage COPD, lack of oxygen may result in hypoxia-driven pulmonary vascular remodeling. However, over the last decade, convincing evidence suggested that pulmonary vascular remodeling in COPD is not secondary to hypoxia, but rather an early phenomenon of the disease and a possible driver of parenchymal destruction (Gredic et al., 2020; Weissmann, 2018). This line of investigation was mainly initiated by the finding that pulmonary vascular remodeling, resembling the changes in PH patients, occurs in smokers who had not yet developed COPD (Santos et al., 2002). Investigations in rodent models of smoke exposure supported this time-course of pathological events in COPD, as pulmonary vascular alterations preceded changes in lung function and emphysema development (Ferrer et al., 2009; Seimetz et al., 2011; Wright & Churg, 1991). This novel concept emphasized the need for understanding the pathophysiology of COPD-PH, as the efficient treatment for vascular alterations could prevent or even contribute to the reversal of emphysema.

The group in which the current thesis was done previously identified inducible nitric oxide synthase (iNOS) as an essential enzyme for the development and reversal of smoke-induced PH and emphysema, and showed that iNOS expression in bone marrow-derived cells drives pulmonary vascular remodeling, while emphysema

development depends on iNOS expression in non-bone marrow cells (Seimetz et al., 2011). However, it remained unclear which bone marrow-derived cell type drives smoke-induced pulmonary vascular remodeling and what the respective mechanism is. On the one hand, this intriguing observation could be explained by a derivation of a portion of PASMC from bone marrow cells (Sata et al., 2002). Alternatively, iNOS expression in non-vascular cell types could be contributing to pulmonary vascular remodeling in COPD.

The hypothesis of the current dissertation proposes that pathological signaling underlying smoke-induced pulmonary vascular remodeling is triggered by elevated iNOS expression in myeloid cells and that a similar process as in the mouse may occur in humans.

My study revealed that myeloid cell-specific deletion of iNOS 1) is sufficient to prevent the development of smoke-induced PH, but not emphysema, 2) counteracts the increase in expression of the marker of M2 polarization (CD206), on interstitial macrophages in smoke-exposed lungs. Additionally, results of my *in vitro* experiments demonstrated that 3) crosstalk between macrophages and PASMC includes factors that induce PASMC proliferation through the ERK pathway activation and whose expression, activity or release by M2-polarized macrophages is modulated by exposure to smoke and, importantly, iNOS activity (Figure 31). Crucially, despite the involvement of M2 macrophages, I showed that 4) observed changes in inflammatory cells and pulmonary vasculature are hypoxia-independent but rather caused directly by cigarette smoke, as myeloid-cell iNOS did not play a role in the development of hypoxic PH.

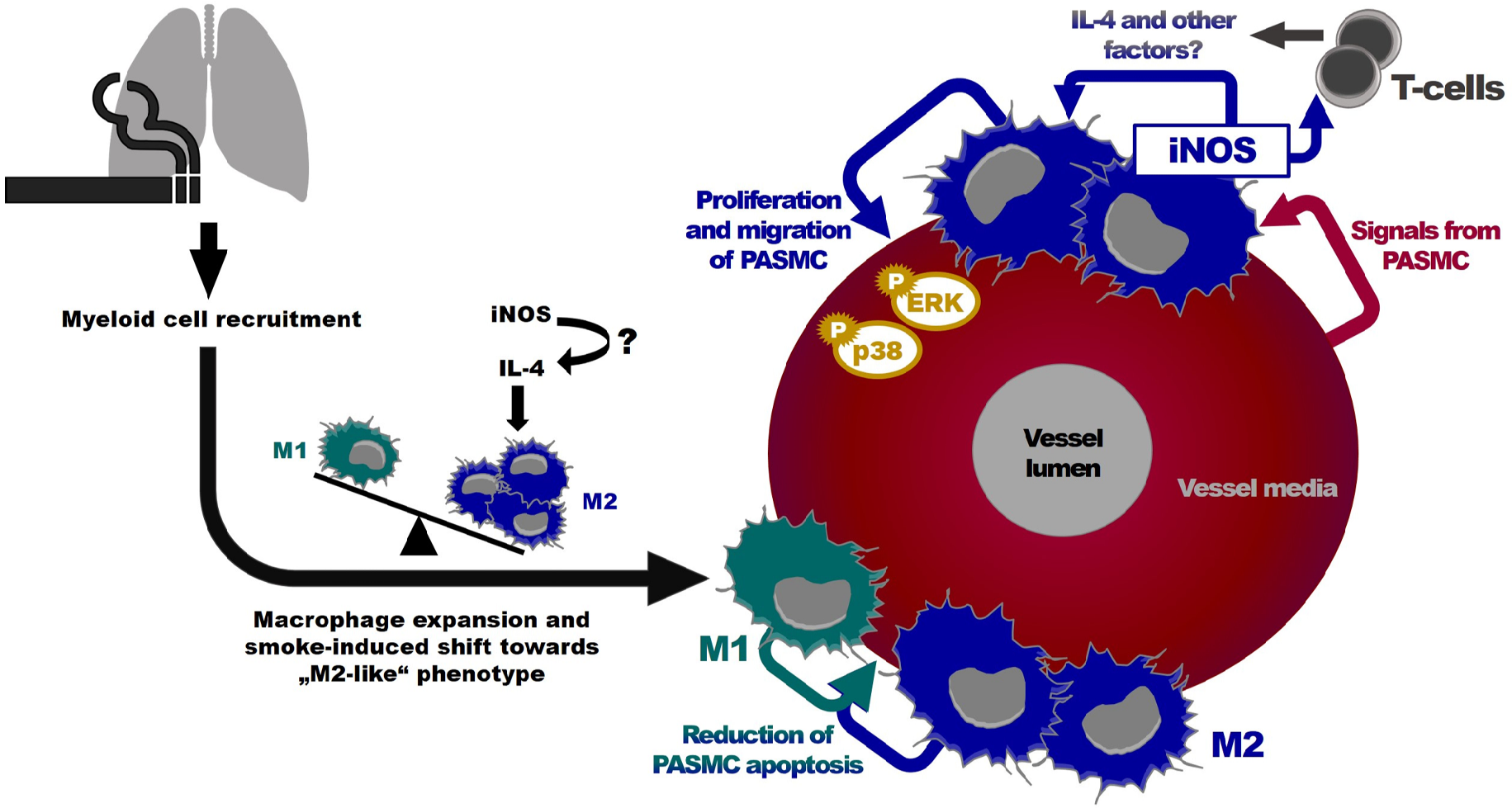

Figure 31. Scheme of the proposed pathological mechanism.

Communication between M2 macrophages and PASMC that leads to PASMC proliferation is potentiated by smoke exposure of macrophages and depends on iNOS expression in those cells and IL-4 concentration in the environment.

IL-4: Interleukin-4. iNOS: Inducible nitric oxide synthase. PASMC: Pulmonary artery smooth muscle cell. ERK: Extracellular signal-regulated kinase. P: Phosphate group.

4.1. Dichotomy of iNOS signaling in COPD pathology

My data demonstrate that iNOS expression in myeloid cells is responsible for development of smoke-induced PH, pulmonary vascular remodeling and RV hypertrophy, but not emphysema. These findings are supported by the abovementioned study from our group (Seimetz et al., 2011). Namely, experiments with bone marrow transplantation revealed dichotomy in pathological consequences of iNOS upregulation in smoke-exposed animals, showing that pulmonary vascular remodeling and emphysema can occur independently, driven by iNOS expression in different cell types. These and my novel findings suggest that smoke-induced pulmonary vascular remodeling may not explicitly lead to the development of emphysema. However, they offer a new, refined picture of the pathological cascade in COPD. On the one hand, the absence of pulmonary vascular remodeling and hemodynamic changes in the myeloid cell-specific knockout animals does not necessarily mean prevention of all smoke-induced molecular changes in PASMC. On the other, Seimetz et al. demonstrated that emphysematous changes were driven by iNOS upregulation in the lung compartment, which was localized primarily in the lung vasculature. Taken together, these findings support the recent hypothesis (Gredic et al., 2020; Karnati et al., 2021; Seimetz et al., 2011; Weissmann, 2018) that molecular alterations in the vasculature (and not vascular remodeling *per se*) are driving parenchymal destruction. Such a situation would explain emphysema development in the absence of pulmonary vascular remodeling, which occurred in the myeloid cell-specific iNOS knockout mice.

4.2. Macrophages as a driver of smoke-induced PH

Although the pivotal role of inflammatory cells and their mediators in other forms of PH is well substantiated by experimental evidence from rodent models and by findings in patients, only a few studies have addressed the role of inflammation in COPD-PH. As already mentioned in the introduction, it has been found that systemic levels of inflammatory mediators such as TNF-α, CRP, IL-6 and IL-17 are increased in COPD patients with PH (Eddahibi et al., 2006; Joppa et al., 2006; Wang et al., 2019). In addition, the study from Peinado and colleagues reported a correlation between the number of inflammatory cells in the adventitia and the degree of pulmonary vascular remodeling (Peinado et al., 1999). In animals, a few substances known to affect inflammatory cell function, such as myeloperoxidase inhibitors and statins, were able

to prevent or reverse smoke-induced pulmonary vascular remodeling (Churg et al., 2012; J. H. Lee et al., 2005; Wright et al., 2011). My study, however, to the best of my knowledge, is the first to implicate macrophages as the inflammatory cells critically involved in smoke-induced PASMC proliferation and consequent pulmonary vascular remodeling. I used a driver line targeting all myeloid cells, which by its specificity goes beyond previous studies from bone-marrow transplantation experiments and rules out obstacles of such an experimental approach as the effect of radiation and reconstitution (Ajami et al., 2007; Ferreira et al., 2019; Kierdorf et al., 2013; Seimetz et al., 2011). My experiments revealed that macrophages seem the most important candidates from myeloid cells, because 1) of the important role of iNOS in these cells (Forstermann & Sessa, 2012; Nathan & Hibbs, 1991), 2) their presence in pulmonary vessels upon smoke exposure, and 3) their effect on PASMC proliferation and migration in my *in vitro* experiments. In this regard, I demonstrated that there is a crosstalk between macrophages and PASMC, which drives the proliferation of those vascular cells and can be modulated by targeting M2 macrophage-derived iNOS. In agreement with my findings, a recent study reported a two-way communication between M2 macrophages and PASMC, which relies on both CCR2 and CCR5 and drives proliferation of PASMC *in vitro* and pulmonary vascular remodeling in IPAH and animal hypoxia and SU5416/hypoxia models of PH *in vivo* (Abid et al., 2019). Although my data support the concept of M2 macrophage-derived signals as important contributors to pulmonary vascular remodeling, I was not able to find smoke- or iNOS-dependent changes in the levels of CCR2 and CCR5 (unpublished observations), suggesting that there is indeed a unique molecular signature of the vasculature in COPD-PH, as previously reported by the group (Seimetz et al., 2011).

4.3. iNOS as a modulator of inflammatory cell phenotype and composition in smoke-induced PH

Results from my *in vitro* system suggest that iNOS deletion in M2 macrophages abolishes smoke-induced proliferation and migration of co-cultured PASMC. While this alone could explain the observed protection of myeloid cell-specific iNOS knockout animals against smoke-induced PH, the anti-proliferative outcome could be further amplified *in vivo* by two important effects of myeloid cell-specific iNOS deletion on the composition of inflammatory cell infiltrates in lungs of smoke-exposed mice.

First, a smoke-induced increase in the expression of an M2-like polarization marker CD206 was not observed on lung interstitial macrophages of the knockout mice, suggesting protection against the smoke-induced shift towards M2 macrophage phenotype, either by interference with polarization or accumulation mechanisms of these cells.

In this regard, recent and partially contradicting reports suggest that iNOS can indeed influence the polarization of expressing macrophages. Van den Bossche and colleagues reported that iNOS expression prevents repolarization of macrophages from M1 to M2 phenotype, presumably through the inhibitory effect on oxidative phosphorylation (Van den Bossche et al., 2016). Conversely, Lu and colleagues recently showed that myeloid cell-derived iNOS suppresses M1 macrophage polarization and speculated that it supports dedifferentiation and phenotypic plasticity of these cells, without affecting the M2 macrophage population (G. Lu et al., 2015). Although the concept that iNOS is a regulator of gene expression phenotype of macrophages can be easily applied to my findings, none of the described scenarios can completely explain the protection of myeloid cell-specific iNOS knockout against smoke-induced PH or differential smoke-induced effects of WT and iNOS-deficient M2 macrophages on PASMC proliferation in co-culture. Having in mind the dynamic nature of macrophage phenotypes, one can conceive that micro-environmental factors such as smoke and signals from PASMC *in vitro*, and additionally the age of animals, apoptosis of lung epithelial cells and presence of other inflammatory cell types and mediators *in vivo* contribute to specific behavior of macrophages observed in my model systems.

The importance of iNOS activity for the accumulation of M2 macrophages of even more interest, as iNOS is considered a classical marker of M1 polarization. However, the picture of iNOS as M1-macrophage-specific, potent antimicrobial defense is being modified and enriched by findings that small amounts of iNOS-derived NO can affect the phenotype of other inflammatory cells, in which expression of this enzyme remains on a low level and has not even been detected until recently. For example, Jianjun et al. demonstrated that iNOS expression in T cells suppresses Th17 responses, through nitration of tyrosine residues within the transcription factor retinoic acid receptor-related orphan receptor (ROR)-γT and consequent impairment of its ability to activate expression of *Il-17* gene (Jianjun et al., 2013). Similarly, iNOS derived NO is required for the functional maturation of NK cells and their responsiveness to IL-12, through the

regulation of auto-kinase activity of the Janus tyrosine kinase (TYK)-2 downstream of IL-12 receptor (Diefenbach et al., 1999). Having in mind these examples of non-canonical, immunomodulatory roles of iNOS, it is conceivable that small amounts of iNOS-derived NO in M2 macrophages have important effects on the activity and phenotype of these cells and consequently contribute to their accumulation and their pathological role in smoke-induced pulmonary vascular remodeling.

Additionally, I showed that IL-4 levels are reduced in co-cultures with iNOS-deficient M2 macrophages. If these *in vitro* data are transferrable to the *in vivo* situation, myeloid cell-specific iNOS deletion might lead to the impaired accumulation of M2 macrophages through their proliferation *in situ*, as IL-4 was shown to be essential for this process (Jenkins et al., 2011).

The second important consequence of myeloid cell-specific iNOS deletion on the composition of inflammatory cell infiltrates is the preserved proportion of T cells in the population of lung immune cells, as opposed to the situation in smoke-exposed WT mice, where the portion of T cells in lung inflammatory infiltrates is increased. Although assessment of absolute numbers is difficult, due to smoke-induced dynamic changes of most cell populations in the lungs, this could suggest that the lungs of smoke-exposed knockout mice have decreased T cell numbers. This finding is of interest as an increased number of T cells is implicated in other forms of PH (Bonnet et al., 2007; Pullamsetti et al., 2011; Tuder et al., 1994) and found in perivascular inflammatory infiltrates of COPD patients (Peinado et al., 1999; Saetta et al., 1999). Macrophage derived-iNOS could influence endothelial activation and T cell diapedesis, as described for the T cell extravasation into tumors. Alternatively, changes in T cell populations might be the consequence of the abovementioned, still largely uninvestigated role of macrophage-derived iNOS on T cell differentiation and activity. However, as Lysozyme M also labels a small portion of T and B cells, a more specific driver line is needed for the further investigation of this phenomenon (Ye et al., 2003).

4.4. The distinctiveness of smoke-induced inflammatory milieu leading to pulmonary vascular remodeling in COPD

Alveolar hypoxia resulting from the impaired respiratory function has long been considered the main cause of pulmonary vascular remodeling seen in COPD patients. My identification of M2 macrophages, which were previously implicated in the development of hypoxia-induced PH (Abid et al., 2019; Amsellem et al., 2017; Vergadi

et al., 2011), as a critical cell type driving smoke-induced pulmonary vascular remodeling could indeed suggest that this pathological event is driven by the similar, hypoxia-dependent mechanism. However, I investigated this possibility and showed that myeloid cell type-specific iNOS knockout animals develop hypoxia-induced PH and RV hypertrophy. In other words, although M2 macrophages are implicated in the development of both smoke- and hypoxia-induced PH, manipulation of iNOS pathway in these cells prevents the first, but not the latter pathology. Here, it is important to emphasize the phenotypical plasticity of macrophages and the spectrum of activation states that these cells are able to acquire. With this in mind, it is not surprising that specific pathways will be activated and preferentially involved in (pathological) signaling depending on external stimuli and microenvironmental milieu such as one present in hypoxia- or smoke-challenged lungs. Additionally, these results are in line with the recent hypothesis that pulmonary vascular remodeling is an early pathological event in COPD that occurs prior to the alveolar destruction and resulting hypoxemia. . In this regard, the group in which this thesis was performed previously showed that 8 months of cigarette smoke exposure in mice did not lead to hypoxemia (Seimetz et al., 2011). The proposed sequence of pathological events is substantiated by evidence from the animal model (Ferrer et al., 2009; Seimetz et al., 2011; Seimetz et al., 2020; Wright & Churg, 1991) and humans (Peinado et al., 1999; Santos et al., 2002); however, to the best of my knowledge only NOXO1-based redox signaling pathway has been described as unique for smoke-induced pulmonary vascular remodeling so far (Seimetz et al., 2020). This makes my study among the first to provide evidence for the smoke-specific signaling events in the remodeling of the pulmonary vasculature. My findings, if transferable to the human situation, can have an impact on the development of new treatment strategies for COPD-PH.

4.5. Signaling pathways mediating the smoke-induced, inflammation-driven pulmonary vascular remodeling

Regarding the potential molecular mechanisms, my results point to a regulatory role of iNOS in macrophage polarization, in response of M2 macrophages to smoke and in pro-proliferative and pro-migratory communication between PASMC and M2 macrophages. The ability of M2 macrophages to potentiate PASMC proliferation and migration was previously reported (Abid et al., 2019; Huang et al., 2020; Vergadi et al., 2011), but to my best knowledge I am the first to investigate the effects of smoke and

iNOS activity in this regard. Since the pro-proliferative and pro-migratory effects of these two factors were observed only in co-cultures of PASMC with M2, and not M1 macrophages, mechanistically they are probably not caused by the production of large amounts of nitric oxide and consequent nitrosative stress, but rather by protein nitration as a regulatory posttranslational modification. Contrary to the prevailing, simplified picture of iNOS as a source of large amounts of NO for the antimicrobial defense, recent evidence from T cells and NK cells suggest that this enzyme is well capable of fine, tight regulation of intracellular signaling pathways through posttranslational modification of their components (Bogdan, 2015). Such a situation was observed before for the regulation of Janus tyrosine kinase (TYK)-2 downstream of IL-12 receptor and retinoic acid receptor-related orphan receptor (ROR)-γT, in the processes of functional maturation of NK and T-cells, respectively (Diefenbach et al., 1999; Jianjun et al., 2013). The role of iNOS in the precise regulation of signaling pathways in M2 macrophages is further supported by the findings from the co-culture system. Here, iNOS deletion abolished smoke-induced proliferative signaling of M2 cells to PASMC in co-culture, but did not influence anti-apoptotic effects that conditioned medium from such co-cultures exerted on PASMC, as it would be the case that it merely suppressed cellular metabolism or reduced viability of expressing M2 cells. This is of importance, as I noted that iNOS deficiency in naïve and M2-polarized macrophages slightly potentiates inhibitory effect of cigarette smoke on metabolic activity of these cells. This finding is surprising at a glance since NO is a known inhibitor of the complex IV (Sarti et al., 2003), a component of the mitochondrial respiratory chain. However, the result can be explained by the anti-apoptotic effect that activation of the NO-sGC-cGMP pathway has in macrophages (Shaw et al., 2009).

Importantly, judging from my *in vitro* experiments, the regulatory role of iNOS in pro-proliferative signaling of M2 cells is limited to specific conditions, which include both exposure of macrophages to smoke and cross-communication between macrophages and PASMC. However, immunohistochemical staining of human lungs suggests that similar conditions exist in COPD, as the macrophages that accumulated in close vicinity to remodeled vessels in the lungs of COPD patients were positive for iNOS and CD206.

Going beyond, my findings implicate IL-4 as the factor that controls responsiveness of M2 macrophages to CSE stimulation and thus regulates their pro-proliferative signaling to PASMC. The connection between iNOS and IL-4 is another intriguing observation

that needs further investigation. As iNOS is known to promote glycolysis (Li et al., 2017; Van den Bossche et al., 2016) and lactate stimulates IL-4 and IL-13 production (Wagner et al., 2016), it is conceivable that metabolic changes are the missing link connecting these two important players in CSE-induced PASMC proliferation.

Importantly, Kumar and colleagues recently demonstrated that IL-4, acting in concert with IL-13, plays a key pathogenic role in TGF-β mediated, *Schistosoma mansoni*-induced PAH. The literature suggests that IL-4 and IL-13 (independently or together) can directly stimulate TGF-β production in human bronchial epithelial cells, and that IL-4 alone can up-regulate TGF-β expression in human eosinophils (Elovic et al., 1998; F. Q. Wen et al., 2002). However, in accordance with my findings, the authors did not find increased levels of total TGF-β in *Schistosoma mansoni*-induced PAH; instead, they propose that M2 macrophages receiving IL-4/IL-13 signals activate a latent form of this growth factor via a mechanism that has yet to be elucidated. Importantly, TGF-β is known to induce vascular smooth muscle cell proliferation through activation of ERK and p38 pathways (Suwanabol, Seedial, Shi, et al., 2012; Suwanabol, Seedial, Zhang, et al., 2012). Naturally, other M2-macrophage derived growth factors such as PDGF (Ntokou et al., 2021) and FGF-2 (Jetten et al., 2014) might also be implicated in MAP kinase-mediated PASMC proliferation. Therefore, the exact nature of the upstream signaling factors leading to the smoke-induced and iNOS-dependent PASMC proliferation remains to be elucidated by further studies. This is especially true, as levels of IL-4 in conditioned medium collected after 24 h of co-culturing were reduced by iNOS inhibition but unchanged by smoke exposure. This can be explained either by dynamic changes of the IL-4 release during co-culturing (like it was the case with ERK phosphorylation in co-cultured PASMC), or by the involvement of yet unidentified player in this signaling cascade.

Regarding the role of MAP kinase pathways in COPD, they were previously implicated in emphysema development, endothelial cell apoptosis and inflammation (Gaffey et al., 2013; Mercer et al., 2004; Renda et al., 2008; Zong et al., 2018), but until now they were never investigated in the context of PASMC proliferation in COPD-associated pulmonary vascular remodeling. Here, I showed an iNOS-dependent upregulation of ERK in co-cultured PASMC *in vitro*, as well as increased phosphorylation of ERK in mouse pulmonary vessels and lung homogenates. Importantly, inhibition of this pathway in PASMC successfully counteracted pro-proliferative signals from M2 macrophages in my co-culture model. Crucially, I demonstrated the relevance for

human COPD, as the immunohistochemical staining for phosphorylated ERK revealed a positive signal located in the remodeled vessels in lungs of COPD patients.

iNOS inhibition in M2 macrophages also reduced p38 phosphorylation in co-cultured PASMC independent of smoke – an effect that probably does not play a role in the *in vitro* co-culture system. However, it still might be important *in vivo*, where smoke exposure induces accumulation of otherwise scarce perivascular inflammatory cells, which is a prerequisite for described pathological cross-talk of M2 macrophages and PASMC. In support of this idea speaks increased p38 phosphorylation in smoke-exposed WT mice, which could, nevertheless, also come from increased inflammation in smoke-exposed lungs (Renda et al., 2008). However, as augmented p38 phosphorylation was also notable in the medial layer of the pulmonary vessel wall in human COPD, one could speculate that vasculature is least in part responsible for the observed changes in lung homogenates. It is important to highlight that my findings are in line with the previously described role of ERK and p38 signaling pathways in other forms of PH (Church et al., 2015; Jin et al., 2000; J. Lu et al., 2004; Schermuly et al., 2005; Wilson et al., 2015).

4.6. Limitations of the study

Most important findings of this study were supported by the data from human COPD samples. Nevertheless, one has to bear in mind that the employed mouse model has several limitations that urge for the additional confirmations of the transferability of presented findings to the human situation. The pitfalls of the mouse model involve absence of chronic bronchitis and minimal small airway remodeling after chronic smoke exposure in this species. Moreover, smoke-induced loss of respiratory surface in mice is similar to a mild form of emphysema commonly found in human smokers and progresses with the prolonged exposure to smoke, but in general remains subtler than seen in patients with GOLD stage IV COPD (Wright et al., 2008). Importantly, mouse lungs have much higher regenerative potential than human, although it was recently reported that lung regeneration is also possible in humans (Butler et al., 2012; Fehrenbach et al., 2008). However, regarding the smoke-induced PH, which was the focus of this study, the mouse model reflects the time-course and main pathophysiological features of human pathology.

An additional limitation of my study is the fact that iNOS knockout was tested as a preventive intervention, and not as a therapy, which would be closer to the potential

application in COPD patients. Further research is needed to test whether the knockout of macrophage-derived iNOS can also reverse smoke-induced vascular alterations. Such a study should preferably employ a mouse line that would enable more specific targeting of monocytic cells. As already stated before, *iNos LysM-Cre* mouse line by specificity goes beyond previously employed bone-marrow transplantation strategy, but its use nevertheless implies *iNos* knockout in leukocytes, DCs, as well as in small proportion of lymphocytes and alveolar type II cells (Abram et al., 2014; McCubbrey et al., 2017; J. Shi et al., 2018).

Finally, as already mentioned in the introduction, the promotor of the *iNOS/iNos* gene has considerable differences between species, which may impact its responsiveness to different macro- and microenvironmental stimuli tested in this study. Further research, employing human peripheral blood mononuclear cells, PASMC and precision-cut lung slices is planned to overcome this uncertainty.

4.7. Future experimental and clinical perspectives

Despite the fact that even mild elevation in PAP is associated with increased mortality and morbidity in COPD patients, efficient and specific treatment options are missing. Available drugs, developed primarily for the treatment of PAH, might even be harmful when considered for COPD-PH, due to the detrimental effects on V/Q matching and arterial oxygenation. Moreover, the novel concept that vascular alterations are an early phenomenon in COPD pathology and possible driver of parenchymal destruction additionally emphasizes the need for an efficient treatment option for COPD-PH, as curative therapies for vascular (molecular) alterations could prevent or even contribute to the reversal of emphysema.

Pharmacological iNOS inhibition gave promising results in preclinical experiments with smoke-exposed animals, where it prevented and reversed the development of PH and emphysema. However, responsible iNOS-expressing cell types and underlying molecular mechanisms are still insufficiently understood, which hinders the development of efficient therapies. A few iNOS inhibitors have been clinically evaluated for the treatment of various human pathologies (Bailey et al., 2007; Brindicci et al., 2007; Brindicci et al., 2009; Connor et al., 2012; Hansel et al., 2003; Hellio le Graverand et al., 2013; Singh et al., 2007), but not a one so far has been approved for human use. The insufficient understanding of iNOS' complex functions and the dual modalities of iNOS and NO in a disease state (i.e. concentration-dependent protective

versus harmful effects) might be in part responsible for the iNOS inhibition failures in states like sepsis and pain (Cinelli et al., 2020). Importantly, another possible shortcoming of the iNOS inhibition strategy in conditions such as cardiogenic shock, where it showed promise in preclinical studies and small human trials, might be the lack of the specificity of the employed inhibitors (Bailey et al., 2007; Cinelli et al., 2020; Heemskerk et al., 2009). This might be of even greater importance when considered for the treatment of pulmonary hypertension, having in mind important (beneficial) effects of eNOS in this context.

With regard to selectivity, the exception among arginine-based NOS inhibitors is L-NIL, a compound with moderate selectivity for iNOS (Vitecek et al., 2012). So far, L-NIL has been tested in clinical setup for the oral application in asthma patients, where it reduced exhaled breath NO levels without producing the side effects observed following systemic administration of nonselective NOS inhibitors (Hansel et al., 2003). The same is true for the GW274150, a sulfur-substituted acetamidine amino acid derivative of L-lysine, a potent and selective iNOS inhibitor (Singh et al., 2007). Although none of them produced the desired effect on lung function or airway hyperreactivity, good tolerability of these compounds and their marked inhibitory effect on iNOS provide support for the potential use of iNOS inhibitors to treat a range of inflammatory clinical disorders.

Future research directions should focus on the precise description of underlying molecular pathways and identification of cell types responsible for the pathological signaling, which may open the way for the identification of novel (iNOS-targeting) pharmacologically active drug candidates or at least better utilization of existing inhibitors. In addition, further *in vivo* studies using relevant animal models of COPD-PH may help to test the desirable properties of potential inhibitors and to determine the optimal route of their administration until the final application for clinical use.

In conclusion, my data demonstrate that iNOS deletion in myeloid cells protects mice against smoke-induced PH. They further support the concept that pulmonary vascular remodeling and emphysema can occur independently, but parenchymal destruction might be driven by molecular alterations in vascular cell types. Finally, the results of this study implicate M2-polarized macrophages as a major driver of smoke-induced pulmonary vascular remodeling and suggest that iNOS expression in this activation state is an important factor in such processes.

5. Abbreviations and acronyms

µCT	Micro-computed tomography
AngII	Angiotensin II
ANOVA	Analysis of variance
AP	Alkaline phosphatase
AP-1	Activator protein-1
APS	Ammonium persulfate
BALF	Bronchoalveolar lavage fluid
BH4	Tetrahydrobiopterin
BMDM	Bone marrow-derived macrophages
BrdU	Bromodeoxyuridine
BSA	Bovine serum albumin
C/EBP	CCAAT-enhancer-binding protein
CaM	Calmodulin
CCL	Chemokine (C-C motif) ligand
CD	Cluster of differentiation
cDNA	Complementary DNA
cGMP	Cyclic guanosine monophosphate
CM	Culture-conditioned medium
COPD	Chronic obstructive pulmonary disease
COPD-PH	COPD-associated PH
CREB	Cyclic adenosine monophosphate-response element binding protein
CRP	C-reactive protein
CSE	Cigarette-smoke extract
CXCL	Chemokine (C-X-C motif) ligand
DC	Dendritic cell
DMEM	Dulbecco's Modified Eagle Medium
DMSO	Dimethylsulfoxide
EDTA	Ethylenediaminetetraacetic acid
ELISA	Enzyme-linked immunosorbent assay
eNOS	Endothelial nitric oxide synthase
ER	Endoplasmic reticulum

ERK	Extracellular signal-regulated kinase
ET-1	Endothelin-1
FACS	Fluorescence-activated cell sorting
FAD	Flavin adenine dinucleotide
FBS	Fetal bovine serum
FEV1	Forced expiratory volume in one second
FMN	Flavin mononucleotide
FMT	Fluorescence molecular tomography
FRC	Functional residual capacity
FVC	Forced vital capacity
HBSS	Hank's balanced salt solution
HIF-1	Hypoxia-inducible factor-1
HIV	Human immunodeficiency virus
HPRT	Hypoxanthine-guanine phosphoribosyltransferase
HPV	Hypoxic vasoconstriction
HRP	Horseradish peroxidase
IFN	Interferon
IL	Interleukin
iNOS	Inducible nitric oxide synthase
IPAH	Idiopathic pulmonary arterial hypertension
JAK	Janus kinase
JAK/STAT-1	Janus kinase/signal transducer and activator of transcription-1
KLF	Krüppel-like factor
L-NIL	N6-(1-iminoethyl)-L-lysine
LPS	Lipopolysaccharide
LV+S	Left ventricle and septum
MAPK	Mitogen-activated protein kinase
M-CSF	Macrophage colony-stimulating factor
MHC	Major histocompatibility complex
MMP	Metalloproteinase
mPAP	Mean pulmonary arterial pressure
MPO	Myeloperoxidases
NADPH	Nicotinamide adenine dinucleotide phosphate
NF-AT	Nuclear factor of activated T-cells

NFκB	Nuclear factor kappa-light-chain-enhancer of activated B-cells
NK cells	Natural killer cells
nNOS	Neuronal nitric oxide synthase
NO	Nitric oxide
NOXO1	NADPH oxidase organizer 1
Nrf2	Nuclear factor erythroid 2–related factor 2
OCT	Octamer transcription factor
$ONOO^-$	Peroxynitrite
PAH	Pulmonary arterial hypertension
PARP	Poly(ADP-ribose) polymerase
PASMC	Pulmonary artery smooth muscle cells
PBS	Phosphate buffered saline
PCR	Polymerase chain reaction
PDE	Phosphodiesterase
PEEP	Positive end-expiratory pressure
PFA	Paraformaldehyde
PGI(2)	Prostacyclin
PH	Pulmonary hypertension
PMSF	Phenylmethansulfonylfluorid
PV	Pressure-volume
PVDF	Phenylmethylsulfonyl fluoride
PVR	Pulmonary vascular resistance
qPCR	Quantitative PCR
RBC	Red blood cell
ROR-γT	Retinoic acid receptor-related orphan receptor-γT
ROS	Reactive oxygen species
RT	Room temperature
RV	Right ventricle
RVSP	Right ventricular systolic pressure
SDS	Sodium dodecyl sulfate
SEM	Standard error of the mean
sGC	Soluble guanylate cyclase
TAPSE	Tricuspid annular plane systolic excursion
TBS	Tris-buffered saline

TBST	TBS with Tween
TGF-β	Transforming growth factor-β
TNF-α	Tumor necrosis factor-α
WT	Wildtype

6. Summary

COPD, comprising chronic bronchitis and emphysema, represents one of the five leading causes of death worldwide. The disease is progressive and currently incurable, with the treatment options limited to those controlling the symptoms. Underlying molecular mechanisms leading to COPD include increased oxidative stress, the imbalance between proteolytic activity and anti-proteolytic defense and influx of inflammatory cells. Moreover, recent findings from preclinical models and COPD patients prompted the hypothesis that pulmonary vascular alterations are an early phenomenon of the COPD pathology and a possible driver of parenchymal destruction. In addition, abnormally high mean pulmonary arterial pressure is present in up to 90% of COPD patients. Although PH is associated with increased risk of exacerbations and decreased survival in COPD patients, efficient pharmacological options are not available. Some of the mechanisms implicated in the pathogenesis of COPD-PH are endothelial dysfunction, hypoxia, vascular pruning and loss of capillary bed. Moreover, activation of inflammatory cells might be a contributing factor to PH development in COPD.

The previous work from the group in which the current thesis was done suggested that iNOS may represent a key player in the pathogenesis of smoke-induced PH as well as emphysema. In smoke-exposed mice, iNOS inhibition prevented and reversed parenchymal destruction, PH and pulmonary vascular remodeling. Moreover, experiments with chimeric mice showed that iNOS expression in bone marrow-derived cells is driving the pulmonary vascular alterations, but not emphysema development. However, it remained unclear which bone marrow-derived cell type drives the process and what the respective mechanism is. In this study, I aimed to identify the iNOS-expressing cell type driving smoke-induced PH and to decipher pro-proliferative pathways involved in this process. To address this question I used myeloid cell-specific iNOS knockout mice in chronic smoke exposure to monitor the development of PH and emphysema and co-cultures of macrophages and PASMC to decipher underlying pathways.

Interestingly, myeloid cell-specific iNOS knockout mice were protected against smoke-induced PH but not emphysema. Moreover, myeloid cell-specific iNOS deletion ameliorated several smoke-induced changes in lung inflammatory cell composition and phenotype. Specifically, iNOS knockout in myeloid cells prevented the increase in

expression of CD206, a marker of M2 polarization, on interstitial macrophages in smoke-exposed lungs. *In vitro*, smoke-induced pro-proliferative signaling in co-cultures of M2-polarized macrophages and PASMC was abolished by iNOS deletion in phagocytic cells. Importantly, numerous CD206-positive and iNOS-positive macrophages accumulated in the proximity of remodeled vessels in the lungs of COPD patients, as shown by immunohistochemistry. Interestingly, described effects on the composition and activity of lung macrophages were hypoxia-independent and represented the smoke-specific signaling events in the remodeling of the pulmonary vasculature, as myeloid cell-specific knockout mice developed PH after chronic exposure to hypoxia. Regarding the underlying molecular pathways, I found differences in IL-4 signaling between WT and iNOS-deficient M2 macrophages. Moreover, I demonstrated increased phosphorylation of ERK and p38 kinases, previously implicated in the proliferation of vascular cells, in PASMC co-cultured with iNOS-expressing macrophages, smoke-induced WT animals, as well as in remodeled pulmonary vessels in the lung of COPD patients.

In summary, my results demonstrate that iNOS deletion in myeloid cells confers protection against PH in smoke-exposed mice and provide evidence for the communication between M2-like macrophages and PASMC in underlying pulmonary vascular remodeling.

7. Zusammenfassung

COPD umfasst die chronische Bronchitis und das Emphysem und ist eine der fünf häufigsten Todesursachen weltweit. Die Krankheit ist derzeit unheilbar, die Behandlungsmöglichkeiten beschränken sich auf die Kontrolle der Symptome. Zu den zugrundeliegenden molekularen Mechanismen, die zu COPD führen, gehören erhöhter oxidativer Stress, das Ungleichgewicht zwischen proteolytischer Aktivität und anti-proteolytischer Abwehr sowie die Einwanderung von Entzündungszellen. Jüngste Erkenntnisse aus präklinischen Modellen und von COPD-Patienten haben zudem zu der Hypothese geführt, dass pulmonale Gefäßveränderungen ein frühes Phänomen der COPD-Pathologie und ein möglicher Auslöser für die Zerstörung des Parenchyms sind. Darüber hinaus liegt bei bis zu 90% der COPD-Patienten ein zu hoher mittlerer pulmonalarterieller Druck vor. Obwohl die PH mit einem erhöhten Risiko von Exazerbationen und einer geringeren Überlebensrate bei COPD-Patienten in Verbindung gebracht wird, gibt es keine wirksamen pharmakologischen Optionen. Einige der Mechanismen, die bei der Entstehung der COPD-PH eine Rolle spielen, sind endotheliale Dysfunktion, Hypoxie, Gefäßverengung und der Verlust des Kapillarbettes. Darüber hinaus könnte die Aktivierung von Entzündungszellen ein Faktor sein, der zur Entwicklung der PH bei COPD beiträgt.

Frühere Arbeiten der Gruppe, in der die vorliegende Arbeit entstand, legten nahe, dass iNOS eine Schlüsselrolle in der Pathogenese der rauchinduzierten PH und des Emphysems spielen könnte. Bei rauchexponierten Mäusen konnte die Hemmung von iNOS die Zerstörung des Parenchyms, die PH und den Umbau der Lungengefäße verhindern und umkehren. Darüber hinaus zeigten Experimente mit chimären Mäusen, dass die iNOS-Expression in Zellen, die aus dem Knochenmark stammen, die pulmonalvaskulären Veränderungen, aber nicht die Emphysementwicklung vorantreibt. Es blieb jedoch unklar, welcher aus dem Knochenmark stammende Zelltyp diesen Prozess antreibt und wie der entsprechende Mechanismus abläuft. Ziel dieser Studie war es den iNOS-exprimierenden Zelltyp zu identifizieren, der für die rauchinduzierte PH verantwortlich ist, und die an diesem Prozess beteiligten proproliferativen Signalwege zu entschlüsseln. Um diese Frage zu klären, habe ich myeloide Zell-spezifische iNOS-Knockout-Mäuse chronischer Rauchbelastung ausgesetzt, um die Entwicklung von PH und Emphysem zu beobachten und zusätzlich

Ko-Kulturen von Makrophagen und PASMC verwendet, um die zugrundeliegenden Signalwege zu entschlüsseln.

Interessanterweise waren die myeloiden Zell-spezifischen iNOS-Knockout-Mäuse vor der rauchinduzierten PH geschützt, jedoch nicht vor dem Emphysem. Außerdem verbesserte die myeloide Zell-spezifische iNOS-Deletion mehrere rauchinduzierte Veränderungen, wie den Phänotyp und die Zusammensetzung der Entzündungszellen in der Lunge. Insbesondere verhinderte der iNOS-Knockout in myeloiden Zellen den Anstieg der CD206 Expression, einem Marker der M2-Polarisierung, auf interstitiellen Makrophagen in rauchexponierten Lungen. In vitro wurde die rauchinduzierte proproliferative Signalübertragung in Ko-Kulturen von M2-polarisierten Makrophagen und PASMC durch die Deletion von iNOS in phagozytischen Zellen aufgehoben. Immunhistochemische Untersuchungen zeigten, dass sich zahlreiche CD206-positive und iNOS-positive Makrophagen in der Nähe umgebauter Gefäße in der Lunge von COPD-Patienten ansammelten. Die beschriebenen Auswirkungen auf die Zusammensetzung und Aktivität der Lungenmakrophagen waren dabei Hypoxie unabhängig. Sie repräsentierten die rauchspezifischen Signalwege beim Umbau der Lungengefäße, da myeloid Zell-spezifische Knockout-Mäuse nach chronischer Hypoxieexposition nach wie vor eine PH entwickelten. Was die zugrundeliegenden molekularen Signalwege betrifft, so fand ich Unterschiede in der IL-4-Signalübertragung zwischen WT- und iNOS-defizienten M2-Makrophagen. Darüber hinaus konnte ich eine erhöhte Phosphorylierung von ERK- und p38-Kinasen, die zuvor bereits mit der Proliferation von Gefäßzellen in Verbindung gebracht wurden, in PASMC ko-kultiviert mit iNOS-exprimierenden Makrophagen, in rauchinduzierten WT-Tieren sowie in veränderten Lungengefäßen aus den Lungen von COPD-Patienten nachweisen.

Zusammenfassend zeigen meine Ergebnisse, dass die Deletion von iNOS in myeloiden Zellen einen Schutz vor PH in rauchexponierten Mäusen bietet. Außerdem liefern sie Beweise für die Kommunikation zwischen M2-ähnlichen Makrophagen und PASMC bei dem zugrunde liegenden pulmonalen Gefäßumbau.

8. Reference list

Abid, S., Marcos, E., Parpaleix, A., Amsellem, V., Breau, M., Houssaini, A., Vienney, N., Lefevre, M., Derumeaux, G., Evans, S., Hubeau, C., Delcroix, M., Quarck, R., Adnot, S., & Lipskaia, L. (2019). CCR2/CCR5-mediated macrophage-smooth muscle cell crosstalk in pulmonary hypertension. *Eur Respir J, 54*(4). doi:10.1183/13993003.02308-2018

Abram, C. L., Roberge, G. L., Hu, Y., & Lowell, C. A. (2014). Comparative analysis of the efficiency and specificity of myeloid-Cre deleting strains using ROSA-EYFP reporter mice. *J Immunol Methods, 408*, 89-100. doi:10.1016/j.jim.2014.05.009

Adnot, S., Amsellem, V., Boyer, L., Marcos, E., Saker, M., Houssaini, A., Kebe, K., Dagouassat, M., Lipskaia, L., & Boczkowski, J. (2015). Telomere Dysfunction and Cell Senescence in Chronic Lung Diseases: Therapeutic Potential. *Pharmacol Ther, 153*, 125-134. doi:10.1016/j.pharmthera.2015.06.007

Ajami, B., Bennett, J. L., Krieger, C., Tetzlaff, W., & Rossi, F. M. (2007). Local self-renewal can sustain CNS microglia maintenance and function throughout adult life. *Nat Neurosci, 10*(12), 1538-1543. doi:10.1038/nn2014

Alderton, W. K., Cooper, C. E., & Knowles, R. G. (2001). Nitric oxide synthases: structure, function and inhibition. *Biochem J, 357*(Pt 3), 593-615. doi:10.1042/0264-6021:3570593

Amsellem, V., Abid, S., Poupel, L., Parpaleix, A., Rodero, M., Gary-Bobo, G., Latiri, M., Dubois-Rande, J. L., Lipskaia, L., Combadiere, C., & Adnot, S. (2017). Roles for the CX3CL1/CX3CR1 and CCL2/CCR2 Chemokine Systems in Hypoxic Pulmonary Hypertension. *Am J Respir Cell Mol Biol, 56*(5), 597-608. doi:10.1165/rcmb.2016-0201OC

Angelini, D. J., Su, Q., Yamaji-Kegan, K., Fan, C., Teng, X., Hassoun, P. M., Yang, S. C., Champion, H. C., Tuder, R. M., & Johns, R. A. (2009). Resistin-Like Molecule-β in Scleroderma-Associated Pulmonary Hypertension. *41*(5), 553-561. doi:10.1165/rcmb.2008-0271OC

Bailey, A., Pope, T. W., Moore, S. A., & Campbell, C. L. (2007). The tragedy of TRIUMPH for nitric oxide synthesis inhibition in cardiogenic shock: where do we go from here? *Am J Cardiovasc Drugs, 7*(5), 337-345. doi:10.2165/00129784-200707050-00003

Barbera, J. A., Peinado, V. I., & Santos, S. (2003). Pulmonary hypertension in chronic obstructive pulmonary disease. *Eur Respir J, 21*(5), 892-905. doi:10.1183/09031936.03.00115402

Barbera, J. A., Peinado, V. I., Santos, S., Ramirez, J., Roca, J., & Rodriguez-Roisin, R. (2001). Reduced expression of endothelial nitric oxide synthase in pulmonary arteries of smokers. *Am J Respir Crit Care Med, 164*(4), 709-713. doi:10.1164/ajrccm.164.4.2101023

Bogdan, C. (2001). Nitric oxide and the immune response. *Nat Immunol, 2*(10), 907-916. doi:10.1038/ni1001-907

Bogdan, C. (2015). Nitric oxide synthase in innate and adaptive immunity: an update. *Trends Immunol, 36*(3), 161-178. doi:10.1016/j.it.2015.01.003

Bogdan, C., Rollinghoff, M., & Diefenbach, A. (2000). The role of nitric oxide in innate immunity. *Immunol Rev, 173*, 17-26. doi:10.1034/j.1600-065x.2000.917307.x

Bonnet, S., Rochefort, G., Sutendra, G., Archer, S. L., Haromy, A., Webster, L., Hashimoto, K., Bonnet, S. N., & Michelakis, E. D. (2007). The nuclear factor of activated T cells in pulmonary arterial hypertension can be therapeutically targeted. *Proc Natl Acad Sci U S A, 104*(27), 11418-11423. doi:10.1073/pnas.0610467104

Braun, M., Klingelhofer, D., Muller, R., & Groneberg, D. A. (2021). The impact of second-hand smoke on nitrogen oxides concentrations in a small interior. *Sci Rep, 11*(1), 11703. doi:10.1038/s41598-021-90994-x

Braune, J., Weyer, U., Hobusch, C., Mauer, J., Bruning, J. C., Bechmann, I., & Gericke, M. (2017). IL-6 Regulates M2 Polarization and Local Proliferation of Adipose Tissue Macrophages in Obesity. *J Immunol, 198*(7), 2927-2934. doi:10.4049/jimmunol.1600476

Brindicci, C., Ito, K., Barnes, P. J., & Kharitonov, S. A. (2007). Effect of an inducible nitric oxide synthase inhibitor on differential flow-exhaled nitric oxide in asthmatic patients and healthy volunteers. *Chest, 132*(2), 581-588. doi:10.1378/chest.06-3046

Brindicci, C., Ito, K., Torre, O., Barnes, P. J., & Kharitonov, S. A. (2009). Effects of aminoguanidine, an inhibitor of inducible nitric oxide synthase, on nitric oxide production and its metabolites in healthy control subjects, healthy smokers, and COPD patients. *Chest, 135*(2), 353-367. doi:10.1378/chest.08-0964

Bunel, V., Guyard, A., Dauriat, G., Danel, C., Montani, D., Gauvain, C., Thabut, G., Humbert, M., Castier, Y., Dorfmuller, P., & Mal, H. (2019). Pulmonary Arterial Histologic Lesions in Patients With COPD With Severe Pulmonary Hypertension. *Chest, 156*(1), 33-44. doi:10.1016/j.chest.2019.02.333

Butler, J. P., Loring, S. H., Patz, S., Tsuda, A., Yablonskiy, D. A., & Mentzer, S. J. (2012). Evidence for adult lung growth in humans. *N Engl J Med, 367*(3), 244-247. doi:10.1056/NEJMoa1203983

Carratu, P., Scoditti, C., Maniscalco, M., Seccia, T. M., Di Gioia, G., Gadaleta, F., Cardone, R. A., Dragonieri, S., Pierucci, P., Spanevello, A., & Resta, O. (2008). Exhaled and arterial levels of endothelin-1 are increased and correlate with pulmonary systolic pressure in COPD with pulmonary hypertension. *BMC Pulm Med, 8*, 20. doi:10.1186/1471-2466-8-20

Chaouat, A., Naeije, R., & Weitzenblum, E. (2008). Pulmonary hypertension in COPD. *Eur Respir J, 32*(5), 1371-1385. doi:10.1183/09031936.00015608

Christmann, R. B., Hayes, E., Pendergrass, S., Padilla, C., Farina, G., Affandi, A. J., Whitfield, M. L., Farber, H. W., & Lafyatis, R. (2011). Interferon and alternative activation of monocyte/macrophages in systemic sclerosis-associated pulmonary arterial hypertension. *Arthritis Rheum, 63*(6), 1718-1728. doi:10.1002/art.30318

Chung, K. F., & Adcock, I. M. (2008). Multifaceted mechanisms in COPD: inflammation, immunity, and tissue repair and destruction. *Eur Respir J, 31*(6), 1334-1356. doi:10.1183/09031936.00018908

Church, A. C., Martin, D. H., Wadsworth, R., Bryson, G., Fisher, A. J., Welsh, D. J., & Peacock, A. J. (2015). The reversal of pulmonary vascular remodeling through inhibition of p38 MAPK-alpha: a potential novel anti-inflammatory strategy in pulmonary hypertension. *Am J Physiol Lung Cell Mol Physiol, 309*(4), L333-347. doi:10.1152/ajplung.00038.2015

Churg, A., Marshall, C. V., Sin, D. D., Bolton, S., Zhou, S., Thain, K., Cadogan, E. B., Maltby, J., Soars, M. G., Mallinder, P. R., & Wright, J. L. (2012). Late intervention with a myeloperoxidase inhibitor stops progression of experimental chronic obstructive pulmonary disease. *Am J Respir Crit Care Med, 185*(1), 34-43. doi:10.1164/rccm.201103-0468OC

Churg, A., & Wright, J. L. (2007). Animal models of cigarette smoke-induced chronic obstructive lung disease. *Contrib Microbiol, 14*, 113-125. doi:10.1159/000107058

Cinelli, M. A., Do, H. T., Miley, G. P., & Silverman, R. B. (2020). Inducible nitric oxide synthase: Regulation, structure, and inhibition. *Med Res Rev, 40*(1), 158-189. doi:10.1002/med.21599

Connor, J. R., Rogers, K., Sunyer, T., Le Graverand-Gastineau, M. P. H., & Manning, P. T. (2012). Efficacy of the Selective Inducible Nitric Oxide Synthase Inhibitor Sd-6010 in Nonclinical Inflammatory, Neuropathic, and Osteoarthritis Pain. *Osteoarthritis and Cartilage, 20*, S64-S65. doi:DOI 10.1016/j.joca.2012.02.036

De Cunto, G., Lunghi, B., Bartalesi, B., Cavarra, E., Fineschi, S., Ulivieri, C., Lungarella, G., & Lucattelli, M. (2016). Severe Reduction in Number and Function of Peripheral T Cells Does Not Afford Protection toward Emphysema and Bronchial Remodeling Induced in Mice by Cigarette Smoke. *Am J Pathol, 186*(7), 1814-1824. doi:10.1016/j.ajpath.2016.03.002

Diefenbach, A., Schindler, H., Rollinghoff, M., Yokoyama, W. M., & Bogdan, C. (1999). Requirement for type 2 NO synthase for IL-12 signaling in innate immunity. *Science, 284*(5416), 951-955. doi:10.1126/science.284.5416.951

Dominguez-Fandos, D., Valdes, C., Ferrer, E., Puig-Pey, R., Blanco, I., Tura-Ceide, O., Paul, T., Peinado, V. I., & Barbera, J. A. (2015). Sildenafil in a cigarette smoke-induced model of COPD in the guinea-pig. *Eur Respir J, 46*(2), 346-354. doi:10.1183/09031936.00139914

Douschan, P., Kovacs, G., Avian, A., Foris, V., Gruber, F., Olschewski, A., & Olschewski, H. (2018). Mild Elevation of Pulmonary Arterial Pressure as a Predictor of Mortality. *Am J Respir Crit Care Med, 197*(4), 509-516. doi:10.1164/rccm.201706-1215OC

Eddahibi, S., Chaouat, A., Tu, L., Chouaid, C., Weitzenblum, E., Housset, B., Maitre, B., & Adnot, S. (2006). Interleukin-6 gene polymorphism confers susceptibility to pulmonary hypertension in chronic obstructive pulmonary disease. *Proc Am Thorac Soc, 3*(6), 475-476. doi:10.1513/pats.200603-038MS

El Kasmi, K. C., Pugliese, S. C., Riddle, S. R., Poth, J. M., Anderson, A. L., Frid, M. G., Li, M., Pullamsetti, S. S., Savai, R., Nagel, M. A., Fini, M. A., Graham, B. B., Tuder, R. M., Friedman, J. E., Eltzschig, H. K., Sokol, R. J., & Stenmark, K. R. (2014). Adventitial fibroblasts induce a distinct proinflammatory/profibrotic macrophage phenotype in pulmonary hypertension. *J Immunol, 193*(2), 597-609. doi:10.4049/jimmunol.1303048

Elovic, A. E., Ohyama, H., Sauty, A., McBride, J., Tsuji, T., Nagai, M., Weller, P. F., & Wong, D. T. (1998). IL-4-dependent regulation of TGF-alpha and TGF-beta1 expression in human eosinophils. *J Immunol, 160*(12), 6121-6127.

Fathke, C., Wilson, L., Hutter, J., Kapoor, V., Smith, A., Hocking, A., & Isik, F. (2004). Contribution of bone marrow-derived cells to skin: collagen deposition and wound repair. *Stem Cells, 22*(5), 812-822. doi:10.1634/stemcells.22-5-812

Fehrenbach, H., Voswinckel, R., Michl, V., Mehling, T., Fehrenbach, A., Seeger, W., & Nyengaard, J. R. (2008). Neoalveolarisation contributes to compensatory lung growth following pneumonectomy in mice. *Eur Respir J, 31*(3), 515-522. doi:10.1183/09031936.00109407

Ferreira, F. M., Palle, P., Vom Berg, J., Prajwal, P., Laman, J. D., & Buch, T. (2019). Bone marrow chimeras-a vital tool in basic and translational research. *J Mol Med (Berl), 97*(7), 889-896. doi:10.1007/s00109-019-01783-z

Ferrer, E., Peinado, V. I., Diez, M., Carrasco, J. L., Musri, M. M., Martinez, A., Rodriguez-Roisin, R., & Barbera, J. A. (2009). Effects of cigarette smoke on endothelial function of pulmonary arteries in the guinea pig. *Respir Res, 10*, 76. doi:10.1186/1465-9921-10-76

Forstermann, U., & Sessa, W. C. (2012). Nitric oxide synthases: regulation and function. *Eur Heart J, 33*(7), 829-837, 837a-837d. doi:10.1093/eurheartj/ehr304

Fujita, M., Shannon, J. M., Irvin, C. G., Fagan, K. A., Cool, C., Augustin, A., & Mason, R. J. (2001). Overexpression of tumor necrosis factor-alpha produces an increase in lung volumes and pulmonary hypertension. *Am J Physiol Lung Cell Mol Physiol, 280*(1), L39-49. doi:10.1152/ajplung.2001.280.1.L39

Gaffey, K., Reynolds, S., Plumb, J., Kaur, M., & Singh, D. (2013). Increased phosphorylated p38 mitogen-activated protein kinase in COPD lungs. *Eur Respir J, 42*(1), 28-41. doi:10.1183/09031936.00170711

Gassmann, M., Cowburn, A., Gu, H., Li, J., Rodriguez, M., Babicheva, A., Jain, P. P., Xiong, M., Gassmann, N. N., Yuan, J. X., Wilkins, M. R., & Zhao, L. (2020). Hypoxia-induced pulmonary hypertension-Utilizing experiments of nature. *Br J Pharmacol*. doi:10.1111/bph.15144

Gouveia, L., Kraut, S., Hadzic, S., Vazquez-Liebanas, E., Kojonazarov, B., Wu, C. Y., Veith Berger, C., He, L., Mermelekas, G., Schermuly, R. T., Weissmann, N., Betsholtz, C., & Andrae, J. (2020). Lung developmental arrest caused by PDGF-A deletion: consequences for the adult mouse lung. *Am J Physiol Lung Cell Mol Physiol*. doi:10.1152/ajplung.00295.2019

Graham, B. B., Chabon, J., Gebreab, L., Poole, J., Debella, E., Davis, L., Tanaka, T., Sanders, L., Dropcho, N., Bandeira, A., Vandivier, R. W., Champion, H. C., Butrous, G., Wang, X. J., Wynn, T. A., & Tuder, R. M. (2013). Transforming growth factor-beta signaling promotes pulmonary hypertension caused by Schistosoma mansoni. *Circulation, 128*(12), 1354-1364. doi:10.1161/CIRCULATIONAHA.113.003072

Gredic, M., Blanco, I., Kovacs, G., Helyes, Z., Ferdinandy, P., Olschewski, H., Barbera, J. A., & Weissmann, N. (2020). Pulmonary hypertension in chronic obstructive pulmonary disease. *Br J Pharmacol*. doi:10.1111/bph.14979

Hadzic, S., Wu, C. Y., Avdeev, S., Weissmann, N., Schermuly, R. T., & Kosanovic, D. (2020). Lung epithelium damage in COPD - An unstoppable pathological event? *Cell Signal, 68*, 109540. doi:10.1016/j.cellsig.2020.109540

Han, S. X., He, G. M., Wang, T., Chen, L., Ning, Y. Y., Luo, F., An, J., Yang, T., Dong, J. J., Liao, Z. L., Xu, D., & Wen, F. Q. (2010). Losartan attenuates chronic cigarette smoke exposure-induced pulmonary arterial hypertension in rats: possible involvement of angiotensin-converting enzyme-2. *Toxicol Appl Pharmacol, 245*(1), 100-107. doi:10.1016/j.taap.2010.02.009

Hansel, T. T., Kharitonov, S. A., Donnelly, L. E., Erin, E. M., Currie, M. G., Moore, W. M., Manning, P. T., Recker, D. P., & Barnes, P. J. (2003). A selective inhibitor of inducible nitric oxide synthase inhibits exhaled breath nitric oxide in healthy volunteers and asthmatics. *FASEB J, 17*(10), 1298-1300. doi:10.1096/fj.02-0633fje

Hashimoto-Kataoka, T., Hosen, N., Sonobe, T., Arita, Y., Yasui, T., Masaki, T., Minami, M., Inagaki, T., Miyagawa, S., Sawa, Y., Murakami, M., Kumanogoh, A., Yamauchi-Takihara, K., Okumura, M., Kishimoto, T., Komuro, I., Shirai, M., Sakata, Y., & Nakaoka, Y. (2015). Interleukin-6/interleukin-21 signaling axis is critical in the pathogenesis of pulmonary arterial hypertension. *Proc Natl Acad Sci U S A, 112*(20), E2677-2686. doi:10.1073/pnas.1424774112

Heemskerk, S., Masereeuw, R., Russel, F. G., & Pickkers, P. (2009). Selective iNOS inhibition for the treatment of sepsis-induced acute kidney injury. *Nat Rev Nephrol, 5*(11), 629-640. doi:10.1038/nrneph.2009.155

Hellio le Graverand, M.-P., Clemmer, R. S., Redifer, P., Brunell, R. M., Hayes, C. W., Brandt, K. D., Abramson, S. B., Manning, P. T., Miller, C. G., & Vignon, E.

(2013). A 2-year randomised, double-blind, placebo-controlled, multicentre study of oral selective iNOS inhibitor, cindunistat (SD-6010), in patients with symptomatic osteoarthritis of the knee. *72*(2), 187-195. doi:10.1136/annrheumdis-2012-202239 %J Annals of the Rheumatic Diseases

Hogg, J. C., & Timens, W. (2009). The pathology of chronic obstructive pulmonary disease. *Annu Rev Pathol, 4*, 435-459. doi:10.1146/annurev.pathol.4.110807.092145

Huang, S., Yue, Y., Feng, K., Huang, X., Li, H., Hou, J., Yang, S., Huang, S., Liang, M., Chen, G., & Wu, Z. (2020). Conditioned medium from M2b macrophages modulates the proliferation, migration, and apoptosis of pulmonary artery smooth muscle cells by deregulating the PI3K/Akt/FoxO3a pathway. *PeerJ, 8*, e9110. doi:10.7717/peerj.9110

Hurdman, J., Condliffe, R., Elliot, C. A., Davies, C., Hill, C., Wild, J. M., Capener, D., Sephton, P., Hamilton, N., Armstrong, I. J., Billings, C., Lawrie, A., Sabroe, I., Akil, M., O'Toole, L., & Kiely, D. G. (2012). ASPIRE registry: assessing the Spectrum of Pulmonary hypertension Identified at a REferral centre. *Eur Respir J, 39*(4), 945-955. doi:10.1183/09031936.00078411

Ichinose, M., Sugiura, H., Yamagata, S., Koarai, A., & Shirato, K. (2000). Increase in reactive nitrogen species production in chronic obstructive pulmonary disease airways. *Am J Respir Crit Care Med, 162*(2 Pt 1), 701-706. doi:10.1164/ajrccm.162.2.9908132

Icochea, A., Cooper, B. S., & Kuhn, C. (1982). The effect of oxygen on Cor pulmonale in experimental emphysema induced by elastase or elastase and beta-aminopropionitrile in hamsters. *Am Rev Respir Dis, 126*(5), 792-796. doi:10.1164/arrd.1982.126.5.792

Ishii, G., Sangai, T., Sugiyama, K., Ito, T., Hasebe, T., Endoh, Y., Magae, J., & Ochiai, A. (2005). In vivo characterization of bone marrow-derived fibroblasts recruited into fibrotic lesions. *Stem Cells, 23*(5), 699-706. doi:10.1634/stemcells.2004-0183

Jenkins, S. J., Ruckerl, D., Cook, P. C., Jones, L. H., Finkelman, F. D., van Rooijen, N., MacDonald, A. S., & Allen, J. E. (2011). Local macrophage proliferation, rather than recruitment from the blood, is a signature of TH2 inflammation. *Science, 332*(6035), 1284-1288. doi:10.1126/science.1204351

Jetten, N., Verbruggen, S., Gijbels, M. J., Post, M. J., De Winther, M. P., & Donners, M. M. (2014). Anti-inflammatory M2, but not pro-inflammatory M1 macrophages promote angiogenesis in vivo. *Angiogenesis, 17*(1), 109-118. doi:10.1007/s10456-013-9381-6

Jianjun, Y., Zhang, R., Lu, G., Shen, Y., Peng, L., Zhu, C., Cui, M., Wang, W., Arnaboldi, P., Tang, M., Gupta, M., Qi, C. F., Jayaraman, P., Zhu, H., Jiang, B., Chen, S. H., He, J. C., Ting, A. T., Zhou, M. M., Kuchroo, V. K., Morse, H. C., 3rd, Ozato, K., Sikora, A. G., & Xiong, H. (2013). T cell-derived inducible nitric oxide synthase switches off Th17 cell differentiation. *J Exp Med, 210*(7), 1447-1462. doi:10.1084/jem.20122494

Jin, N., Hatton, N., Swartz, D. R., Xia, X., Harrington, M. A., Larsen, S. H., & Rhoades, R. A. (2000). Hypoxia activates jun-N-terminal kinase, extracellular signal-regulated protein kinase, and p38 kinase in pulmonary arteries. *Am J Respir Cell Mol Biol, 23*(5), 593-601. doi:10.1165/ajrcmb.23.5.3921

Joppa, P., Petrasova, D., Stancak, B., & Tkacova, R. (2006). Systemic inflammation in patients with COPD and pulmonary hypertension. *Chest, 130*(2), 326-333. doi:10.1378/chest.130.2.326

Karnati, S., Seimetz, M., Kleefeldt, F., Sonawane, A., Madhusudhan, T., Bachhuka, A., Kosanovic, D., Weissmann, N., Kruger, K., & Ergun, S. (2021). Chronic Obstructive Pulmonary Disease and the Cardiovascular System: Vascular Repair and Regeneration as a Therapeutic Target. *Front Cardiovasc Med, 8*, 649512. doi:10.3389/fcvm.2021.649512

Kessler, R., Faller, M., Fourgaut, G., Mennecier, B., & Weitzenblum, E. (1999). Predictive factors of hospitalization for acute exacerbation in a series of 64 patients with chronic obstructive pulmonary disease. *Am J Respir Crit Care Med, 159*(1), 158-164. doi:10.1164/ajrccm.159.1.9803117

Kierdorf, K., Katzmarski, N., Haas, C. A., & Prinz, M. (2013). Bone marrow cell recruitment to the brain in the absence of irradiation or parabiosis bias. *PLoS One, 8*(3), e58544. doi:10.1371/journal.pone.0058544

Knust, J., Ochs, M., Gundersen, H. J., & Nyengaard, J. R. (2009). Stereological estimates of alveolar number and size and capillary length and surface area in mice lungs. *Anat Rec (Hoboken), 292*(1), 113-122. doi:10.1002/ar.20747

Kojonazarov, B., Hadzic, S., Ghofrani, H. A., Grimminger, F., Seeger, W., Weissmann, N., & Schermuly, R. T. (2019). Severe Emphysema in the SU5416/Hypoxia Rat Model of Pulmonary Hypertension. *Am J Respir Crit Care Med, 200*(4), 515-518. doi:10.1164/rccm.201902-0390LE

Kosanovic, D., Dahal, B. K., Peters, D. M., Seimetz, M., Wygrecka, M., Hoffmann, K., Antel, J., Reiss, I., Ghofrani, H. A., Weissmann, N., Grimminger, F., Seeger, W., & Schermuly, R. T. (2014). Histological characterization of mast cell chymase in patients with pulmonary hypertension and chronic obstructive pulmonary disease. *Pulm Circ, 4*(1), 128-136. doi:10.1086/675642

Kovacs, G., Avian, A., Tscherner, M., Foris, V., Bachmaier, G., Olschewski, A., & Olschewski, H. (2014). Characterization of patients with borderline pulmonary arterial pressure. *Chest, 146*(6), 1486-1493. doi:10.1378/chest.14-0194

Kuebler, W. M., Bonnet, S., & Tabuchi, A. (2018). Inflammation and autoimmunity in pulmonary hypertension: is there a role for endothelial adhesion molecules? (2017 Grover Conference Series). *Pulm Circ, 8*(2), 2045893218757596. doi:10.1177/2045893218757596

Kumar, R., Mickael, C., Chabon, J., Gebreab, L., Rutebemberwa, A., Garcia, A. R., Koyanagi, D. E., Sanders, L., Gandjeva, A., Kearns, M. T., Barthel, L., Janssen, W. J., Mauad, T., Bandeira, A., Schmidt, E., Tuder, R. M., & Graham, B. B. (2015). The Causal Role of IL-4 and IL-13 in Schistosoma mansoni Pulmonary Hypertension. *Am J Respir Crit Care Med, 192*(8), 998-1008. doi:10.1164/rccm.201410-1820OC

Lee, J. H., Lee, D. S., Kim, E. K., Choe, K. H., Oh, Y. M., Shim, T. S., Kim, S. E., Lee, Y. S., & Lee, S. D. (2005). Simvastatin inhibits cigarette smoking-induced emphysema and pulmonary hypertension in rat lungs. *Am J Respir Crit Care Med, 172*(8), 987-993. doi:10.1164/rccm.200501-041OC

Lee, M., Rey, K., Besler, K., Wang, C., & Choy, J. (2017). Immunobiology of Nitric Oxide and Regulation of Inducible Nitric Oxide Synthase. *Results Probl Cell Differ, 62*, 181-207. doi:10.1007/978-3-319-54090-0_8

Li, L., Zhu, L., Hao, B., Gao, W., Wang, Q., Li, K., Wang, M., Huang, M., Liu, Z., Yang, Q., Li, X., Zhong, Z., Huang, W., Xiao, G., Xu, Y., Yao, K., & Liu, Q. (2017). iNOS-derived nitric oxide promotes glycolysis by inducing pyruvate kinase M2 nuclear translocation in ovarian cancer. *Oncotarget, 8*(20), 33047-33063. doi:10.18632/oncotarget.16523

Lu, G., Zhang, R., Geng, S., Peng, L., Jayaraman, P., Chen, C., Xu, F., Yang, J., Li, Q., Zheng, H., Shen, K., Wang, J., Liu, X., Wang, W., Zheng, Z., Qi, C. F., Si,

C., He, J. C., Liu, K., Lira, S. A., Sikora, A. G., Li, L., & Xiong, H. (2015). Myeloid cell-derived inducible nitric oxide synthase suppresses M1 macrophage polarization. *Nat Commun, 6*, 6676. doi:10.1038/ncomms7676

Lu, J., Shimpo, H., Shimamoto, A., Chong, A. J., Hampton, C. R., Spring, D. J., Yada, M., Takao, M., Onoda, K., Yada, I., Pohlman, T. H., & Verrier, E. D. (2004). Specific inhibition of p38 mitogen-activated protein kinase with FR167653 attenuates vascular proliferation in monocrotaline-induced pulmonary hypertension in rats. *J Thorac Cardiovasc Surg, 128*(6), 850-859. doi:10.1016/j.jtcvs.2004.03.003

Luthje, L., Raupach, T., Michels, H., Unsold, B., Hasenfuss, G., Kogler, H., & Andreas, S. (2009). Exercise intolerance and systemic manifestations of pulmonary emphysema in a mouse model. *Respir Res, 10*, 7. doi:10.1186/1465-9921-10-7

MacNee, W., & Tuder, R. M. (2009). New paradigms in the pathogenesis of chronic obstructive pulmonary disease I. *Proc Am Thorac Soc, 6*(6), 527-531. doi:10.1513/pats.200905-027DS

Maestrelli, P., Paska, C., Saetta, M., Turato, G., Nowicki, Y., Monti, S., Formichi, B., Miniati, M., & Fabbri, L. M. (2003). Decreased haem oxygenase-1 and increased inducible nitric oxide synthase in the lung of severe COPD patients. *Eur Respir J, 21*(6), 971-976. doi:10.1183/09031936.03.00098203

Magee, F., Wright, J. L., Wiggs, B. R., Pare, P. D., & Hogg, J. C. (1988). Pulmonary vascular structure and function in chronic obstructive pulmonary disease. *Thorax, 43*(3), 183-189. doi:10.1136/thx.43.3.183

Marshall, C., Mamary, A. J., Verhoeven, A. J., & Marshall, B. E. (1996). Pulmonary artery NADPH-oxidase is activated in hypoxic pulmonary vasoconstriction. *Am J Respir Cell Mol Biol, 15*(5), 633-644. doi:10.1165/ajrcmb.15.5.8918370

McCubbrey, A. L., Allison, K. C., Lee-Sherick, A. B., Jakubzick, C. V., & Janssen, W. J. (2017). Promoter Specificity and Efficacy in Conditional and Inducible Transgenic Targeting of Lung Macrophages. *8*(1618). doi:10.3389/fimmu.2017.01618

Medrek, S. K., Sharafkhaneh, A., Spiegelman, A. M., Kak, A., & Pandit, L. M. (2017). Admission for COPD Exacerbation Is Associated with the Clinical Diagnosis of Pulmonary Hypertension: Results from a Retrospective Longitudinal Study of a Veteran Population. *COPD, 14*(5), 484-489. doi:10.1080/15412555.2017.1336209

Mercer, B. A., Kolesnikova, N., Sonett, J., & D'Armiento, J. (2004). Extracellular regulated kinase/mitogen activated protein kinase is up-regulated in pulmonary emphysema and mediates matrix metalloproteinase-1 induction by cigarette smoke. *J Biol Chem, 279*(17), 17690-17696. doi:10.1074/jbc.M313842200

Mills, C. D., Kincaid, K., Alt, J. M., Heilman, M. J., & Hill, A. M. (2000). M-1/M-2 macrophages and the Th1/Th2 paradigm. *J Immunol, 164*(12), 6166-6173. doi:10.4049/jimmunol.164.12.6166

Morrell, N. W., Upton, P. D., Kotecha, S., Huntley, A., Yacoub, M. H., Polak, J. M., & Wharton, J. (1999). Angiotensin II activates MAPK and stimulates growth of human pulmonary artery smooth muscle via AT1 receptors. *Am J Physiol, 277*(3), L440-448. doi:10.1152/ajplung.1999.277.3.L440

Nahrendorf, M., & Swirski, F. K. (2016). Abandoning M1/M2 for a Network Model of Macrophage Function. *Circ Res, 119*(3), 414-417. doi:10.1161/CIRCRESAHA.116.309194

Nana-Sinkam, S. P., Lee, J. D., Sotto-Santiago, S., Stearman, R. S., Keith, R. L., Choudhury, Q., Cool, C., Parr, J., Moore, M. D., Bull, T. M., Voelkel, N. F., &

Geraci, M. W. (2007). Prostacyclin prevents pulmonary endothelial cell apoptosis induced by cigarette smoke. *Am J Respir Crit Care Med, 175*(7), 676-685. doi:10.1164/rccm.200605-724OC

Nathan, C. F., & Hibbs, J. B., Jr. (1991). Role of nitric oxide synthesis in macrophage antimicrobial activity. *Curr Opin Immunol, 3*(1), 65-70. doi:10.1016/0952-7915(91)90079-g

Ni, Y., Shi, G., & Qu, J. (2020). Indoor PM2.5, tobacco smoking and chronic lung diseases: A narrative review. *Environ Res, 181*, 108910. doi:10.1016/j.envres.2019.108910

Ntokou, A., Dave, J. M., Kauffman, A. C., Sauler, M., Ryu, C., Hwa, J., Herzog, E. L., Singh, I., Saltzman, W. M., & Greif, D. M. (2021). Macrophage-derived PDGF-B induces muscularization in murine and human pulmonary hypertension. *JCI Insight, 6*(6). doi:10.1172/jci.insight.139067

Oliveira, M. V., Abreu, S. C., Padilha, G. A., Rocha, N. N., Maia, L. A., Takiya, C. M., Xisto, D. G., Suki, B., Silva, P. L., & Rocco, P. R. (2016). Characterization of a Mouse Model of Emphysema Induced by Multiple Instillations of Low-Dose Elastase. *Front Physiol, 7*, 457. doi:10.3389/fphys.2016.00457

Osler, W. (1893). *The principles and practice of medicine*. New York: D. Appleton.

Peinado, V. I., Barbera, J. A., Abate, P., Ramirez, J., Roca, J., Santos, S., & Rodriguez-Roisin, R. (1999). Inflammatory reaction in pulmonary muscular arteries of patients with mild chronic obstructive pulmonary disease. *Am J Respir Crit Care Med, 159*(5 Pt 1), 1605-1611. doi:10.1164/ajrccm.159.5.9807059

Perez-Sala, D., Cernuda-Morollon, E., Diaz-Cazorla, M., Rodriguez-Pascual, F., & Lamas, S. (2001). Posttranscriptional regulation of human iNOS by the NO/cGMP pathway. *Am J Physiol Renal Physiol, 280*(3), F466-473. doi:10.1152/ajprenal.2001.280.3.F466

Pichl, A., Sommer, N., Bednorz, M., Seimetz, M., Hadzic, S., Kuhnert, S., Kraut, S., Roxlau, E. T., Kojonazarov, B., Wilhelm, J., Gredic, M., Gall, H., Tello, K., Richter, M. J., Pak, O., Petrovic, A., Hecker, M., Schermuly, R. T., Grimminger, F., Seeger, W., Ghofrani, H. A., & Weissmann, N. (2019). Riociguat for treatment of pulmonary hypertension in COPD: a translational study. *Eur Respir J, 53*(6). doi:10.1183/13993003.02445-2018

Price, L. C., Wort, S. J., Perros, F., Dorfmuller, P., Huertas, A., Montani, D., Cohen-Kaminsky, S., & Humbert, M. (2012). Inflammation in pulmonary arterial hypertension. *Chest, 141*(1), 210-221. doi:10.1378/chest.11-0793

Pullamsetti, S. S., Savai, R., Janssen, W., Dahal, B. K., Seeger, W., Grimminger, F., Ghofrani, H. A., Weissmann, N., & Schermuly, R. T. (2011). Inflammation, immunological reaction and role of infection in pulmonary hypertension. *Clin Microbiol Infect, 17*(1), 7-14. doi:10.1111/j.1469-0691.2010.03285.x

Rabinovitch, M., Guignabert, C., Humbert, M., & Nicolls, M. R. (2014). Inflammation and immunity in the pathogenesis of pulmonary arterial hypertension. *Circ Res, 115*(1), 165-175. doi:10.1161/CIRCRESAHA.113.301141

Renda, T., Baraldo, S., Pelaia, G., Bazzan, E., Turato, G., Papi, A., Maestrelli, P., Maselli, R., Vatrella, A., Fabbri, L. M., Zuin, R., Marsico, S. A., & Saetta, M. (2008). Increased activation of p38 MAPK in COPD. *Eur Respir J, 31*(1), 62-69. doi:10.1183/09031936.00036707

Roca, H., Varsos, Z. S., Sud, S., Craig, M. J., Ying, C., & Pienta, K. J. (2009). CCL2 and interleukin-6 promote survival of human CD11b+ peripheral blood mononuclear cells and induce M2-type macrophage polarization. *J Biol Chem, 284*(49), 34342-34354. doi:10.1074/jbc.M109.042671

Romberg, E. (1893). *Ueber Sclerose d. Lungenarterie*.

Saetta, M., Baraldo, S., Corbino, L., Turato, G., Braccioni, F., Rea, F., Cavallesco, G., Tropeano, G., Mapp, C. E., Maestrelli, P., Ciaccia, A., & Fabbri, L. M. (1999). CD8 + ve Cells in the Lungs of Smokers with Chronic Obstructive Pulmonary Disease. *160*(2), 711-717. doi:10.1164/ajrccm.160.2.9812020

Santos, S., Peinado, V. I., Ramirez, J., Melgosa, T., Roca, J., Rodriguez-Roisin, R., & Barbera, J. A. (2002). Characterization of pulmonary vascular remodelling in smokers and patients with mild COPD. *Eur Respir J, 19*(4), 632-638. doi:10.1183/09031936.02.00245902

Sarti, P., Arese, M., Bacchi, A., Barone, M. C., Forte, E., Mastronicola, D., Brunori, M., & Giuffre, A. (2003). Nitric oxide and mitochondrial complex IV. *IUBMB Life, 55*(10-11), 605-611. doi:10.1080/15216540310001628726

Sata, M., Saiura, A., Kunisato, A., Tojo, A., Okada, S., Tokuhisa, T., Hirai, H., Makuuchi, M., Hirata, Y., & Nagai, R. (2002). Hematopoietic stem cells differentiate into vascular cells that participate in the pathogenesis of atherosclerosis. *Nat Med, 8*(4), 403-409. doi:10.1038/nm0402-403

Savai, R., Pullamsetti, S. S., Kolbe, J., Bieniek, E., Voswinckel, R., Fink, L., Scheed, A., Ritter, C., Dahal, B. K., Vater, A., Klussmann, S., Ghofrani, H. A., Weissmann, N., Klepetko, W., Banat, G. A., Seeger, W., Grimminger, F., & Schermuly, R. T. (2012). Immune and inflammatory cell involvement in the pathology of idiopathic pulmonary arterial hypertension. *Am J Respir Crit Care Med, 186*(9), 897-908. doi:10.1164/rccm.201202-0335OC

Scharf, S. M., Iqbal, M., Keller, C., Criner, G., Lee, S., Fessler, H. E., & National Emphysema Treatment Trial, G. (2002). Hemodynamic characterization of patients with severe emphysema. *Am J Respir Crit Care Med, 166*(3), 314-322. doi:10.1164/rccm.2107027

Schermuly, R. T., Dony, E., Ghofrani, H. A., Pullamsetti, S., Savai, R., Roth, M., Sydykov, A., Lai, Y. J., Weissmann, N., Seeger, W., & Grimminger, F. (2005). Reversal of experimental pulmonary hypertension by PDGF inhibition. *J Clin Invest, 115*(10), 2811-2821. doi:10.1172/JCI24838

Seimetz, M., Parajuli, N., Pichl, A., Bednorz, M., Ghofrani, H. A., Schermuly, R. T., Seeger, W., Grimminger, F., & Weissmann, N. (2015). Cigarette Smoke-Induced Emphysema and Pulmonary Hypertension Can Be Prevented by Phosphodiesterase 4 and 5 Inhibition in Mice. *PLoS One, 10*(6), e0129327. doi:10.1371/journal.pone.0129327

Seimetz, M., Parajuli, N., Pichl, A., Veit, F., Kwapiszewska, G., Weisel, F. C., Milger, K., Egemnazarov, B., Turowska, A., Fuchs, B., Nikam, S., Roth, M., Sydykov, A., Medebach, T., Klepetko, W., Jaksch, P., Dumitrascu, R., Garn, H., Voswinckel, R., Kostin, S., Seeger, W., Schermuly, R. T., Grimminger, F., Ghofrani, H. A., & Weissmann, N. (2011). Inducible NOS inhibition reverses tobacco-smoke-induced emphysema and pulmonary hypertension in mice. *Cell, 147*(2), 293-305. doi:10.1016/j.cell.2011.08.035

Seimetz, M., Sommer, N., Bednorz, M., Pak, O., Veith, C., Hadzic, S., Gredic, M., Parajuli, N., Kojonazarov, B., Kraut, S., Wilhelm, J., Knoepp, F., Henneke, I., Pichl, A., Kanbagli, Z. I., Scheibe, S., Fysikopoulos, A., Wu, C. Y., Klepetko, W., Jaksch, P., Eichstaedt, C., Grunig, E., Hinderhofer, K., Geiszt, M., Muller, N., Rezende, F., Buchmann, G., Wittig, I., Hecker, M., Hecker, A., Padberg, W., Dorfmuller, P., Gattenlohner, S., Vogelmeier, C. F., Gunther, A., Karnati, S., Baumgart-Vogt, E., Schermuly, R. T., Ghofrani, H. A., Seeger, W., Schroder, K., Grimminger, F., Brandes, R. P., & Weissmann, N. (2020). NADPH oxidase subunit NOXO1 is a target for emphysema treatment in COPD. *Nat Metab, 2*(6), 532-546. doi:10.1038/s42255-020-0215-8

Sektioglu, I. M., Carretero, R., Bender, N., Bogdan, C., Garbi, N., Umansky, V., Umansky, L., Urban, K., von Knebel-Doberitz, M., Somasundaram, V., Wink, D., Beckhove, P., & Hammerling, G. J. (2016). Macrophage-derived nitric oxide initiates T-cell diapedesis and tumor rejection. *Oncoimmunology, 5*(10), e1204506. doi:10.1080/2162402X.2016.1204506

Shapouri-Moghaddam, A., Mohammadian, S., Vazini, H., Taghadosi, M., Esmaeili, S. A., Mardani, F., Seifi, B., Mohammadi, A., Afshari, J. T., & Sahebkar, A. (2018). Macrophage plasticity, polarization, and function in health and disease. *J Cell Physiol, 233*(9), 6425-6440. doi:10.1002/jcp.26429

Shaw, C. A., Webb, D. J., Rossi, A. G., & Megson, I. L. (2009). Cyclic GMP protects human macrophages against peroxynitrite-induced apoptosis. *J Inflamm (Lond), 6*, 14. doi:10.1186/1476-9255-6-14

Shi, J., Hua, L., Harmer, D., Li, P., & Ren, G. (2018). Cre Driver Mice Targeting Macrophages. *Methods Mol Biol, 1784*, 263-275. doi:10.1007/978-1-4939-7837-3_24

Shi, W., Bellusci, S., & Warburton, D. (2007). Lung development and adult lung diseases. *Chest, 132*(2), 651-656. doi:10.1378/chest.06-2663

Simonneau, G., Montani, D., Celermajer, D. S., Denton, C. P., Gatzoulis, M. A., Krowka, M., Williams, P. G., & Souza, R. (2019). Haemodynamic definitions and updated clinical classification of pulmonary hypertension. *Eur Respir J, 53*(1). doi:10.1183/13993003.01913-2018

Singh, D., Richards, D., Knowles, R. G., Schwartz, S., Woodcock, A., Langley, S., & O'Connor, B. J. (2007). Selective inducible nitric oxide synthase inhibition has no effect on allergen challenge in asthma. *Am J Respir Crit Care Med, 176*(10), 988-993. doi:10.1164/rccm.200704-588OC

Stenmark, K. R., Tuder, R. M., & El Kasmi, K. C. (2015). Metabolic reprogramming and inflammation act in concert to control vascular remodeling in hypoxic pulmonary hypertension. *J Appl Physiol (1985), 119*(10), 1164-1172. doi:10.1152/japplphysiol.00283.2015

Sullivan, A. K., Simonian, P. L., Falta, M. T., Mitchell, J. D., Cosgrove, G. P., Brown, K. K., Kotzin, B. L., Voelkel, N. F., & Fontenot, A. P. (2005). Oligoclonal CD4+ T cells in the lungs of patients with severe emphysema. *Am J Respir Crit Care Med, 172*(5), 590-596. doi:10.1164/rccm.200410-1332OC

Sun, J., Steenbergen, C., & Murphy, E. (2006). S-nitrosylation: NO-related redox signaling to protect against oxidative stress. *Antioxid Redox Signal, 8*(9-10), 1693-1705. doi:10.1089/ars.2006.8.1693

Sundar, I. K., Yao, H., Kirkham, P. A., & Rahman, I. (2014). Smoking, Oxidative/Carbonyl Stress, and Regulation of Redox Signaling in Lung Inflammation. In I. Laher (Ed.), *Systems Biology of Free Radicals and Antioxidants* (pp. 817-848). Berlin, Heidelberg: Springer Berlin Heidelberg.

Sussan, T. E., Rangasamy, T., Blake, D. J., Malhotra, D., El-Haddad, H., Bedja, D., Yates, M. S., Kombairaju, P., Yamamoto, M., Liby, K. T., Sporn, M. B., Gabrielson, K. L., Champion, H. C., Tuder, R. M., Kensler, T. W., & Biswal, S. (2009). Targeting Nrf2 with the triterpenoid CDDO-imidazolide attenuates cigarette smoke-induced emphysema and cardiac dysfunction in mice. *Proc Natl Acad Sci U S A, 106*(1), 250-255. doi:10.1073/pnas.0804333106

Suwanabol, P. A., Seedial, S. M., Shi, X., Zhang, F., Yamanouchi, D., Roenneburg, D., Liu, B., & Kent, K. C. (2012). Transforming growth factor-beta increases vascular smooth muscle cell proliferation through the Smad3 and extracellular signal-regulated kinase mitogen-activated protein kinases pathways. *J Vasc Surg, 56*(2), 446-454. doi:10.1016/j.jvs.2011.12.038

Suwanabol, P. A., Seedial, S. M., Zhang, F., Shi, X., Si, Y., Liu, B., & Kent, K. C. (2012). TGF-beta and Smad3 modulate PI3K/Akt signaling pathway in vascular smooth muscle cells. *Am J Physiol Heart Circ Physiol, 302*(11), H2211-2219. doi:10.1152/ajpheart.00966.2011

Suzuki, Y., Ruiz-Ortega, M., Lorenzo, O., Ruperez, M., Esteban, V., & Egido, J. (2003). Inflammation and angiotensin II. *Int J Biochem Cell Biol, 35*(6), 881-900. doi:10.1016/s1357-2725(02)00271-6

Thabut, G., Dauriat, G., Stern, J. B., Logeart, D., Levy, A., Marrash-Chahla, R., & Mal, H. (2005). Pulmonary hemodynamics in advanced COPD candidates for lung volume reduction surgery or lung transplantation. *Chest, 127*(5), 1531-1536. doi:10.1378/chest.127.5.1531

Tuder, R. M. (2017). Pulmonary vascular remodeling in pulmonary hypertension. *Cell Tissue Res, 367*(3), 643-649. doi:10.1007/s00441-016-2539-y

Tuder, R. M., Groves, B., Badesch, D. B., & Voelkel, N. F. (1994). Exuberant endothelial cell growth and elements of inflammation are present in plexiform lesions of pulmonary hypertension. *Am J Pathol, 144*(2), 275-285.

Tuder, R. M., & Petrache, I. (2012). Pathogenesis of chronic obstructive pulmonary disease. *J Clin Invest, 122*(8), 2749-2755. doi:10.1172/JCI60324

Tuder, R. M., Yun, J. H., Bhunia, A., & Fijalkowska, I. (2007). Hypoxia and chronic lung disease. *J Mol Med (Berl), 85*(12), 1317-1324. doi:10.1007/s00109-007-0280-4

Van den Bossche, J., Baardman, J., Otto, N. A., van der Velden, S., Neele, A. E., van den Berg, S. M., Luque-Martin, R., Chen, H. J., Boshuizen, M. C., Ahmed, M., Hoeksema, M. A., de Vos, A. F., & de Winther, M. P. (2016). Mitochondrial Dysfunction Prevents Repolarization of Inflammatory Macrophages. *Cell Rep, 17*(3), 684-696. doi:10.1016/j.celrep.2016.09.008

Vergadi, E., Chang, M. S., Lee, C., Liang, O. D., Liu, X., Fernandez-Gonzalez, A., Mitsialis, S. A., & Kourembanas, S. (2011). Early macrophage recruitment and alternative activation are critical for the later development of hypoxia-induced pulmonary hypertension. *Circulation, 123*(18), 1986-1995. doi:10.1161/CIRCULATIONAHA.110.978627

Vitecek, J., Lojek, A., Valacchi, G., & Kubala, L. (2012). Arginine-based inhibitors of nitric oxide synthase: therapeutic potential and challenges. *Mediators Inflamm, 2012*, 318087. doi:10.1155/2012/318087

Vogelmeier, C., Agusti, A., Anzueto, A., Barnes, P., Bourbeau, J., Criner, G., Frith, P., Halpin, D., Han, M. K., Martinez, F., Montes de Oca, M., Papi, A., Pavord, I., Roche, N., Sin, D. D., Singh, D., Stockley, R., Victorina Lopez Varela, M., Vestbo, J., & Wedzicha, J. (2020). *Global strategy for the diagnosis, management, and prevention of chronic obstructive pulmonary disease* Retrieved from Global Initiative for Chronic Obstructive Lung Disease: https://goldcopd.org/wp-content/uploads/2019/12/GOLD-2020-FINAL-ver1.2-03Dec19_WMV.pdf

Vuillemenot, B. R., Rodriguez, J. F., & Hoyle, G. W. (2004). Lymphoid tissue and emphysema in the lungs of transgenic mice inducibly expressing tumor necrosis factor-alpha. *Am J Respir Cell Mol Biol, 30*(4), 438-448. doi:10.1165/rcmb.2003-0062OC

Wagner, W., Ciszewski, W., Kania, K., & Dastych, J. (2016). Lactate Stimulates IL-4 and IL-13 Production in Activated HuT-78 T Lymphocytes Through a Process That Involves Monocarboxylate Transporters and Protein Hyperacetylation. *J Interferon Cytokine Res, 36*(5), 317-327. doi:10.1089/jir.2015.0086

Wang, L., Liu, J., Wang, W., Qi, X., Wang, Y., Tian, B., Dai, H., Wang, J., Ning, W., Yang, T., & Wang, C. (2019). Targeting IL-17 attenuates hypoxia-induced

pulmonary hypertension through downregulation of beta-catenin. *Thorax, 74*(6), 564-578. doi:10.1136/thoraxjnl-2018-211846

Weisel, F. C., Kloepping, C., Pichl, A., Sydykov, A., Kojonazarov, B., Wilhelm, J., Roth, M., Ridge, K. M., Igarashi, K., Nishimura, K., Maison, W., Wackendorff, C., Klepetko, W., Jaksch, P., Ghofrani, H. A., Grimminger, F., Seeger, W., Schermuly, R. T., Weissmann, N., & Kwapiszewska, G. (2014). Impact of S-adenosylmethionine decarboxylase 1 on pulmonary vascular remodeling. *Circulation, 129*(14), 1510-1523. doi:10.1161/CIRCULATIONAHA.113.006402

Weissmann, N. (2018). Chronic Obstructive Pulmonary Disease and Pulmonary Vascular Disease. A Comorbidity? *Ann Am Thorac Soc, 15*(Suppl 4), S278-S281. doi:10.1513/AnnalsATS.201808-532MG

Weissmann, N., Lobo, B., Pichl, A., Parajuli, N., Seimetz, M., Puig-Pey, R., Ferrer, E., Peinado, V. I., Dominguez-Fandos, D., Fysikopoulos, A., Stasch, J. P., Ghofrani, H. A., Coll-Bonfill, N., Frey, R., Schermuly, R. T., Garcia-Lucio, J., Blanco, I., Bednorz, M., Tura-Ceide, O., Tadele, E., Brandes, R. P., Grimminger, J., Klepetko, W., Jaksch, P., Rodriguez-Roisin, R., Seeger, W., Grimminger, F., & Barbera, J. A. (2014). Stimulation of soluble guanylate cyclase prevents cigarette smoke-induced pulmonary hypertension and emphysema. *Am J Respir Crit Care Med, 189*(11), 1359-1373. doi:10.1164/rccm.201311-2037OC

Weissmann, N., Sommer, N., Schermuly, R. T., Ghofrani, H. A., Seeger, W., & Grimminger, F. (2006). Oxygen sensors in hypoxic pulmonary vasoconstriction. *Cardiovasc Res, 71*(4), 620-629. doi:10.1016/j.cardiores.2006.04.009

Weitzenblum, E., Sautegeau, A., Ehrhart, M., Mammosser, M., & Pelletier, A. (1985). Long-term oxygen therapy can reverse the progression of pulmonary hypertension in patients with chronic obstructive pulmonary disease. *Am Rev Respir Dis, 131*(4), 493-498. doi:10.1164/arrd.1985.131.4.493

Wells, J. M., Washko, G. R., Han, M. K., Abbas, N., Nath, H., Mamary, A. J., Regan, E., Bailey, W. C., Martinez, F. J., Westfall, E., Beaty, T. H., Curran-Everett, D., Curtis, J. L., Hokanson, J. E., Lynch, D. A., Make, B. J., Crapo, J. D., Silverman, E. K., Bowler, R. P., Dransfield, M. T., Investigators, C. O., & Investigators, E. S. (2012). Pulmonary arterial enlargement and acute exacerbations of COPD. *N Engl J Med, 367*(10), 913-921. doi:10.1056/NEJMoa1203830

Wen, F. Q., Kohyama, T., Liu, X., Zhu, Y. K., Wang, H., Kim, H. J., Kobayashi, T., Abe, S., Spurzem, J. R., & Rennard, S. I. (2002). Interleukin-4- and interleukin-13-enhanced transforming growth factor-beta2 production in cultured human bronchial epithelial cells is attenuated by interferon-gamma. *Am J Respir Cell Mol Biol, 26*(4), 484-490. doi:10.1165/ajrcmb.26.4.4784

Wen, L., Krauss-Etschmann, S., Petersen, F., & Yu, X. (2018). Autoantibodies in Chronic Obstructive Pulmonary Disease. *Front Immunol, 9*, 66. doi:10.3389/fimmu.2018.00066

Wilkinson, M., Langhorne, C. A., Heath, D., Barer, G. R., & Howard, P. (1988). A pathophysiological study of 10 cases of hypoxic cor pulmonale. *Q J Med, 66*(249), 65-85.

Wilson, J. L., Yu, J., Taylor, L., & Polgar, P. (2015). Hyperplastic Growth of Pulmonary Artery Smooth Muscle Cells from Subjects with Pulmonary Arterial Hypertension Is Activated through JNK and p38 MAPK. *PLoS One, 10*(4), e0123662. doi:10.1371/journal.pone.0123662

Wright, J. L., & Churg, A. (1991). Effect of long-term cigarette smoke exposure on pulmonary vascular structure and function in the guinea pig. *Exp Lung Res, 17*(6), 997-1009. doi:10.3109/01902149109064331

Wright, J. L., Cosio, M., & Churg, A. (2008). Animal models of chronic obstructive pulmonary disease. *Am J Physiol Lung Cell Mol Physiol, 295*(1), L1-15. doi:10.1152/ajplung.90200.2008

Wright, J. L., Petty, T., & Thurlbeck, W. M. (1992). Analysis of the structure of the muscular pulmonary arteries in patients with pulmonary hypertension and COPD: National Institutes of Health nocturnal oxygen therapy trial. *Lung, 170*(2), 109-124. doi:10.1007/BF00175982

Wright, J. L., Zhou, S., Preobrazhenska, O., Marshall, C., Sin, D. D., Laher, I., Golbidi, S., & Churg, A. M. (2011). Statin reverses smoke-induced pulmonary hypertension and prevents emphysema but not airway remodeling. *Am J Respir Crit Care Med, 183*(1), 50-58. doi:10.1164/rccm.201003-0399OC

Ye, M., Iwasaki, H., Laiosa, C. V., Stadtfeld, M., Xie, H., Heck, S., Clausen, B., Akashi, K., & Graf, T. (2003). Hematopoietic stem cells expressing the myeloid lysozyme gene retain long-term, multilineage repopulation potential. *Immunity, 19*(5), 689-699. doi:10.1016/s1074-7613(03)00299-1

Zong, D., Li, J., Cai, S., He, S., Liu, Q., Jiang, J., Chen, S., Long, Y., Chen, Y., Chen, P., & Ouyang, R. (2018). Notch1 regulates endothelial apoptosis via the ERK pathway in chronic obstructive pulmonary disease. *Am J Physiol Cell Physiol, 315*(3), C330-C340. doi:10.1152/ajpcell.00182.2017

9. Declaration

I declare that I have completed this dissertation single-handedly without the unauthorized help of a second party and only with the assistance acknowledged therein. I have appropriately acknowledged and referenced all text passages that are derived literally from or are based on the content of published or unpublished work of others, and all information that relates to verbal communications. I have abided by the principles of good scientific conduct laid down in the charter of the Justus Liebig University of Giessen in carrying out the investigations described in the dissertation.

10. Acknowledgments

It is my pleasure to express deepest gratitude and appreciation to the people, whose assistance, support and encouragement were indispensable to me during the period of my PhD studies.

First of all, I would like to thank my supervisor Dr. Norbert Weißmann for providing me the opportunity to work in his research group. His guidance and unreserved support made the completion of my PhD thesis possible. I am especially grateful for the given freedom and trust, that allowed me to grow and develop professionally.

I am thankful to Dr. Simone Kraut, not only for the mentoring and guidance, but also for the friendly, supportive and caring manner in which she provided it.

I would like to express a special gratitude to Professor Werner Seeger, as the Chief of the Department of Internal Medicine, Section Head of Respiratory and Critical Care Medicine at Justus Liebig University Giessen, Chairman of the Universities of Giessen & Marburg Lung Center (UGMLC).

I am deeply thankful to Cheng-Yu Wu, Dr. Rajkumar Savai, Dr. Baktybek Kojonazarov, Siddartha Doswada, Dr. Astrid Weiss, Dr. Andreas Weigert, Dr. Andreas Guenther, Dr. Ralf P. Brandes, Dr. Ralph T. Schermuly, Dr. Friedrich Grimminger, Dr. Natascha Sommer, Dr. Jochen Wilhelm and Julia Meike Schaeffer, whose intellectual and practical assistance was a milestone in the completion of this project.

I would like to thank Ewa Bieniek, Nils Schupp, Ingrid Breitenborn-Müller, Carmen Homberger, Susanne Lich, Miriam Wessendorf and Elisabeth Kappes for their valuable technical assistance.

I would like to pay special regard to my dear friends and colleagues, Dr. Oleg Pak, Aleksandar Petrović and Karin Quanz, for the valuable help in my everyday work, and more importantly, their kindness, support, encouragement and friendship. Especially, I would like to thank my best friend, Stefan Hadžić. *Ni mnogo vještiji se ne bi snašli da opišu koliko mi znači tvoja podrška, briga i dobrota, i koliko mi je bitno da naše prijateljstvo opstaje i raste.*

Finally, nothing would have been possible without my family and their unconditional love and support. I would like to thank my parents Zora and Tomislav, sister Jelena, brothers Andrija and Lazar, and husband Đuro. *Sve što jesam i što ću postati, ja sam*

zbog vas i za vas, koji ste vjerovali u mene čak i kada ja nijesam vjerovala u sebe. Mogu se samo nadati da se približim onome, što vi u meni vidite.